Addis Ababa University
Addis Ababa Institute of Technology
African Railway Center of Excellence

Investigating the Influence of Wheel Wear on Vehicle Dynamic Behavior by Introducing Yaw and Track Irregularity

A Research report Submitted to the School of Graduate Studies of Addis Ababa University in Partial Fulfillment of the Requirements for the Degree of Masters of Science in Railway Engineering (Rolling stock)

Prepared By: Biruk Yifru (GSR/0845/13)

Advisor: Daniel Tilahun (PhD)

Co-Advisor: Awel Mohammed Seid (PhD Candidate)

February 2023
Addis Ababa
Ethiopia

Approval Page

ADDIS ABABA UNIVERSITY

Addis Ababa Institute of Technology

African Railway Center of Excellence

Title: Investigating the Influence of Wheel Wear on Vehicle Dynamic Behavior by Introducing Yaw and Track Irregularity

Biruk Yifru (GSR/0845/13)

Dr. Daniel Tilahun	________________	________________
Main Advisor	Signature	Date
Mr. Awel Mohammed Seid	________________	________________
Co-Advisor	Signature	Date
Dr. Mulugeta Habtemariam	________________	________________
Internal Examiner	Signature	Date
Dr. Haileloul Sahile	________________	________________
External Examiner	Signature	Date
________________________	________________	________________
ARCE Center Head	Signature	Date

Declaration Page

I hereby declare that the research work entitled **"Investigating the Influence of Wheel Wear on Vehicle Dynamic Behavior by Introducing Yaw and Track Irregularity"** is my original piece of work and has not been presented for any degree in any other universities

_________________ ________________

Biruk Yifru Date

Acknowledgement

First and foremost, I would like to thank God for giving me the patience to carry out this research work since it took an extended period than I anticipated. I would also like to express my deepest gratitude to Dr. Daniel and Mr. Awel, my research Advisor and Co-advisor. My special thanks go to Mr. Awel, who gave me unpresented support throughout preparing for this research work and other course works. I also like to thank staff from AALRT, specifically Mr. Yoseph, Mr. Dula, Mr. Endalk and Mr. Taddele for their unreserved support in availing the data from AALRT required for the research work. Finally, I would like to thank my family and friends for their support and care during my studies and this research work, as it helped a great deal to finish this work successfully.

Abstract

This research intends to indicate the influence of wheel wear due to yaw and track irregularity on vehicle dynamic behavior demonstrated in terms of waer depth, derailment coefficient and ride index. Software simulation-based and wear data validation was used. A Hertzian contact model was used for the wheel-rail contact while SIMPACK and in house made MATLAB code of Archard wear model were used for multibody modeling and analysis of wear depth of each wheel. Main influencing factors involved in the analysis were curvature radius, speed, yaw, and track irregularities variations which were demonstrated in terms of wear depth and vehicle dynamic behavior expressed in derailment coefficient and ride index. A 1 km track long specified curve radius, speed, and yaw damper values were devised for the analysis process with a wear factor of 10,000 applied for the wear depth calculation.

Based on the analysis, re-profiling analysis was performed till 60,000km with 10,000km interval data extraction and wear depth was found to match close to the values from wear data collected from AALRT. Further case studies also confirmed that 50m radius of curvature resulted the highest wear depth (6.18mm) and higher derailment coefficient (1.01) and unconfortable despite the existence of yaw damper or track irregularity. Yaw at lower running speeds on the other hand didn’t affect much the ride index while it improved the derailment coefficient. But when speed becomes higher and its value increased, wear depth reduced and both ride index and derailment coefficient deteriorated. Finally, track irregularity alone brought only slight disturbance to the derailment coefficient and ride index. But it has significant increase to both values when combined with factors like yaw. As a result, measures shall be taken to minimize the combined effect of yaw and track irregularity.

Keywords: Vehicle dynamic modeling, Archard wear model, wear depth, derailment coefficient, ride index, re-profiling, wear data.

Table of Contents

List of Figures

List of Tables

Nomenclature

Symbols

A: contact Area

D: distance

E: modulus of elasticity

G shear modulus

H: Material hardiness

I: Moment of Inertia

K: wear coefficient

k_v, k_y: *factors of volume wear*

N: Normal force

P: Normal pressure in contact patch

R_w: *radius of the wheel*

r_{x1} *wheel radius*

r_{y1} *rail radius*

S sliding distance

T: Creep Force

W: wear rate

V_{lat}: *lateral velocity of the wheel*

V_w: *forward velocity of the wheel.*

γ: *longitudinal creepage*

ω: *lateral creepage*

ψ *spin creepage*

V_w: *Volume of wear*

μ_f: *Coefficient of friction*

ψ: *yaw angle*

+Y+Tr: Yaw with track irregularity

+Y-Tr: Yaw with no track irregularity

-Y+Tr: No Yaw with track irregularity

-Y-Tr: No Yaw with no track irregularity

MC1: Motored Car 1

MC2: Motored Car 2

TP: Trailor Car

WS: Wheelset, as WS1, WS2, WS3 …

R: Right

L: Left

Abbreviations

Acronym	***Definition***
AALRT	*Addis Ababa Light Rail Transit*
ARCE	*African Railway Center of Excellence*
BRR	*British Rail Research*
DOAJ	*Directory of open-Source Journals*
DOF	*Degree of Freedom*
IEA	*International Energy Agency*
KTH	*KTH Royal Institute of Technology*
LRT	*Light Rail Transit*
MBS	*Multi Body Simulation*
NMV	*Ride comfort Index*
ODE	*Ordinary Differential Equation*
PPHD	*People Per Hour per Direction*
RCF	*Rolling contact Fatigue*
RI	*Ride Index*
UIC	*International Union of Railways*
USFD	*University of Sheffield*

Chapter 1 - Introduction

1.1 Background

The railway is one of the most energy-efficient and Cost-effective modes of transport available nowadays, next to sea transport. It hauls heavy amounts of goods and passengers from one place to another with a cost and energy-efficient contact mode. Yet its history claims that over 200 years ago when the first locomotives were built, people feared that passengers would become unconscious due to the excessive vibration from the locomotives. Over the years, the technology has improved a lot through research and development and now there are trains traveling beyond 300 miles per hours and other new railway technologies emerging to achieve higher speeds and make a breakthrough in the Railway industry [1].

1.1.1. Brief History of Railway

Even though the leads of a railway system can be dated back 2000 years during the civilization of Egypt, Babylon, and Greece, with animals pulling goods with carts and a predetermined path [2], the modern railway started as early as 1550 in Germany where wooden rails (wagon ways) were used as tracks and horses as locomotives to transport coal using wagons from the mine site to production industries [1]. Later on, around the 17th century, iron replaced the wooden rails while horses were still used till the discovery of the steam engine in the 18th century [1]. The first steam-powered locomotive originated in Great Britain in the late 1900s and was mainly used to haul coal from coal mines and was later engineered to haul its first passengers. The Wales adopted the first ever passenger railway servicen 1807 when the Mumbles and Swansea Railways ultimately became passenger based [3]. Until the discovery of cars and airplanes in the early 1900s, trains were the primary mode of transportation in USA, where moststeam powered locomotives were then abandoned, and Diesel and electric powered ones started to rise [1]. The history of Electric rail vehicles dates back to 1837, built in Scotland by the chemist Robert Davidson, designed to run on batteries and later adopted into a large locomotive called 'Galvani', which gave rise to the design of running rails and overhead line by the Germania Werner von Siemens [3]. Yet the starting of diesel-powered trains revolutionized the era of rail travel when the first diesel-powered railway was built in Switzerland in 1906.

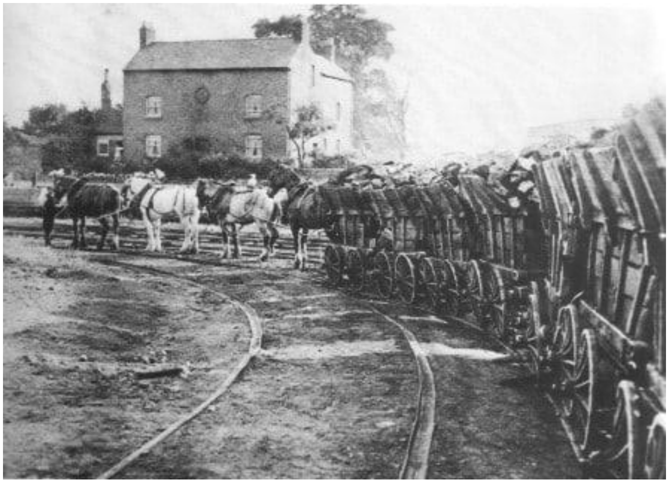

Figure 1.1-Horses being used as locomotives in the early 1500s [1]

The most astonishing effect of the railway that came after diesel-powered railways was the advancement in the electric-powered railways and high-speed trains, leading to new inventions and innovations, like the MAGLEV and Hyperloop, which aimed to improve the performance and energy efficiency of the system to revolutionizing the railway travel experience in these new systems. With our current highly innovative world, we can expect to see trains traveling underwater, trains powered by new energy sources like Hydrogen cells, trains having speeds higher than 1000 km/hr, and many more.

1.1.2. Railway in Ethiopia

The first railway in Ethiopia was a 780km meter gauge line built from Addis Ababa to Djibouti by the Ethiopian Emperor Menelik II to facilitate the transport of goods and passengers to and from the port of Djibouti due to the complicated animal-based transportation system at that time. The first line was constructed from Djibouti to DireDawa and was open for service in 1901 while the second part extending the line from DireDawa to the capital was not constructed till 1917. The line was considered the main logistics route during the time and used to give service till the late 20^{th}/early 21^{st} century and finally closed for service. Later in 2016, a new 760km, 660km lies in Ethiopia, standard gauge electrified railway system replaced the former meter gauge railway and started giving service [4].

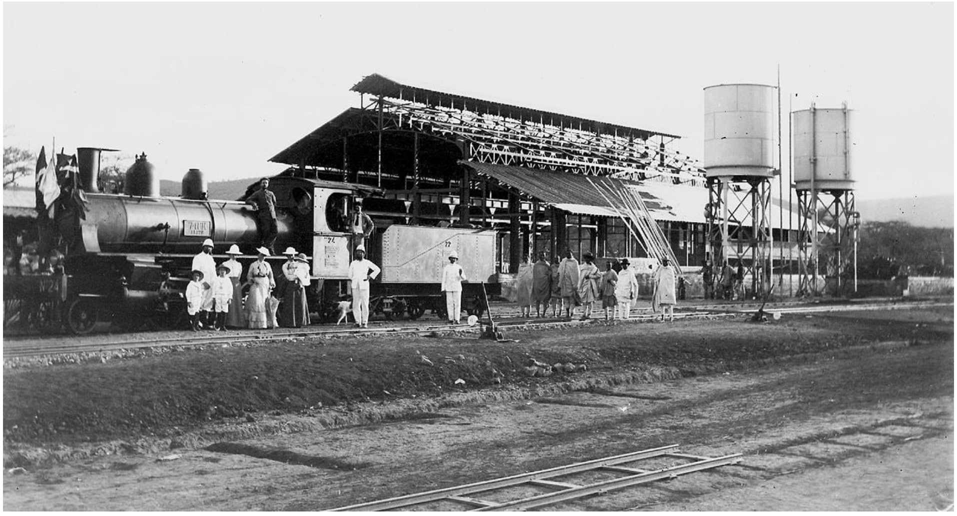

Figure 1.2-Ethio-Djibouti railway at Dire Dawa (Courtesy of Alfred Ilg and his family)

The Ethiopian Railway Corporation also gave the contract for the construction of a 392 km line from Awash to Djibouti to Hara gebeya in 2015, 260 km from Hara Gebeya to Mekele in 2015, 480 km line from Hara Gebeya to Port Tajura in Djibouti and 491 km from Addis Ababa to Bedele. The Addis Ababa to Hara Gebeya is reported to reach 90% by the early 2020, but the rest are under construction. In 2020 also, a feasibility study of a new 1522 km standard gauge railway linking Addis Ababa to Sudan Khartoum to Port Sudan was initiated [4].

Considering LRTs (Light Rail Transit), Addis Ababa Light Rail Transit (AALRT) is the first sub-Saharan renewable energy light rail train network found in Addis Ababa, Ethiopia [5]. It is a 31.6 kms of standard gauge line extending from east to west (17.4 km), stretching from Ayat to Torhailoch and north to the south line (16.9 km) extending from Menelik Square to Kality having a common section of 2.7 km at the Meskel Square area. The project was completed and started giving service in September, 2015, with the north-to-south line giving service before the east-to-west line with a total Expenditure of $475 Million covered by the Ethiopian government and Chinese Export-Import Bank. Trains are expected to run at maximum speed of 70 km/hr with a hauling capacity of 15,000 PPHD on its 41 stations giving service up to 18 hours a day [6]. The below figure 1.3 shows train types currently in operation at AALRT and the corresponding 41 train stations through the two major route of the trains. Each of the trains operating in the two lines have their own color designation, i.e. the N-S line trains are identified by Blue colour while the E-W line trains are Green.

Figure 1.3-AALRT Trains in operation (a) AALRT Route Map (b) [7]

1.1.3. Challenges in the Railway Industry

There are many challenges in the current railway industry related to wear of materials, energy efficiency, material properties, environmental conditions, and many more and they could generally be categorized into the following three major categories [8].

- **Strengthening the attractiveness of the sector:** by ensuring safety, health, and hygiene onboard and around trains and improving passenger comfort
- **Digitalizing the transport system:** by using the latest technologies available in communication operation and control, improving availability at a lower cost

- **Providing Virtuous designs for trains:** will facilitate their ever-known preference over the other land transportation modes due to their at least three times less polluting than road vehicles, according to the figure 1.4 shown below.

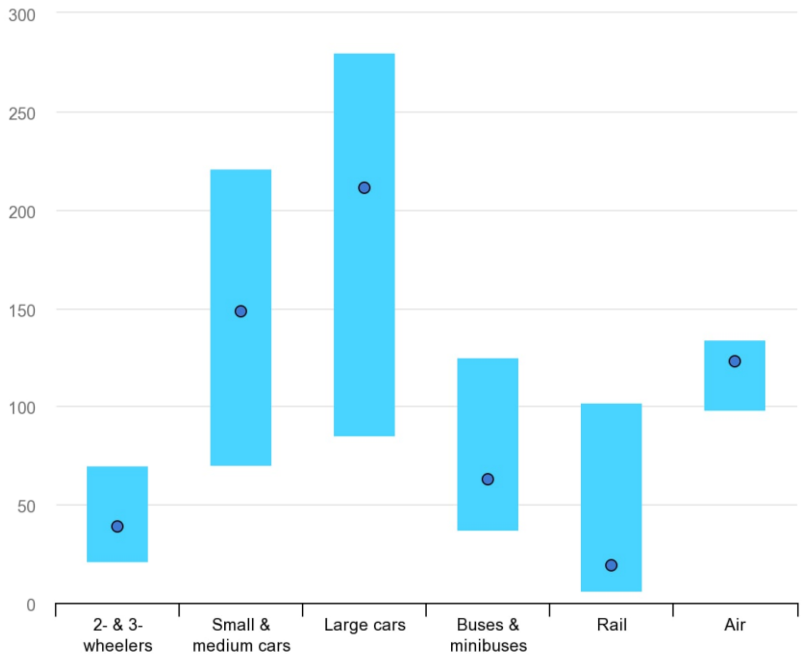

Figure 1.4-The Energy efficiency of Railway compared to other land transportation modes (y-axis: a gram of CO2 emission rate/passenger km, blue dot: area average) [9]

Due to its emense capacity to move passengers and products at once, railway is now the most energy-efficient mode of land transportation. The higher energy efficiency also rises from the low coefficient of rolling friction between the wheel and rail. Though the coefficient of rolling friction is considered to be minimum, the area of contact between the wheel and rail is very small compared to the surface area of the contacting wheel and rail, thus resulting in an elevated amount of stress existing on the interface, i.e., on the contact patch. This, in turn, gives rise to the localized stress being more than the material property, i.e., the yield stress being exceeded, resulting in plastic deformation. When this process is repeated several times while the wheel is rolling on the rail, a cyclic stress results in a fatigue crack forming in the subsurface of the two materials in contact and a final fatigue fracture. This, in general, is the main cause of wheel wear on railway.

1.2 Problem Statement

Wear is one of the most prevalent modes of material damage in machinery parts. According to [10] material loss connected with friction and wear in machines is estimated to take 3-5% of the gross national product. Also, about a quarter of the energy input in the industry is spent on overcoming friction, having direct relation to wear in most of the materials. Wear mechanisms can generally be Abrasive, Adhesive, surface fatigue, and tribo-chemical wear depending on the cause and means of wear propagation. It is also classified as being mild or severe.

In the railway Industry, wear is a very crucial subject because of a metal running on another metal scenario which poses excessive material loss, noise, and discomfort due to this effect. The term ‘wheel wear’ is generally used to denote any damage occurring on the rolling surface of railway wheels, which involves material loss from the surface. This can be viewed as thread wear or flange wear based on the location of the wearing surface and can be caused by the effect of adhesive and/or abrasive wear, rolling contact fatigue (RCF), and sometimes due to material relocation due to plastic deformation [11]. Material is usually removed from the existing profile of the wheel, mostly from the flange contact point due to cornering and hunting effects giving rise to a new wheel profile with reduced flange thickness (15mm min. limit for AALRT Case) as shown in figure 1.5. Since the new profile is undesirable and causes unwanted dynamic effects, wheels are re-profiled after inspections are performed until their dimensional constraints set by the manufacturer (580mm min. limit for the AALRT case) are reached so that there is no further re-profiling recommended unless the wheel is disposed.

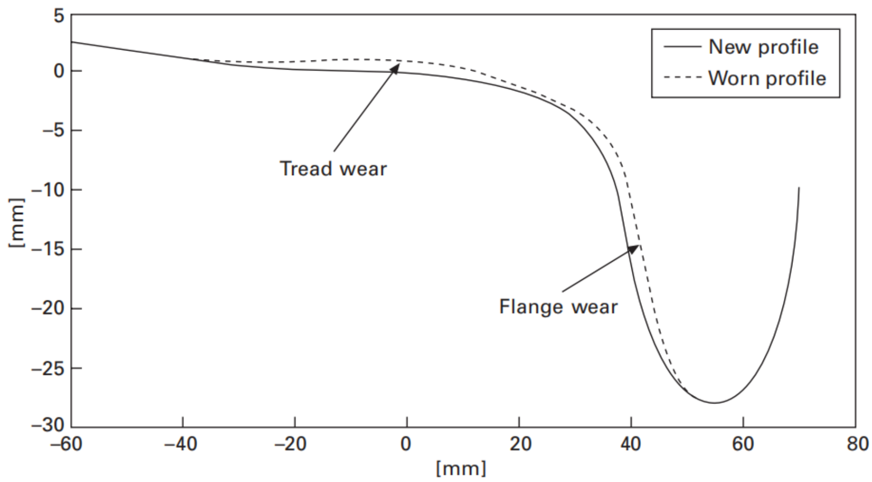

Figure 1.5-New and worn profile of a typical rail vehicle wheel at different locations [12]

Considering AALRT's case, there are many issues related to wheel wear based on data assessment and other researchs done on the related topics. Based on a research done [13], each train carries 400 passengers, while according to the train manufacturer the maximum train carrying capacity is 317 (65 sittings and 252 standing) passengers. This causes overload, which is transferred as vertical, lateral and creep forces into the train's wheels. Since this research was published in 2019, the value is expected to be higher nowadays with the passenger overflow in 2022 with a close to 10% increase in population growth and ever increasing traffic congestion in the city of Addis Ababa. Based on wheel flange thickness and re-profiling history (2019-2021) data collection and analysis done from AALRT, it has been found that out of the 47 trains where wheel re-profiling has been done at the Kality Depot, 38 of them were from Ayat line (East to the west line) which is not the curviest as that of north to the south line and some trains even had repeated re-profiling history due to the overload of passengers on that line.

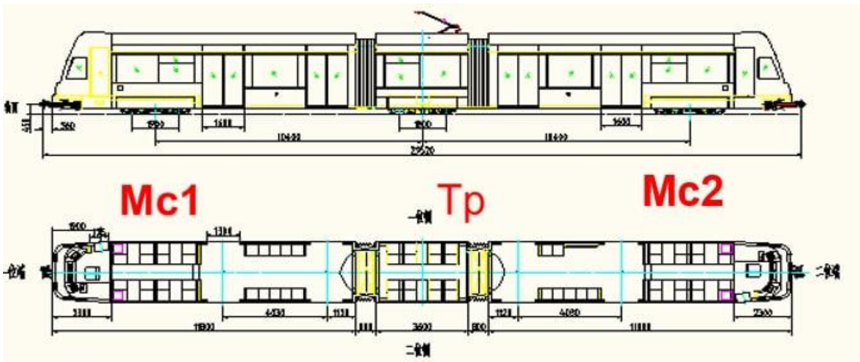

Figure 1.6-Layout of Train Carriages of AALRT (Courtesy of Train Maintenance Manual)

Also, based on the above data analysis, it was found almost all the time severe wheel wear and wheel flange thickness degradation had been found on the wheels of the TP (Trailer Car) of three car bodies of the train. Based on staff interviews performed, the wheels of the trains are wearing prematurely with previously anticipated five years of service with 1mm of wear for each 10,000 km of travel based on track condition promised by the manufacturer. But based on the data collected, wheel change is done for the trains in less than three years, and some trains are currently out of service due to this problem. To compensate for these frequent re-profiling, the technicians place shims between the primary suspension spring and the axle box to protect the onboard device from being hit by on-ground objects, as shown in figure 1.7. As a result, the main objective of this research is to quantify the wear rate based on actual data from the LRT and express it in terms of corresponding vehicle dynamics parameters.

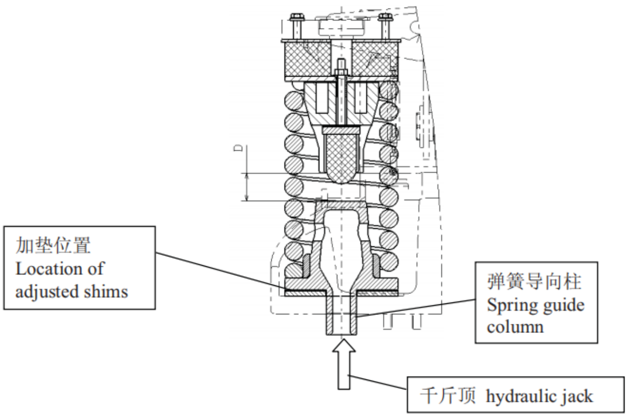

Figure 1.7-Shims between suspension spring and axle box (Courtesy of Train maintenance manual)

1.3 Research Questions

- Which rail vehicle and track-related parameters influence wheel wear in most for the AALRT case?
- How much is single and combined effect of yaw and track irregularities on wear depth?
- How much is the effect of wear due to yaw and track irregularities on ride index, derailment coefficient, and lateral force against the standard allowable values?

1.4 Objective

1.4.1 General objective

The general objective of the research project is to investigate the effect of wear on vehicle dynamic behavior by considering yaw and track irregularity as major factors using computational analysis

1.4.2 Specific Objectives

- To analyze the vehicle and track related factors that influence wheel wear and determine the most prevalent.
- To determine the influence of yaw and track irregularity variation separately and in combination on wheel wear depth.
- To demonstrate the effect of wheel wear depth due to yaw and track irregularity variation on vehicle dynamic behavior, i.e. derailment coefficient and ride index.
- Based on actual track condition and vehicle data of trains, model, simulate and validate the result through a wear data from AALRT.

1.5 Research Significance

The main advantage of performing this research work was to indicate the significant effect of yaw and track irregularities on wheel wear. This is demonstrated by vehicle dynamic analysis of the AALRT trains so that proper maintenance procedure for wheel and track can be devised intended to reduce the effect of wear due to rail irregularities and Yaw. This also showed the importance of considering yaw and track irregularity individually and in combination in wear and vehicle dynamic analysis of rollingstocks as a general case.

1.6 Scope and Limitation of the research

The scope of the study is focused on performing a software simulation based on the actual data of the track and rail vehicle condition for AALRT based on different operational scenarios including operating speeds, track curvature radius, and influencing parameters such as yaw damper and track irregularities. The data collected was focused on flange thickness, re-profiling diameter history, and actual geometrical dimension for the trains. The research outcome is limited to the effect of yaw and track irregularity on wheel wear and vehicle dynamic behaviors even though there are many other factors that need to be considered to get the full picture of the real scenario. But including other many factors will introduce higher computation time and memory size and is left for further research work. Also, the unavailability of complete wear data for the Ayat (East to the west) line from AALRT can be taken as a limitation since the change of values couldn’t be compared for the two railway lines.

Chapter 2 - Literature Review

2.1 Introduction

In the operation of a railway line, the wear of wheel and rail is one of unavoidable phenomena where the material is removed from the surface as a result of wheel-rail interaction. The wheel profile and material selection were mostly led by strength, fatigue and wear. But recently, the effect of wear has dominated due to its effect on vehicle dynamic behavior due to the excessive modification of the original wheel profile [12]. This imposes significant performance and cost related issues since wheels shall be re-profiled to regain their original profile by compromising the diameter of the wheel. The wheel wear, in general, could be classified as regular wear, having a wear pattern along the circumferential direction formed due to slow variation of with longitudinal and lateral contact forces and creepage associated while irregular wear (wheel out of roundness) due to fast variation of wheel-rail contact condition affecting vertical vibration of the system [15]. Considering this research regular wheel wear is under concern.

In the literature review process, well-known scientific Journals, including Scopus (www.scopus.com), Science Direct (www.sciencedirect.com), Tylor and Francis (www.tandonline.com), and Directory of open access Journals (DOAJ) has been used to search for relevant published literature, and Lit maps (app.litmaps.com) has been used to find the most related literature to the topics under consideration. Keywords and phrases including “wheel wear and vehicle dynamics”, “wheel wear prediction”, “vehicle dynamics due to wear”, “wheel wear and yaw”, “wheel wear and track irregularities,” and many other related words and phrases were used to collect related published papers; then screening has been done for considering the effect of wheel wear on vehicle dynamics and using Multibody dynamic simulation tools like SIMPACK. Finally, the most relevant literatures to the topic have been chosen and reviewed in the following sections.

2.1.1 Wear and wear mechanisms

In general, wear is the process of material removal from the surface of an object due to a mechanical, thermal or chemical effect, the mechanical one being due to friction interaction between two or more surfaces resulting in the harder material putting a print on the softer one or due to a blending effect made between the materials, one of the materials could take away part of the softer one. Different wear mechanisms are found on the motion type between the interfacing surfaces or tribo-pairs [16]. These include: -

- **Abrasive wear**: in this wear mechanism, significant hardness differences between the interfacing materials or a third body in between will cause a material removal from the surfaces due to fracture of piece of material from the softer one during loading and motion. [16]

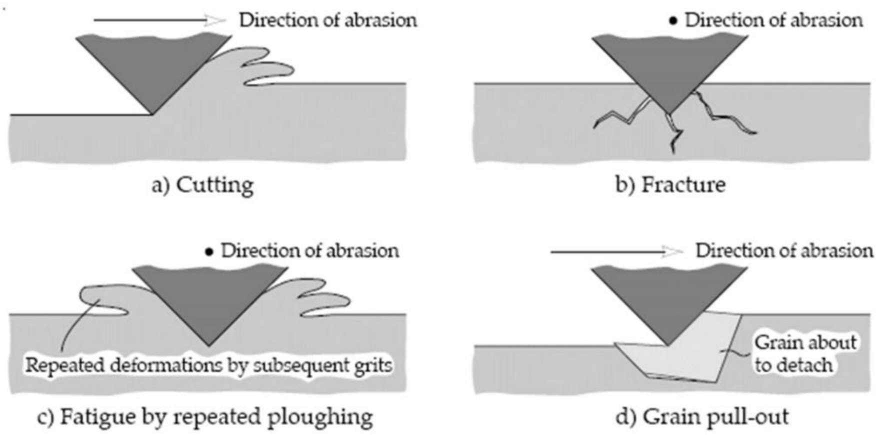

Figure 2.1-Abrasive wear modes [16]

- **Adhesive wear:** this occurs when two surfaces are in sliding contact and bonding occurs between surface layers. Then when the load is applied, the asperities in contact will break away from either of the surfaces to the other, causing wear. [16]

Figure 2.2-Adhesive wear [16]

- **Surface fatigue:** is caused by repeated cyclic loading causing a fatigue crack in the subsurface of either of the contacting surfaces, which then propagates and material detachment occurs. The sub-layers could also experience plastic deformation due to the fatigue strength of the material being lower than the applied load. [16]

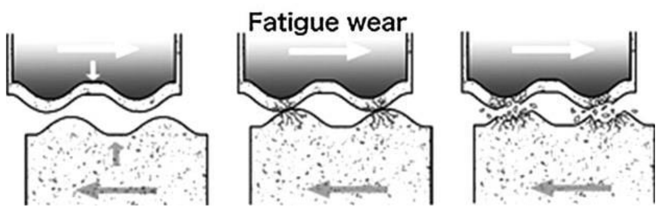

Figure 2.3-Fatigue wear [16]

- **Tribo-chemical (corrosive) wear:** in this case, materials are first removed due to a chemical reaction occurring between the surfaces due to corrosion and surface rubbing leading those debris to cause a further damage on to the surface. [16]

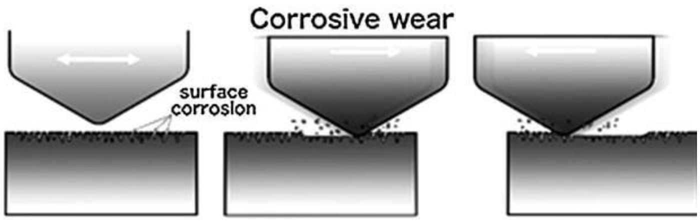

Figure 2.4-Corrosive wear [16]

In practice, each wear mechanism doesn't exist by itself but rather combined with the others to give out significant material damage. To identify the possible wear mechanism existing in a damaged surface, analyzing the motion type as sliding, rolling, impact, or oscillating type can help a lot. But the most efficient way is to analyze the damaged surface deeply and depict the wear mechanism involved. Also, each wear mechanism has its mitigation techniques and measures so that its effect couldn't trigger catastrophic damage to the contacting surfaces.

2.1.2 Wear regimes

Wear regime vary based on the type of load and direction of motion as sliding wear, and rolling wear [17]. Wear could also result from a combination of the mechanical, chemical, and thermal types expressed in terms of micro-cutting, plastic deformation, cracking, fracture, welding, or melting. Wear is not a material property but a system response that is highly affected by its operating environment, i.e., the presence of a dry, wet, oily condition or, in general, having a third body in between highly affects the wear rate of the interface.

Surface disturbance / Relative motion	Generation of defects		Generation of heat	
	Storage of defects	Motion of defects	Chemical interaction	Physical interaction
Fretting	Fretting fatigue	Fretting wear		
Sliding	Fatigue wear	Abrasive wear		Adhesive wear
Rolling	Pitting	Solid-particle crushing		
Impact	Impact wear			
Flow	Liquid-impact erosion	Solid-particle erosion		Ablation erosion

Figure 2.5-Different Types of Wear [17]

Based on the material lost from the surface of the tribo-pairs due to increased normal load, sliding speed or bulk (contact interface) temperature, we can also classify wear regime as: [18]

- **Mild wear**: wear process occurs on the outermost surface layers, which are usually smooth, and surfaces are oxide layer protected, usually debris up to 100nm long.
- **Sever wear**: the surfaces are worn deep into the sublayers with debris up to 100 µm. Mostly it is associated with thermal and adhesive wear mechanisms.
- **Catastrophic wear**: increased temperature in contact results in thermal softening leading to further transition from severe wear. It is later discovered after the two wear regimes described above.

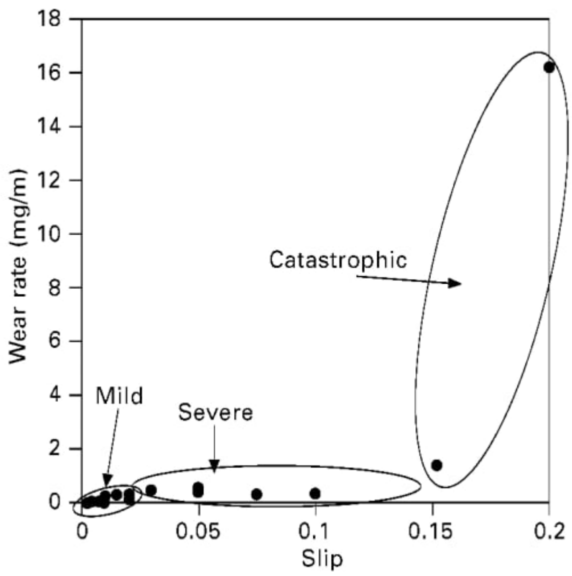

Figure 2.6-wear regimes for sample R8T wheel material on twin disc test [18]

2.2. Wheel-Rail contact mechanics and wear

Adhesion is the main reason trains safely, efficiently, and reliably operate in a railway network. In accelerating, braking, and stopping keeping an optimum amount of adhesive force is an important subject to be dealt with. Wheel rail contact is also a critical issue in railways because it determines the tractive or braking force that could be applied by minimizing slip [18]. As it is known, contacting surfaces are both metals for trains and there is a very small area of contact between the components (wheel and rail) compared to their surface area, imposing a tremendous amount of stress on the surfaces at the contacting interface (Contact patch). In addition, since there are no steering mechanisms for train wheels, they accommodate curving by performing a wheel slide on the rail causing even higher stress at the interface. The main intention here is therefore to determine the stress, deformation and shape of the contact patch under these operating conditions.

The contact mechanics is highly influenced by the following important factors [18]:

- Number of bodies under contact
- The geometry of the bodies
- The material property of the bodies
- Deformation mode of the bodies
- Contact force imposed between the bodies
- Type of relative motion between them (static, sliding, rolling)
- The velocity of the relative motion

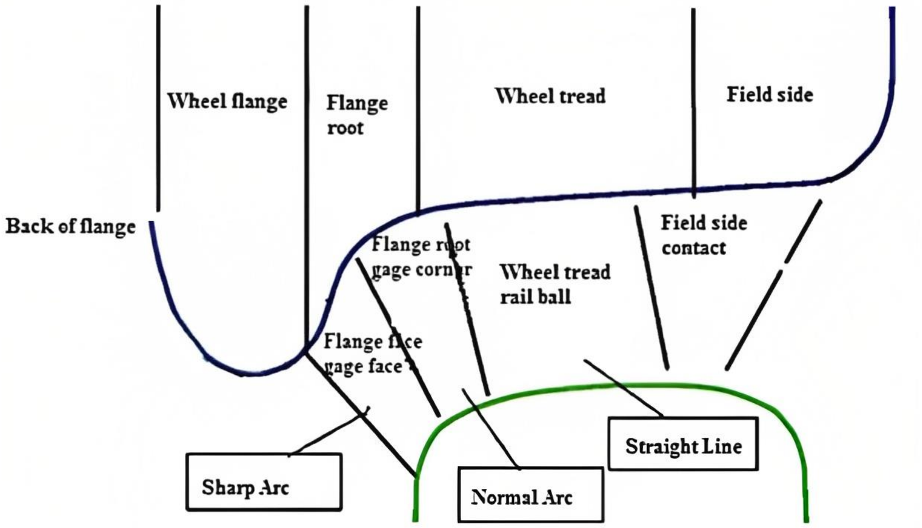

Figure 2.7-Contact surfaces description [19]

In general, there are two types of contact between wheel and rail, i.e., thread contact and flange contact, and a combination of them at some points. Thread contact denotes contact between the wheel and rail at the thread portion of the wheel and rail and Flange contact where the contact occurs in the flange section, as shown in the figure 2.7 above.

The general contact theory was developed by Hertz in 1882. Based on his fringes experiment; he proposed the contact area between two non-conformal bodies revolving on one another as elliptical shape and normal pressure distribution is taken to be semi-ellipsoid by taking the following assumptions during the process [18].

- Materials in contact are homogeneous and yield stress is not exceeded

- The effect of surface roughness is negligible
- The normal load causes contact stress to tangent contact plane/ no tangential force
- The contact area is very small compared to the whole dimension of the bodies

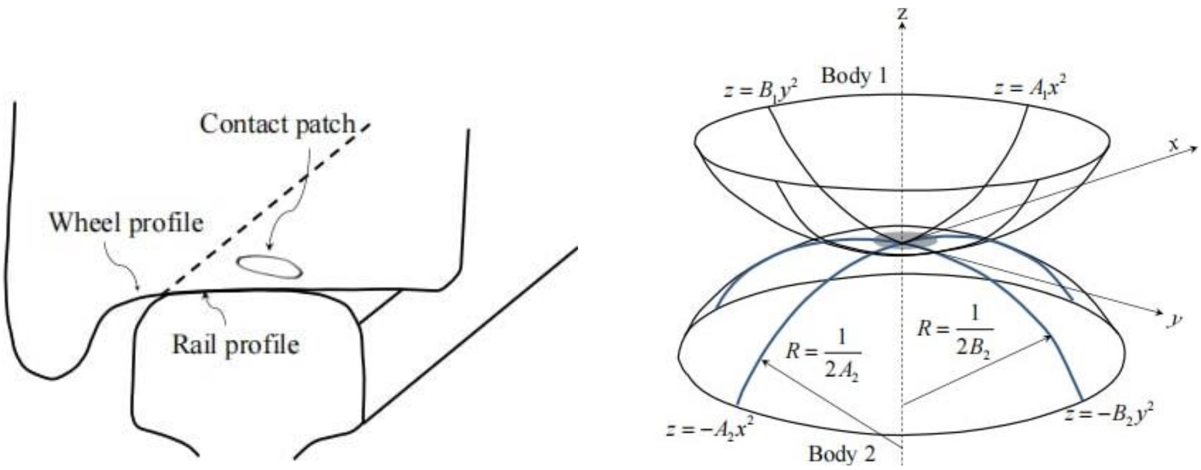

Figure 2.8-Contact patch representation [20]

In the following contact mechanics analysis's, R_w and R_r are the radius of curvature of wheel thread and rail head at the contact point, r is radius of wheel, N is the normal force acting on the contact area, a and b are the major and minor axis semi-lengths given by [21]:

$$(a/m)^3 = (b/n)^3 = 3N(1-v^2)/E(1/r + 1/R_r - 1/R_w) \quad \text{Eq 2.1}$$

$$\cos\beta = (1/r + 1/R_r - 1/R_w)/(1/r - 1/R_r + 1/R_w) \quad \text{Eq 2.2}$$

Where: E = Youngs modulus v = Poisson Ratio, m and n = hertzian parameters tabulated in terms of hertzian contact constant beta

Table 2.1-Hertzian contact coefficients (m and n) [21]

(^{0})	m	n	(^{0})	m	n
0		0	50	1.754	0.641
1	36.89	0.131	55	1.611	0.678
10	6.612	0.319	60	1.486	0.717
20	3.778	0.408	65	1.378	0.759
25	3.152	0.456	70	1.284	0.802
30	2.731	0.493	75	1.202	0.846
35	2.397	0.530	80	1.128	0.893
40	2.136	0.567	85	1.061	0.944
45	1.926	0.604	90	1.000	1.000

Using the above analysis, the value of the elliptical contact patch's major and minor axis length (2a and 2b) can be found. The maximum normal pressure and shear stress along the contact patch for Hertzian contact and railhead, respectively could also be found as follows:

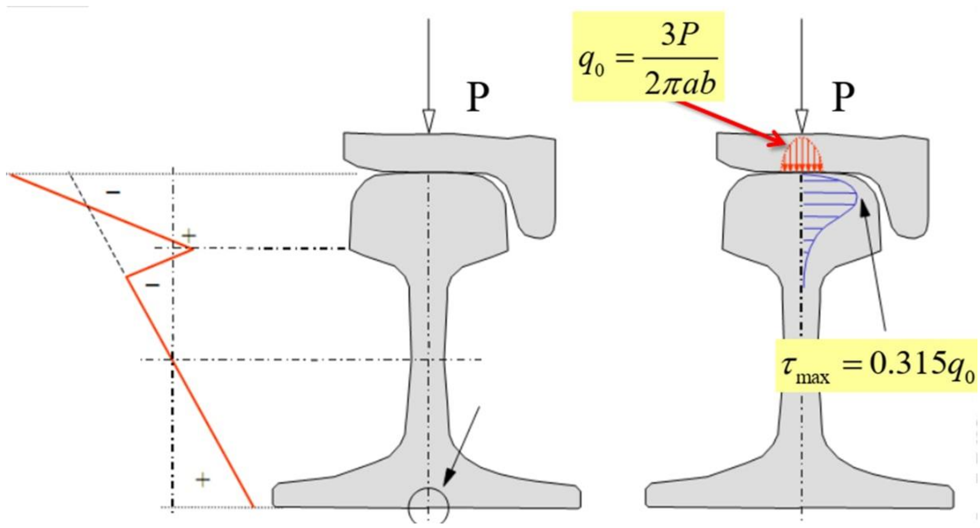

Figure 2.9-Maximum normal and shear pressure acting on the contact patch [21]

But the above assumptions don't always hold true, especially in contact conditions at rail gauge, wheel flange, and worn profile wheels. Many other non-Hertzian or modified Hertzian contact models are found in different literatures, which account for these factors in the contact mechanics.

When a longitudinal force is applied to wheels, a deviation from rolling motion occurs, i.e., slippage or Creepage. A deviation in relative velocity in the longitudinal direction between the wheel and rail concerning the forward speed is called longitudinal creepage. On the other hand, Lateral creepage is the incremental relative lateral velocity concerning wheel and rail about the forward speed. Finally, spin is the relative angular motion between the wheel and rail about the normal contact axis. Mathematically, these are expressed as [21]:

$$\gamma_1 = \frac{(V_x^w - V_x^r)}{V} \qquad \gamma_2 = \frac{(V_y^w - V_y^r)}{V} \qquad \omega_3 = \frac{(\Omega_z^w - \Omega_z^r)}{V} \qquad \text{Eq 2.3}$$

Where: γ_1 = Longitudinal creepage, γ_2 = Lateral creepage, ω_3 = Spin creepage, and V and Ω represent translational and angular velocities of wheel or rail (w or r as superscript).

For the small value of creepages and spin, adhesion prevails along the whole contact patch. As shown in the following expressions, creep forces have a linear relationship with creepage.

$$T_1 = -f_{11}\gamma_1 \qquad T_2 = -f_{22}\gamma_2 - f_{23}\omega_3 \qquad M_3 = f_{23}\gamma_2 - f_{33}\omega_3 \qquad \text{Eq 2.4}$$

Where: T_1, T_2 and M_3 are longitudinal, lateral and spin creep forces, respectively

The constants f_{ij} were analyzed by Kalker as follows:

$$f_{11} = Gc^2C_{11} \qquad f_{22} = Gc^2C_{22} \qquad f_{23} = Gc^3C_{23} \qquad \text{Eq 2.5}$$

Where: c^2 = ab, and G = Elastic modulus of rigidity and C_{ij} can be found from Appendix 3. Taking f_{11} and f_{22} as equal is a useful approximation during analysis [21]. For an arbitrary creepage condition, Kalker provided a faster approach in the computer program known as FASTSIM and if flexibility in the contact area is to be isotropic, the following relations is a rearrangement of the f_{ij} factors for the small creepage case.

$$f_1 = 8a/3C_{11}G \qquad f_2 = 8a/3C_{22}G \qquad f_3 = \pi a\sqrt{a/b}/4C_{23}G \qquad \text{Eq 2.6}$$

For other complex non-Hertzian contact mechanics conditions, different researchers proposed other methodologies to analyze the real scenario under consideration. For example, a faster and more reliable method of contact calculation was proposed in [22] and [23] based on semi-elliptical pressure distribution in the direction of rolling and curved contact surface approaches, respectively.

Considering the vehicle dynamics of the wheelsets and wheel-rail geometry, the velocity components of the wheels are given by [21]:

Wheel Related		Rail related	
$V_{1l}{}^{w} = \Omega r_l + l\dot{\psi}$	Eq 2.7	$V_{1r}{}^{r} = -V\left(1 - \frac{l}{R_0}\right)$	Eq 2.8
$V_{2r}{}^{w} = \left(\dot{u}_y^* + \Omega r_r \psi\right)\sec\delta_r$	Eq 2.9	$V_{1l}^{r} = -V\left(l + \frac{l}{R_0}\right)$	Eq 2.10
$V_{2l}{}^{w} = \left(\dot{u}_y^* + \Omega r_l \psi\right)\sec\delta_l$	Eq 2.11	$V_{2r}^{r} = 0, V_{2l}{}^{r} = 0$	Eq 2.12
$\Omega_{3r}{}^{w} = \Omega\sin\delta_r + \dot{\psi}\cos\delta_r$	Eq 2.13	$\Omega_{3r}^{r} = -\frac{V\cos\delta_r}{R_0}$	Eq 2.14
$\Omega_{3l}{}^{w} = -\Omega\sin\delta_l + \dot{\psi}\cos\delta_l$	Eq 2.15	$\Omega_{3l}^{r} = -\frac{V\cos\delta_l}{R_0}$	Eq 2.16

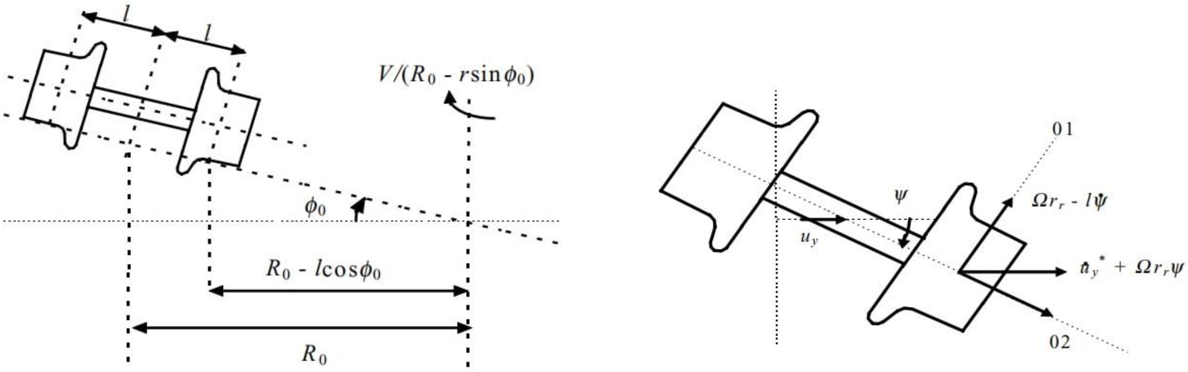

Figure 2.10-Velocity components of wheel and wheelsets [21]

Based on this analysis as the previous case of a single wheel, the wheelset creep forces and creepages for small creepage are calculated as:

Creepage		Creep Forces	
$\gamma_{1r} = \frac{\Omega r_r}{V} + 1 - \frac{l\dot{\psi}}{V} - \frac{l}{R_0}$	Eq 2.17	$T_{xr} = T_{lr}$	Eq 2.18
$\gamma_{1l} = \frac{\Omega r_l}{V} + 1 + \frac{l\dot{\psi}}{V} + \frac{l}{R_0}$	Eq 2.19	$T_{yr} = T_{2r}\cos\delta_r + T_{3r}\sin\delta_r$	Eq 2.20
$\gamma_{2r} = \left(\dot{u}_y^* + \Omega r_r \psi\right)\frac{\sec\delta_l}{V}$	Eq 21	$T_{zr} = T_{3r}\cos\delta_r - T_{2r}\sin\delta_r$	Eq 2.22
$\gamma_{2l} = \left(\dot{u}_y^* + \Omega r_l \psi\right)\frac{\sec\delta_l}{V}$	Eq 2.23	$T_{xl} = T_{ll}$	Eq 2.24
$\omega_{3r} = (\frac{\Omega}{V})\sin\delta_r + (\frac{\dot{\psi}}{V})\cos\delta_r + \frac{\cos\delta_r}{R_0}$	Eq 2.25	$T_{yl} = T_{2l}\cos\delta_l - T_{3l}\sin\delta_l$	Eq 2.26
$\omega_{3l} = -(\frac{\Omega}{V})\sin\delta_l + (\frac{\dot{\psi}}{V})\cos\delta_l + \frac{\cos\delta_l}{R_0}$	Eq 2.27	$T_{zl} = T_{3l}\cos\delta_l + T_{2l}\sin\delta_l$	Eq 2.28

The final resultant creep forces are found by the following relation based on summation of forces along the direction of application of forces:

$$T_x = T_{xr} + T_{xl} \qquad \text{Eq 2.29}$$

$$T_y = T_{yr} + T_{yl} \qquad \text{Eq 2.30}$$

$$T_z = T_{zr} + T_{zl} \qquad \text{Eq 2.31}$$

$$M_x = T_{zr}l - T_{zl}l - T_{yr}r_r - T_{yl}r_l \qquad \text{Eq 2.32}$$

$$M_y = \left(T_{xr} + T_{yr}\psi - T_{zr}\psi\tan\delta_r\right)r_r + \left(T_{xl} + T_{yl}\psi + T_{zl}\psi\tan\delta_l\right)r_l \qquad \text{Eq 2.33}$$

$$M_z = T_{xl}l - T_{xy}l \qquad \text{Eq 2.34}$$

2.3. Vehicle Dynamics

2.3.1. Longitudinal Dynamics

The longitudinal dynamic behavior is expressed in terms of combination of differential equations by considering each wagon (MC_1, MC_2 and TP) as a single mass connected by couplers.

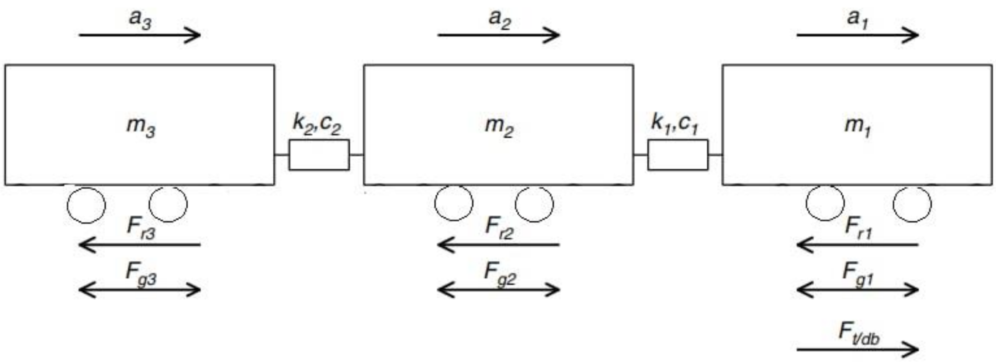

Figure 2.11-Longitudinal dynamics of AALRT Train [24]

The longitudinal equation of motion for the ith wagon is given by:

$$m_i a_i + c_{i-1}(v_i - v_{i-1}) + c_i(v_i - v_{i+1}) + k_{i-1}(x_i - x_{i-1}) + k_i(x_i - x_{i+1}) = F_{\mathrm{t/db}i} - F_{\mathrm{r}i} - F_{\mathrm{g}i} \quad \text{Eq 2.35}$$

Where, m_i = mass, a_i = acceleration, v_i = speed, x_i = distance travel, C_i = coupler damping of ith wagon, $F_{t/db}$ = force from locomotive (tractive and braking), F_r = sum of resistances including propulsion, curve, and braking related resistances and F_g= gravitational force due to grade difference.

Since we don't have a locomotive in our case, the $F_{t/db}$ is power supplied for each motored bogie (MC) and zero for TP, while the rest of them will be accounted based on the conditions. Once the system of equation is arranged in the above way, they are collected in terms of the following expression for convenience of calculation.

$$\mathrm{M}\frac{\mathrm{d}^2\mathrm{X(t)}}{\mathrm{dt}^2} + \mathrm{C}\frac{\mathrm{dX(t)}}{\mathrm{dt}} + \mathrm{KX(t)} = \mathrm{f(t)} \quad \text{In time domain}$$

$$\mathrm{MS}^2 + \mathrm{CS} + \mathrm{K} = \frac{\mathrm{F(S)}}{\mathrm{X(S)}} \quad \text{In frequency domain}$$

Analyzing the above equation in a numerical analysis algorithm, state-space method, or other ODE analysis methods will give the system variables of the longitudinal dynamic behavior of each component.

2.3.2. Lateral Dynamics

Considering the lateral dynamics, we have the lateral distance expressed in terms of the conicity and radius of curvature as:

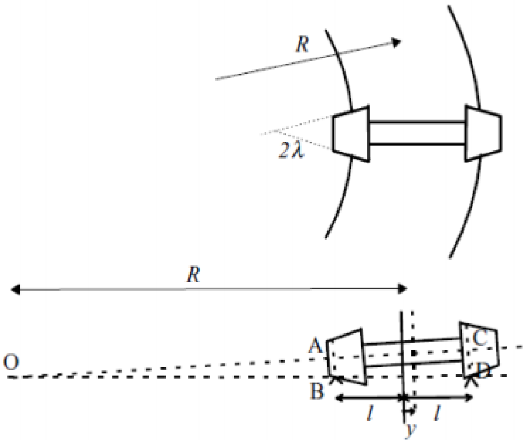

$$\mathrm{OAB} = \mathrm{OCD}$$

$$(r_0 - \lambda y)/(R - l) = (r_0 + \lambda y)/(R + l)$$

$$y = r_0 l / R\lambda$$

Figure 2.12-Lateral position of wheelset [24]

By taking the components contributing to the lateral motion of the wheelset, assuming a small stiffnes of lateral and yaw springs with small displacement and conicity and using summation of forces and yaw torque in the lateral direction with final simplification gives us the following governing equation for the lateral motion of the wheelset.

$$m\ddot{y} + \frac{2f_{22}\dot{y}}{V} + K_y y - 2f_{22}\psi + \left(\frac{2f_{23}}{V} - \frac{I_y \kappa V}{r_0 l}\right)\dot{\psi} = Q_y \qquad \text{Eq 2.36}$$

$$I_z\ddot{\psi} + \frac{2f_{11}\lambda_0 l y}{r_0} - \left(\frac{2f_{23}}{V} - \frac{I_y \delta_0 V}{r_0}\right)\dot{y} + 2f_{11} l^2 \frac{\dot{\psi}}{V} + K_\psi \psi = Q_\psi \qquad \text{Eq 2.37}$$

Where:

$$Q_y = -\frac{mV^2}{R_o} + mg\phi_0 + \frac{\delta_0 I_y V^2}{R_0 r_o} + 2f_{23}/R_0 \qquad \text{Eq 2.38}$$

$$K_y = k_y + \left(\frac{2N_0\varepsilon_0^*}{l}\right)\left(1 - \frac{f_{23}}{N_0 r_0}\right) \qquad \text{Eq 2.39}$$

$$Q_\psi = \frac{I_y V \dot{\phi}_0}{r_0} - I_z V \frac{d}{dt} R_0 - \frac{2f_{11} l^2}{R_0} \qquad \text{Eq 2.40}$$

$$K_\psi = k_\psi + 2N_0 l(-\delta_0 + f_{23}/N_0 l) \qquad \text{Eq 2.41}$$

$$\varepsilon_0^* = l\left(1 + \frac{R_r\delta_0}{l}\right)/(R_w - R_r)\left(1 - \frac{r_0\delta_0}{l}\right) \qquad \text{Eq 2.42}$$

Solving the above equation in the appropriate numerical tool gives the necessary system variables to define the lateral motion of the wheelset.

2.3.3. Vertical Dynamics

In the vertical dynamic analysis, the important factors to consider are suspensions (primary and secondary), masses, springs, and dampers, irregularities of rails and external forces applied on them. First the system is modeled as a spring, mass and damper system as shown below.

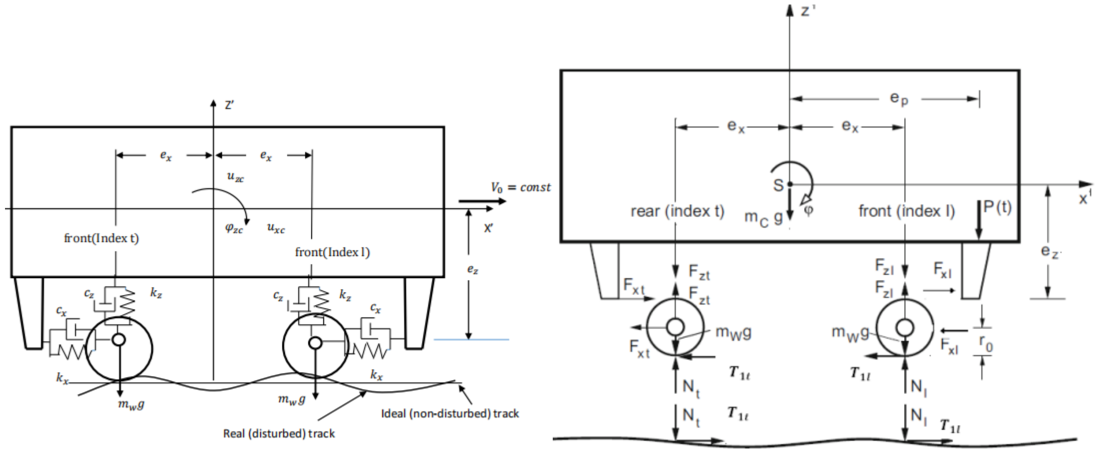

Figure 2.13-Free body model of Train using spring, mass, and damper system [24]

Based on the free body diagram, the equilibrium of forces on the Car body and the two wheels is done, and the equation of motion extracted by applying the sum of force and moment on each body and making the necessary arrangements gives the following general expression, which can be solved using state space, Eigenvalue, numerical method or other ODE solving methods to get the system variables.

$$\mathrm{M}\frac{\mathrm{d}^2\mathrm{X(t)}}{\mathrm{dt}^2} + \mathrm{C}\frac{\mathrm{dX(t)}}{\mathrm{dt}} + \mathrm{KX(t)} = \mathrm{F} \qquad \text{Eq 2.43}$$

Where:

$$M = \begin{bmatrix} m_{cb} & 0 & 0 & 0 & 0 \\ 0 & m_{cb} & 0 & 0 & 0 \\ 0 & 0 & I_{cb} & 0 & 0 \\ 0 & 0 & 0 & m_w + \frac{I_w}{r_0^2} & 0 \\ 0 & 0 & 0 & m_w + \frac{I_w}{r_0^2} & \end{bmatrix}, \quad C = \begin{bmatrix} 2c_x & 0 & -2c_x e_z - c_x & -c_x & \\ 0 & 2c_z & 0 & 0 & \\ -2c_x e_z & 0 & 2c_x e_z^2 + 2c_z e_x^2 & c_x e_z & c_x e_z \\ -c_x & 0 & c_x e_z & c_x & 0 \\ -c_x & 0 & c_x e_z & 0 & c_x \end{bmatrix}, X = \begin{Bmatrix} u_{xcb} \\ u_{zcb} \\ \varphi \\ u_{xl} \\ u_{xt} \end{Bmatrix},$$

$$K = \begin{bmatrix} 2k_x & 0 & & -2k_x e_z & -k_x & -k_x \\ 0 & 2k_z & 0 & 0 & 0 & \\ -2k_x e_z & 0 & 2k_x e_z^2 + 2k_z e_x^2 & k_x e_z & k_x e_z & \\ -k_x & 0 & k_x e_z & k_x & 0 & \\ -k_x & 0 & 0 & k_x e_z & 0 & k_x \end{bmatrix} F = \begin{Bmatrix} 0 \\ m_{cb}g - P(t) + k_z(z_l + z_t) + c_z(\dot{z}_l + \dot{z}_t) \\ P(t)e_p - k_z e_x(z_l - z_t) - c_z e_x(\dot{z}_l - \dot{z}_t) \\ 0 \\ 0 \end{Bmatrix}$$

2.4. Wear Modeling and Prediction

Prediction of wear due to wheel-rail interaction is important since it affects the running stability, safety, and comfort of passengers and freight being transported by rolling stocks. The most practical method used to construct the wheel wear profile of a given rail vehicle is through experimental data collection, which is time and finance intensive and tedious process. But there are acceptable alternatives using multi-body simulation software-based solutions accompanied by consecutive updating of the wear profile with a programming tool, though their efficiency shall be validated through an experiment or actual wear data. The wheel geometry is then adjusted and fed back to the MBS software so that a step-wise analysis is performed until the analysis limit distance is reached for the wheel.

The below Figure shows the schematic of the overall wearing process modeling and re-profiling operation of a generic railway wheel. The initial new wheel is primarily subjected to creepage and forces due to wheel-rail contact leading to wearing, where a wear model is prepared and predict new profile using software programming. This profile is then fed back to the vehicle dynamic model, and the cycle continues until a final distance for minimum wheel geometric constraint is reached.

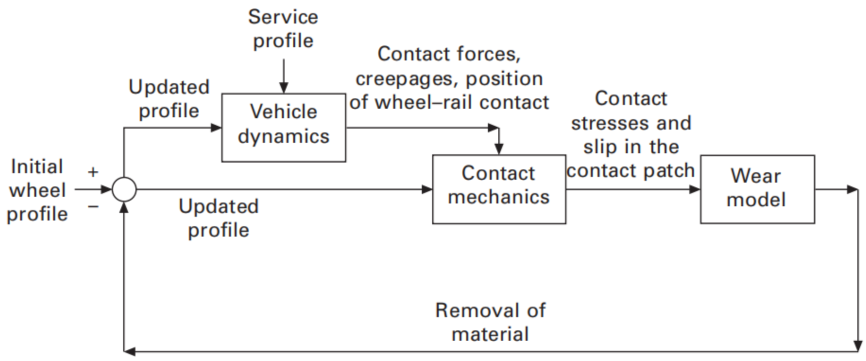

Figure 2.14-Schematics for re-profiling grinding operation of wheel profile [12]

2.4.1. Arcard wear Model

Predicting the wear using models is important to establish theories to quantify the material loss. One of the most used equations to quantify wear is the Arcard wear model, as proposed by Holm and Arcard in 1953 [25]. The model assumes a full plastic deformation of spherical asperities in adhesive wear conditions. As a result of this assumption, the contact patch is a circle of area equal to πa^2 with a radius of "a". The volume wear **(V_t)** for total travel distances' is given by: [25]

$$V_t = kPS/H \qquad \text{Eq 2.44}$$

Where: k = K/s, K = probability of hemispherical debris formation, P = normal load, H = hardness of the softer material.

Differentiating the above equation also gives us:

$$\frac{dV_t}{dt} = \frac{\frac{kP_c}{H}dS}{dt} = \frac{kPv}{H} \qquad \text{Eq 2.45}$$

Where: v = sliding speed, this expression can be used to calculate wear rate locally.

To find the right value of Archard wear coefficient (k), the following chart shall be used depending on the wear regime under consideration. Since this is for a dry case, some scaling factors shall be applied to get the real scenario during analysis that accounts for environmental, lubrication, and other factors.

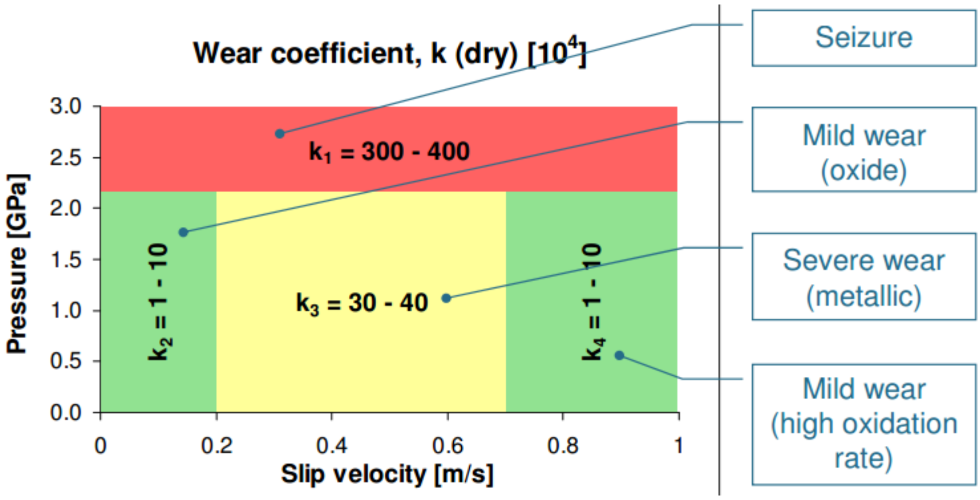

Figure 2.15-Archard wear Coefficient chart [15]

The slip speed is the important parameter here used to obtain the slip distance and is calculated as [26]:

$$v_{\text{slip}} = v_{\text{vehicle}}\left[(v_\xi - \phi\eta, v_\eta + \phi\xi) - \frac{\partial}{\partial\xi}(u_\xi, u_\eta)\right] \qquad \text{Eq 2.46}$$

Where: ξ, η = local contact surface coordinates, v_ξ, v_η, ϕ = local longitudinal, lateral, and spin creepages and (u_ξ, u_η) = elastic displacement vector of the contact surface.

By dividing volume wear (V_t) with contact surface area, we get wear depth **(h)** as:

$$h = V_t/A = kP_cS/H \qquad \text{Eq 2.47}$$

Where: P/A = P_c = local contact pressure.

From other accepted methodologies, the quantity proportional to wear is the wear index and the most conventional method to calculate it is the Derby wear index method which assumes proportionality of wear with work done at the wheel-rail contact. These use the longitudinal, lateral creepage and creep forces dot product sum to obtain the Tγ so that the wear index could be computed.

$$WI = K\,(T_1\gamma_1 + T_2\gamma_2) \qquad \text{Eq 2.48}$$

Once this value is determined, the wear regime could be determined as mild, severe or catastrophic based on where it lies on the wear map for the specific wheel and rail material on twin-disc testing carried out in early research.

2.4.2. USFD Wear Model

The USFD wear model is proposed based on the weight loss of material per distance rolled per contact area, which is proportional to the total Tγ. The relation for wear rate (K) is expressed as follows [27]:

$$K\,(wear\ rate) = K_w \frac{T_\gamma}{A} \qquad \text{Eq 2.49}$$

Where: K_w = empirical wear constant depending on materials in contact, A = contact area.

The wear map of the wear model based on the Tγ Vs K will then be plotted based on the experimental output of twin-disc analysis for the specific wheel and rail materials. According to Braghin [28], the wear rate has its own regimes based on the value of Tγ/A as shown in the Figure below. The expression used to construct these wear regimes is as follows:

$$K\,(\mu g/m/mm) = \begin{array}{l} \frac{5.3\mathrm{T\gamma}}{\mathrm{A}} \ldots for\ \frac{\mathrm{T\gamma}}{\mathrm{A}} < 10.4 \\ 55 \ldots for\ 10.4 < \frac{\mathrm{T\gamma}}{\mathrm{A}} < 77.2 \\ \frac{61.9\mathrm{T\gamma}}{\mathrm{A}} \ldots for\ 77.2 < \mathrm{T\gamma/A} \end{array} \qquad \text{Eq 2.50}$$

Where: A = area of contact patch (m^2)

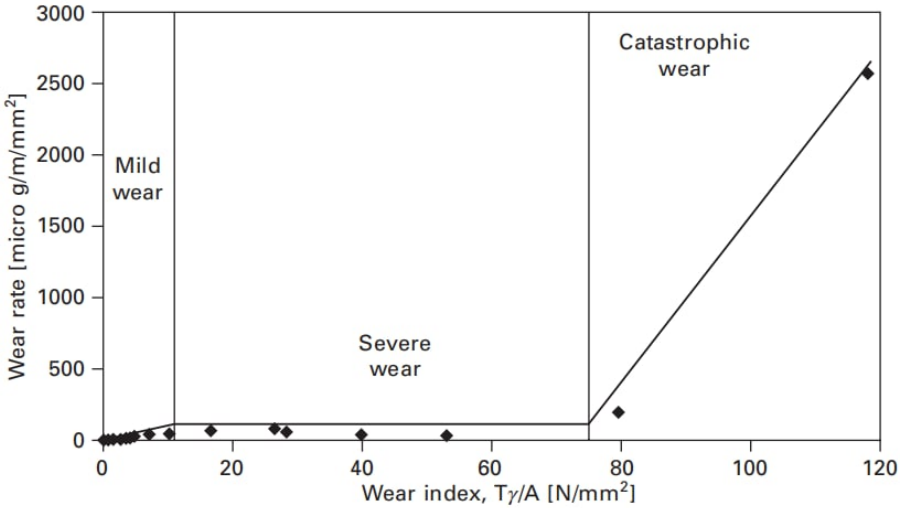

Figure 2.16-Sample wear rate and regime for R8T wheel and UIC60 rail material [12]

The incremental wear depth is also calculated considering wear occurring at a given time instant and at a particular wheel transversal and longitudinal position and spread over the whole circumference of the wheel according to the ratio between the real travelled distance (vΔt) and the length of the circumference (2πR), Δt being the time interval between subsequent integration steps and R the rolling radius of the wheel [28].

$$\delta(x,y) = K\left(\frac{T\gamma}{A}\right)\frac{v\Delta t}{\rho}\frac{v\Delta t}{2\pi R} \qquad \text{Eq 2.51}$$

Where: δ(x,y) = incremental wear depth at cell coordinate (x,y) (mm).

2.5. Wear profile updating and smoothing

To do a wear analysis and profile updating, using data extracted from Simpack is inconvenient as it is bulky. Instead, researchers used sample length in the simulation process. But care shall be taken to elongate the sample length as much as possible so as it gives fewer sampling distances for the whole route, but not long enough to reduce the precision of the calculation. Based on this assumption, [26] took a wheel revolution ($L_{sample}=2\pi R_{nom}$ = 4.15m) of sampling length being enough for analysis with the best percision to be found. The number of sample elements is then calculated as:

$$n_i = \frac{L_i}{L_{sample}} \qquad \text{Eq 2.52}$$

Where: L_i= Length of the type curve i

The wear generated on wheel, *j* from a type *I*, *Wj,I* on a single wear step is then given as the sum of the corresponding samples given by [26]:

$$w_{j,i}(y) = \sum_{k=1}^{n_i} w_{j,k}(y) \quad \text{Eq 2.53}$$

Next, all the wear in each type curve is weighted according to the whole network as follows [26]:

$$w_{w,m}(y) = \left(w_{1,i}(y), w_{2,i}(y), \dots, w_{J,i}(y)\right) \cdot \begin{pmatrix} L_{tot,1}/L_{tot,nw} \\ L_{tot,2}/L_{tot,nw} \\ L_{tot,I}/L_{tot,nw} \end{pmatrix} \quad \text{Eq 2.54}$$

$$L_{tot,m} = (L_1, L_2, \dots, L_I) \cdot \begin{pmatrix} L_{tot,1}/L_{tot,nw} \\ L_{tot,2}/L_{tot,nw} \\ \dots \\ L_{tot,I}/L_{tot,nw} \end{pmatrix} \quad \text{Eq 2.55}$$

Where: $w_{w,(y)}$ = weighted wear, *w* means weighted and *m* means wear step, *J* = the total number of wheels on the simulated car, *I* = the total type curve number, $L_{tot,i}$ = the tack length that a certain type curve, and $L_{tot,n}$ = the total network length after considering the traffic condition?

But during the analysis, the maximum allowable wear depth and maximum running distance in each step are limited to 0.1x10^{-3}m and 1500km to avoid few executions of the multi-body system that results in a large variation of contact points with the real situation when wear depth is large [26]. Based on this, the wear depth and running distance are scaled up or down depending on their calculated value to a different value of *y* as follows [26]:

$$w_{\text{wearstep },m}(y) = \frac{0.1\times10^{-3}}{max(w_{w,m}(y))} w_{w,m}(y) \quad \text{Eq 2.56}$$

$$L_{\text{wearstep },m} = \frac{0.1\times10^{-3}}{max(w_{w,m}(y))} L_{\text{tot },m} \quad \text{Eq 2.57}$$

Based on this new wear step value the new updated locations of the worn profile are given by [26]:

$$y_{\text{update}} = y + w_{\text{wearstep },m}(y)\sin\Gamma(y) \quad \text{Eq 2.58}$$

$$z_{\text{update}} = z + w_{\text{wearstep },m}(y)\cos\Gamma(y) \quad \text{Eq 2.59}$$

Where: $(\boldsymbol{y})$ = profile angle along the wheel profile. $\boldsymbol{y_{update}}, \boldsymbol{z_{updat}}$ = new coordinate for each point on the wheel profile after updating. For these research on the otherhand, profile updation is done in simpack itself by deducting the weardepth at sampling points from the original wheel profile and curve smoothning before importing to the next round of calculation.

2.6. Track Irregularities

Track irregularities are deviations from the original geometry of the track. They are the main continuous ground-based excitations regarding railway operation, resulting in a dynamic effect that shall be mitigated. Especially in high-speed train operation, such small irregularities could result in a high probability of response, resulting in catastrophic accidents due to derailment. This means a track that kept the predefined track layout for longer is said to have good ride quality, i.e., less irregularities.

According to Karis T. [29], there are four main types of track irregularities in general. These are:

- **Longitudinal level irregularities** exist in the vertical (z-axis) direction and are defined as the mean value of both rails' vertical deviation from their nominal vertical position.
- **Alignment irregularities**: found in the lateral (y-axis) direction, defined as their deviation from the nominal track center.
- **Cant irregularities**: the unintentional rotation of a track around its longitudinal axis and expressed as the difference in height between the two rails.
- **Gauge irregularities**: the smallest deviation from the track gauge between the inside of the two rails, usually measured 14mm below the running surface.

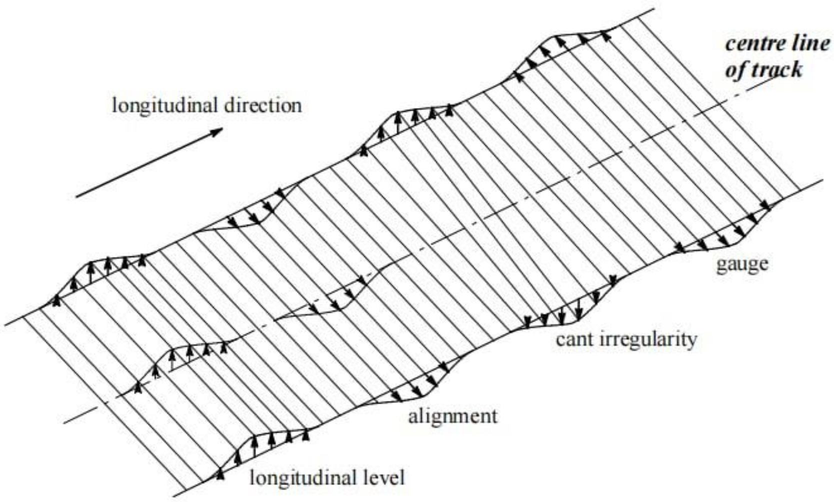

Figure 2.17-Four types of track irregularities [29]

The above track-related track irregularities are equivalent to the lateral and vertical rail irregularities [29] and can be used interchangeably.

Track irregularities are usually measured using vehicles equipped with inertia-based measurement devices, i.e., Accelerometers, gyroscopes, and laser recording devices. Some railway operators place accelerometers in the axle box of rail car's so that they can measure the estimated irregularities of the track, which can be used for a condition-based track maintenance process [29]. Track irregularities affect the vehicle dynamic response by altering the contact mechanics existing on the contact patch and imposing unexpected paths for the wheels so that they won't follow the predefined path. This affects the creepage and creep forces between the wheel and rail, resulting in unwanted vibration, wear, and fatigue on the wheel and rail material. There effect is usually measured in wheel-rail forces, and acceleration is felt vertically and laterally.

2.7. Stability and Safety

2.7.1. Nadal's Formula for Safety Criteria

The derailment of wheels from the rail is one of the most devastating failures that could occur in a railway system yet sometimes deliberate derailer tools are used for safety during accidents or protection during construction. Derailment is a process by which the lateral force imposed on the wheel pushes it against the rail at the contact patch, raising the wheel above the rail gauge, resulting in wheel climbing and further wheel derailment. To avoid this phenomenon, safety criteria are put to quantify the possible limit to derailment. These include Weinstock axle-sum L/V criteria, High-speed passenger limit criteria (US), L/V time duration criterion (Japan), and Nadal's single-wheel L/V limit criterion [24]. From the above, Nadal and Weinstock criteria are related to L/V ratio limits, while the rest are related to the time and distance exceeding limits of L/V. The Nadal's safety criterion is proposed for French railways based on a subsequent flange contact due to excess lateral force and it is expressed as follows.

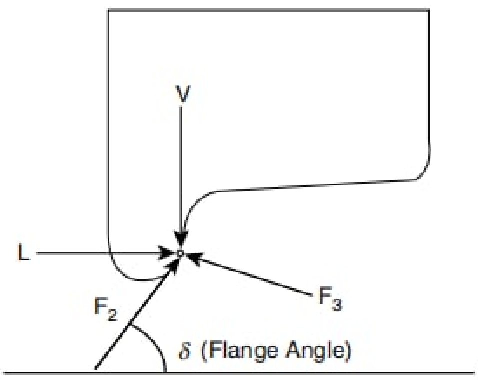

Figure 2.18-Vertical and lateral force application at contact patch [24]

$$\frac{L}{V} = \frac{\tan\delta - \mu}{1 + \mu\tan\delta} \qquad \text{Eq 60}$$

Where: L = Lateral force, V = Vertical force, μ = friction coefficient and δ = flange angle

According to the safety criteria, the value L/V shall not exceed value of 0.8 for avoiding wheel climbing during operation of the trains.

2.7.2. Comfort

For general comfort conditions according to the UIC approach takes the following expression for ride quality computation [24]:

$$N_{\mathrm{MV}} = 6\sqrt{(a_{\mathrm{XP}})^2 + (a_{\mathrm{YP}})^2 + (a_{\mathrm{ZP}})^2} \qquad \text{Eq 61}$$

Where: N_{MV} = Ride Quality, a_{xp} = acceleration in the longitudinal direction, a_{yp} = acceleration in the lateral direction, a_{zp} = acceleration in the vertical direction.

The maximum peak acceleration that can be achieved in all directions is estimated at 0.3g = 2.943m/s^2 by taking 30% adhesion contact at most [24]. Further, for N<1 = very comfortable, 1<N<2 = Comfortable, 2<N<4 = medium comfort, 4<N<5 = Uncomfortable, and N>5 = Very uncomfortable conditions limiting conditions exist. Thes value is refered as ride index in the following SIMPACK analysis and the best comfort condition, it shall be taken below 2 based on above analysis.

2.8. Additional Published literatures

Most of the researchs done around this topic constitut the following four main components of the overall system modeling under condideration, i.e., Vehicle Dynamic Model, Wheel-rail interaction model, wear model and finally, a validation system for confirmation of the results.

Pradhan [20] stated that most previous papers didn't address the plastic deformation of contact patch during contact, whether the contact pattern was elliptical or non-elliptical. Also, the lab tests on wheelsets failed to replicate the real scenario of varying loads, creepages, and vehicle dynamic effects. On the other hand, he also tried to address this by considering the real track layout of the Indian railway by using ADAMS VI MBS software with MATLAB a wear re-profiling tool. A semi-hertzian/STRIP approach and modified kalker's FASTSIM approach were used to calculate the normal and tangential contact stresses, respectively.

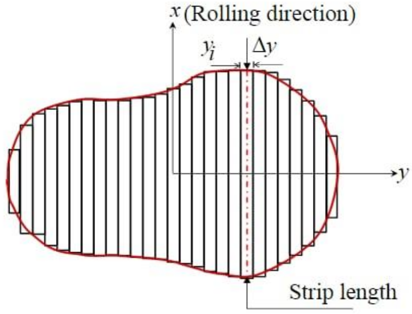

Figure 2.19-Discretized Strip of contact patch [20]

Based on the analysis done in the research, the wheel re-profiling schedule and the total life of wheels were obtained for Indian network trains. The influence of wheel wear on vehicle dynamic response due to curve performance, critical speed, and ride comfort was also justified.

Tao [14] mentioned that direct wear data collection is a time-consuming process, even though reliable. Instead, a field-measured wheel profiles of high-speed train on the Wuhan-Guangzhou high-speed railway line was used to modify the USFD wear function. SIMPACK was used as multibody analysis software with Hertzian and FaStrip methods to calculate normal and tangential forces and the USFD wear model used for material removal calculation.

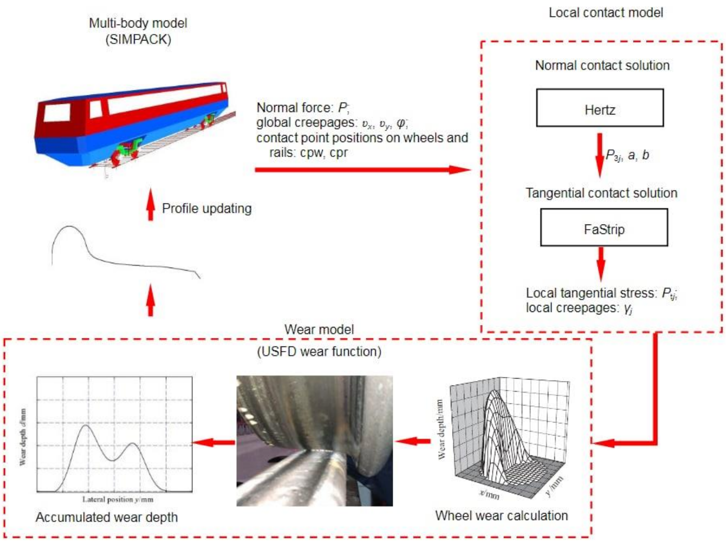

Figure 2.20-Wheel wear prediction model used [14]

Based on the validation wear data of the CRH3 train, the simulated data were in good agreement as the results show wear spreading in the range from -25mm to 25mm relative to the nominal rolling circle of the wheels, as shown in the figure 2.21 below.

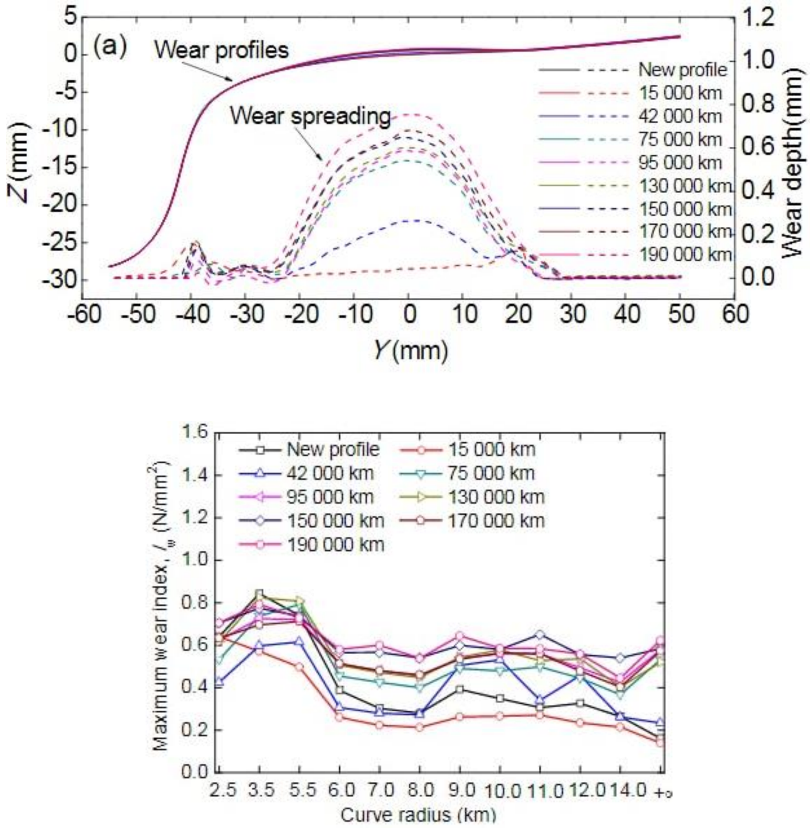

Figure 2.21-(a) Measured wheel profiles and wear spread with respect to millage (b) maximum wear index based on different curve radiuses [14]

On the other hand, Boyang et al. [30] stated most of the researchers used offline mode of calculation to evaluate wear and rolling contact fatigue. Gap of fewer studies showing the difference between the outputs of the two major wear models, i.e., Arcard and USFD in accordance with the fast non-Hertzian methods was also identified. To address this, four non-Hertzian wheel-rail contact models, i.e., kik-Piotrowskis, Linder's, Ayarechollet's stips algorithm and ANAYLN algorithm, for normal contact and FASTSIM and FaStrip were used for tangential contact modeling. Finally, Kalker's CONTACT code was used to validate the results of the fast non-Hertzian method. Results show that ANALYN + FaStrip was found to be the best model for Arcard wear model of wheel-rail rolling contact model. Also, STRIPS + FASTSIM provides the best accuracy for maximum wear depth prediction for USFD wear model**.**

Yunguang et al. [31] considered the yaw effect in the wear prediction of wheels, which is inevitable when trains pass along small curvatures.

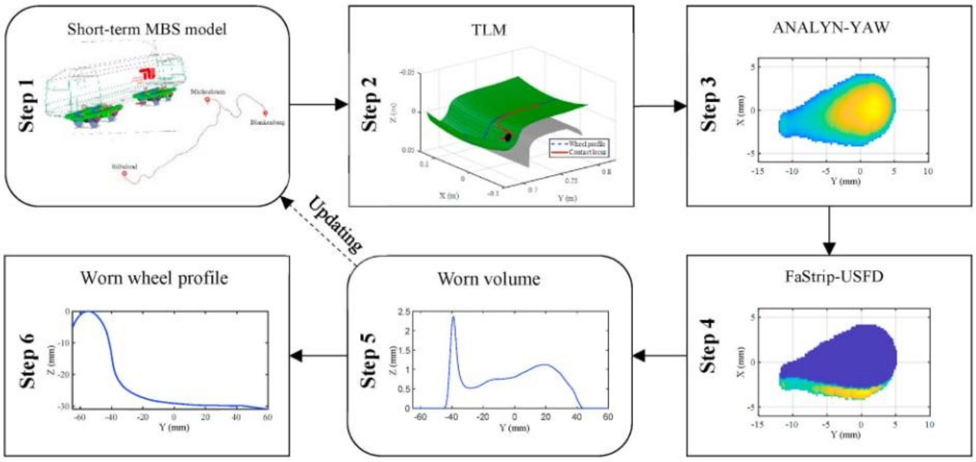

Figure 2.22-Process followed in the analysis and wheel profile updating [31]

As a result, field test validated the ANALYN – YAW – FaStrip adjusted wheel wear prediction model was more plausible than the models avoiding Yaw or standard Hertzian-FaStrip adjusted USFD method, which was adopted by prior researches.

Auciello [32] used experimental data validation by the ALSTOM ALn 501 ‘Minuetto’ train in Italy by selecting an appropriate step size for updating the wheel geometry for simulation, as it is an important aspect of the wear prediction process. SIMPACK was used as multibody modelling software, and MATLAB was used in wear modeling with Hertzian and Kalker’s contact models for normal and tangential contact models.

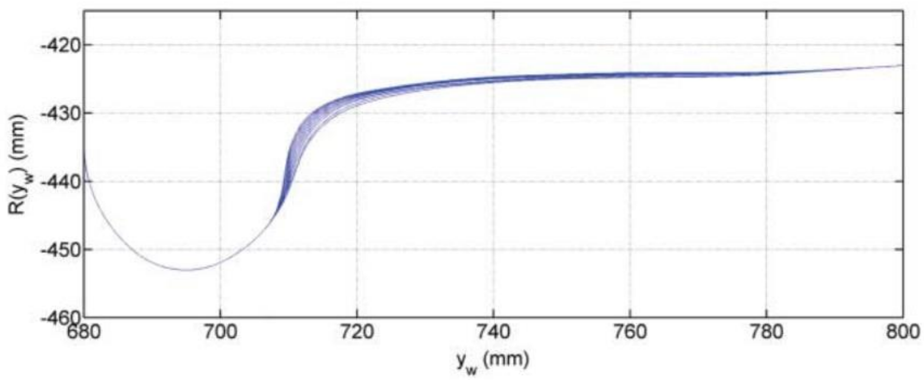

Figure 2.23-Evolution of wear on wheel profile [32]

The created model was afterwards tested against experimental data and found to accurately and closely match the data.Since most previous literature were done -based on experiment, Pombo [33] presented and compared three wear function model functions, i.e., British rail research (BRR), KTH (Arcard-based), and USFD models, and comparison between global and local models for wheel-rail contact to determine the wheel profile concerning the run distance. The equations used to find the wear rate in the three wear models are given as follows.

Equation for KTH (Arcard) wear model:

$$V_{\text{worn}} = K_A \frac{N \cdot d}{H} \quad \text{Eq 62}$$

Equation for USFD wear model:

$$\text{Wear rate} = K \frac{T\gamma}{A} \quad \text{Eq 63}$$

Table 2.2-BRR wear model equations

Wear Regime	Wear index Tγ (N)	Area of material Loss on profile (mm^2)
Mild	Tγ<100	0.25 Tγ/D
Sever	100≤ Tγ<200	25/D
Catastrophic	Tγ≥200	(1.19 Tγ-154)/D

VAMPIRE was used as an MBS tool, with MATLAB as a wear modeling tool. The analysis results were found to be in good agreement with the experimental results.

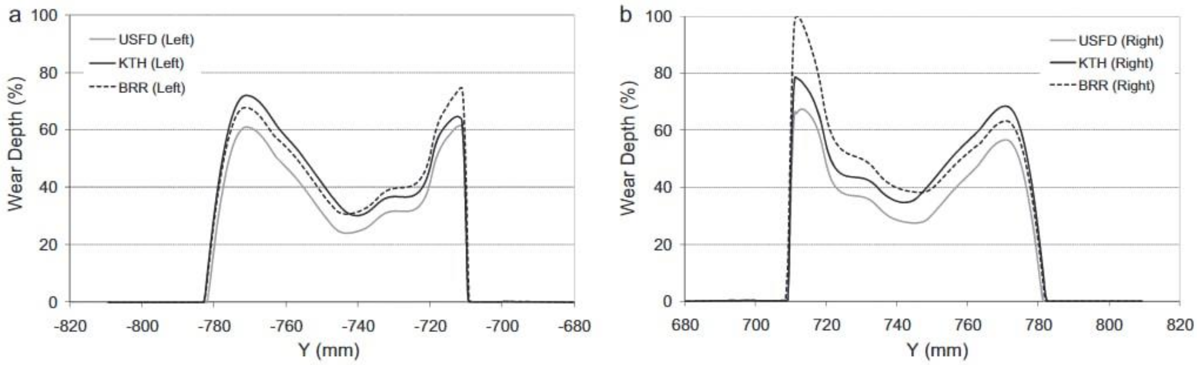

Figure 2.24-Comparison of the three wear models based on wear depth result [33]

The slight variations were mentioned due to variations in different materials used in experimental tests when developing the wear functions. Based on the USFD wear model, using the local model gave better stress distribution results along the contact patch but needed twice the computation time than others yet giving not more than 4% error in variation with the others. As a result, it is recommended to use the other methods based on the output result requirment.

Ren Luo et al. [34] also tried to consider the stochastic parameters (track geometry and wheel-rail interaction correlations) to predict wheel profile wear using the Archard wear model and the FASTSIM contact algorithm. Vertical and lateral track irregularities were also attributed as external excitationsto simulate the Real-time condition. The wheel profile was also updated for each 1500km while the train runs for 30,000 km, i.e., 200 steps involved. Based on the non-linear MBS analysis, the simulation results were in coherence with the field test, in terms of the given stochastic parameters.

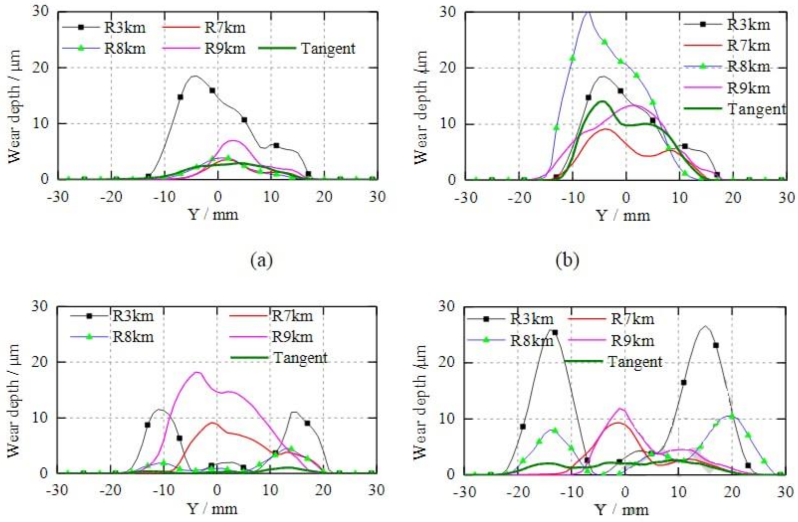

Figure 2.24-Wear depth results for 1500kms intervals (a) 0kms (b) 10,000kms (c) 20,000kms (d) 30,000kms [34]

Finally, Tao again [35] tried to analyze wheel wear prediction analysis for locomotives due to dry condition traction/braking effect and wet PI-based creep control with similar procedures commonly followed in the other papers. The influence of frequent traction and braking in locomotives has been justified in the following data regarding wear area.

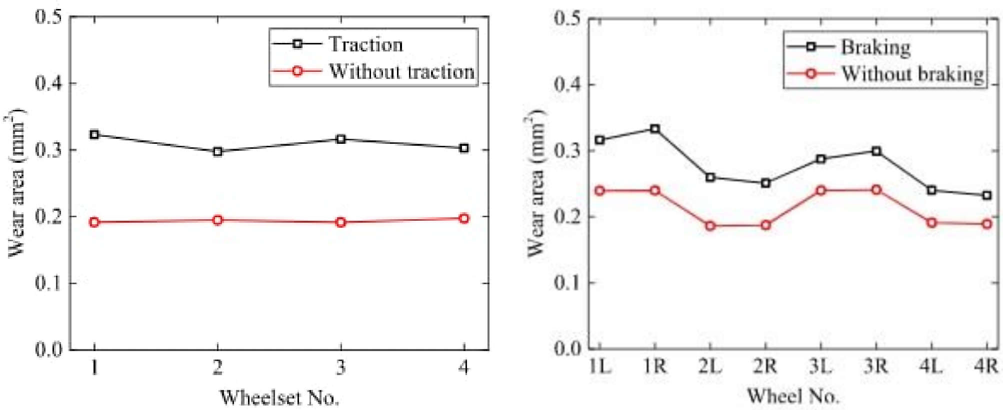

Figure 2.25-Wear area Vs Traction (a) and Braking (b) [35]

The intension of the researcher is using traction and braking as a means for elevated creepage and creep forces so that wear is aggravated, and demonstrate by using a creep controlling circuit to calculate the creep and use PI controller to modulate the AC drive in order to reduce wear as shown in the schematic diagram below.

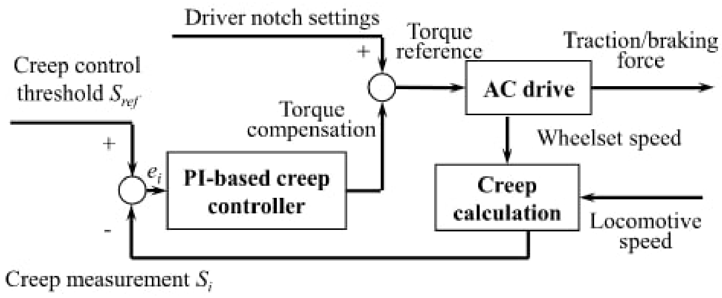

Figure 2.26-Creep control diagram for the locomotive [35]

Results show traction/braking greatly influences wheel wear in locomotives, and optimal creep control gives good exertion of tractive/braking force, thereby lowering wheel wear.

2.9. Measurment and factors influencing wheel wear

Considering parametric wear analysis and measurement, Abdullah [36] used a Caliper measurement of the wheel profile wear to avoid a human error for future predictive maintenance scheduling.

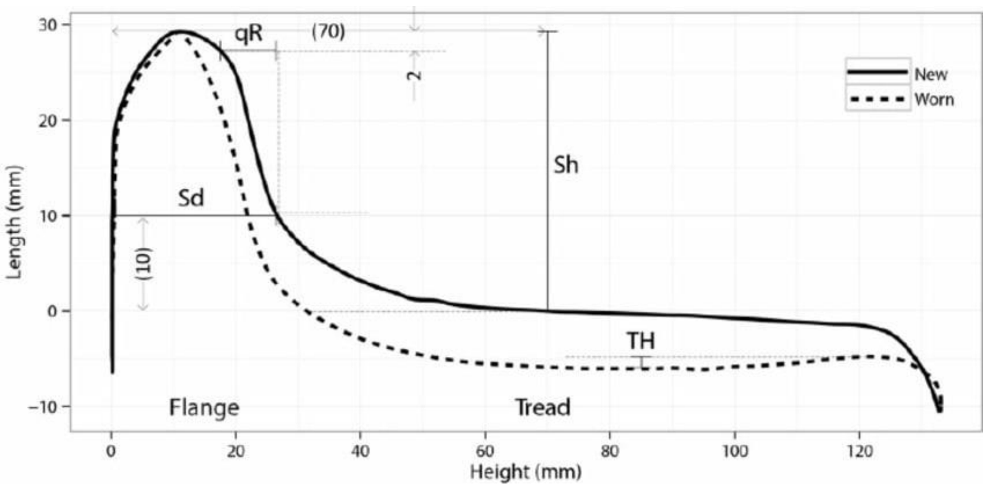

Figure 2.27-Railway wheel dimensions [37]

Mainly measurement for wheel flange height (S_h) and thickness (S_d), figure 2.27, was done so that material removal is found with respect to distance traveled, and Zhu et al. [38] used the Arcards wear coefficient method using a field test-based method accompanied by numerical simulation on SIMPACK to calculate the wear rate. On the other hand, Sui and Wang [39] tried to consider the effect of wheel diameter difference on tread wear rate based on an extensive field measuring and numerical simulations. The analysis used non-Hertzian contact and found initial wheel diameter difference significantly affecting the shapes and stress distributions of wheel-rail contact patches by leading to asymmetric wear, which facilitates further wheel diameter difference. Spangenberg [40] also tried to analyze the effect of RCF (Rolling contact fatigue) mitigation measures i.e., changes in suspension stiffness in an attempt to spread wheel wear across the tread and changes in rail profile design on wheel wear based on multibody dynamic simulation. The results showed that changes in suspension stiffness and rail profile design caused concentrated hollow wear on the wheel. Zhang and Rezende [41], [42] on the other hand tried to change the material properties of wheel in order to improve the friction and wear behavior of the system and found promising approaches. Lastly, Lyu [43] performed a pin-on-disc machine investigation to examine the influence of environmental conditions and iron oxides on the wear type and performance of thewheel–rail contact. On the result of clean contacts, adhesive wear was found predominant, and for high moisture and at room temperature, oxidative wear is the main wear mechanism, and under dry conditions, severe wear appears as delamination wear while raising the moisture level helps the pins to avoid severe wear.

Considering the local not published researches done in ARCE concerning AALRT, [48] studied wear generation on the tracks of AALRT based on SIMPACK analysis due to parameters including critical speed, friction coefficenit and overloading on the wear index developed. His results showed that maximum critical speed of 40km/hr, friction coefficient of 0.55 and and overload of 20 tons resulted in maximum wear index. [49] also analyzed the effect of crossings on wheel wear at varied speeds and loading conditions resulting in maximum wear index at the crossings when fully loaded and at empty load cases showing that crossingovers had a contribution to the wheel wear of AALRT. On the other hand, [50] also considered the effect of wet and dry loading conditions (Friction Coefficient) on wheel wear which showed the dry loading condition and higher speeds resulting in the maximum wear indexes.

Table 2.3-Objetives of the articles summery

Research Paper	Train Type	Research Gap Identified	W/R Interaction Models	MBS software	Wear Model	Wear Modeling tool	Validation Method
[20]	Passenger	Plastic deformation of contact patch Not considered, lab tests failing to replicate the real scenario	semi hertzian/STRIP approach and modified kalker's FASTSIM	ADAMS VI	ARCARD	MATLAB	Wear Data of Indian Railway
[14]	Passenger	Direct wear data collection is a time-consuming process	Hertzian and FaStrip	SIMPACK	USFD	-	Wear Data of CRH3
[30]	General case	Researchers used offline mode of calculation	Non-Hertzian (kik-Piotrowskis, Linder's, Ayarechollet's stips algorithm and ANAYLN) & FaStrip	-	Arcard and USFD	-	Kalker's CONTACT code
[31]	General case	Didn't consider yaw effect in wear prediction of wheels	Non-Heartzian (Yaw Adusted ANALYN FaStrip)	-	USFD	-	Field Test
[32]	Passenger	not take appropriate step size for updating wheel geometry	Hertzian and Kalker's contact models	SIMPACK	-	MATLAB	Experiment
[33]	General Case	Compared three wear function model functions	-	VAMPIRE	BRR, Archard and USFD	MATLAB	-
[34]	General Case	Didn't use stochastic parameters	FASTSIM contact	non-linear MBS analysis	Archard Model	-	Field Test
[35]	Locomotive	Different whether condition and traction/braking effect and wet PI based creep control	Modified FASTSIM (spiryangin's method)	SIMPACK	USFD	-	-

2.10. Research Gap

In general, based on summarized view points of various researchers in the Table 2.3 above, even though most of the related published research papers consider many factors influencing wheel wear and vehicle dynamics and were reasoned out well, yaw and track irregularities were considered less often, except Ye and Zhu [31], [38]. Yet, even though the previous considered the effect of yawing on the wear rate based on a field test-based validation by continuous measurement of wheel profile, they were both concerned with high-speed trains rather than low or medium-speed. On the otherhand, AALRT trains are grouped under low-speed division according to [44], and the North to the south line is the curviest route as low as 50m. By considering researchs from ARCE, [48] studied wear but has not included Track irregularity as a factor for analysis while [49] analyzed the effect of crossings on wheel wear. On the other hand, [50] also considered the effect of wet and dry loading conditions (Friction Coefficient) on wheel wear. As a result, few were performed considering track irregularities and yaw as main varying input factors for simulation. Based on this ground, considering yaw and rail irregularity is reasonable as main inputs for the analysis, especially for the specific case of AALRT. This research will be based on incorporating these two major parameters into the existing wear prediction process with contact and wear models of Hertzian and Archard methods, respectively.

Chapter 3 - Methedology

3.1. Introduction

The overall research process is divided into three major stages. The first stage is the pre-analysis stage, which includes a literature review, Wheel and rail profile data collection, and analysis parameters determination phase. This section major inputs for the next analysis phase mainly are collected from relevant literatures and AALRT rolling stock depot. Here also, data used for validation, including wear data recorded by the maintenance department in AALRT and other similar literatures are collected. Once this is done, the second phase, which is the analysis phase follows where multibody system modeling of the railway system, including wheel/rail contact modeling, SIMPACK vehicle dynamic modeling, and simulation and wear modeling of the system is done. Hertzian contact and Kalkers FASTSIM contact models between wheel and rail are used for normal and tangential contact, and Arcards Wear model based on Matlab is used for the wear modeling process.

Once this is done, the simulation proceeds in SIMPACK, and for each analysis step distance factor of 10,000 with different track conditions (curve radius), operational speeds, input excitations and lateral distance, lateral and vertical creep forces and creepages are recorded with their corresponding wheel-worn profile or wear depth. During this simulation period, continuous wear analysis and wheel profile updating process is done at the end of each step distance using Matlab until it reaches its final analysis limiting distance. This is done because the system couldn’t accommodate the whole simulation distance at once due to simulation memory size and time limitation. So a step by step analysis of the system is necessary [14]. Then the final data, including wear depth, derailment coefficient, ride index, and lateral force are extracted from SIMPACK and Matlab. With the post-processor stage, results will be interpreted using the SIMPACK Post-processor module at each stage of simulation. The main comparison parameters here will be the existence or absence of yaw and track irregularities and their effect on the other pre-determined parameters. Finally, the result from this analysis will be compared and validated to wear data found from AALRT for the years 2019 to 2021. An intermediate data extraction from SIMPACK and input to the Matlab code, then a back extraction of wear depth at sampling points and deduction from the original profile and feeding these profile back to SIMPACK for the next round is performed in the midway of the analysis stage as shown clearly in the figure below.

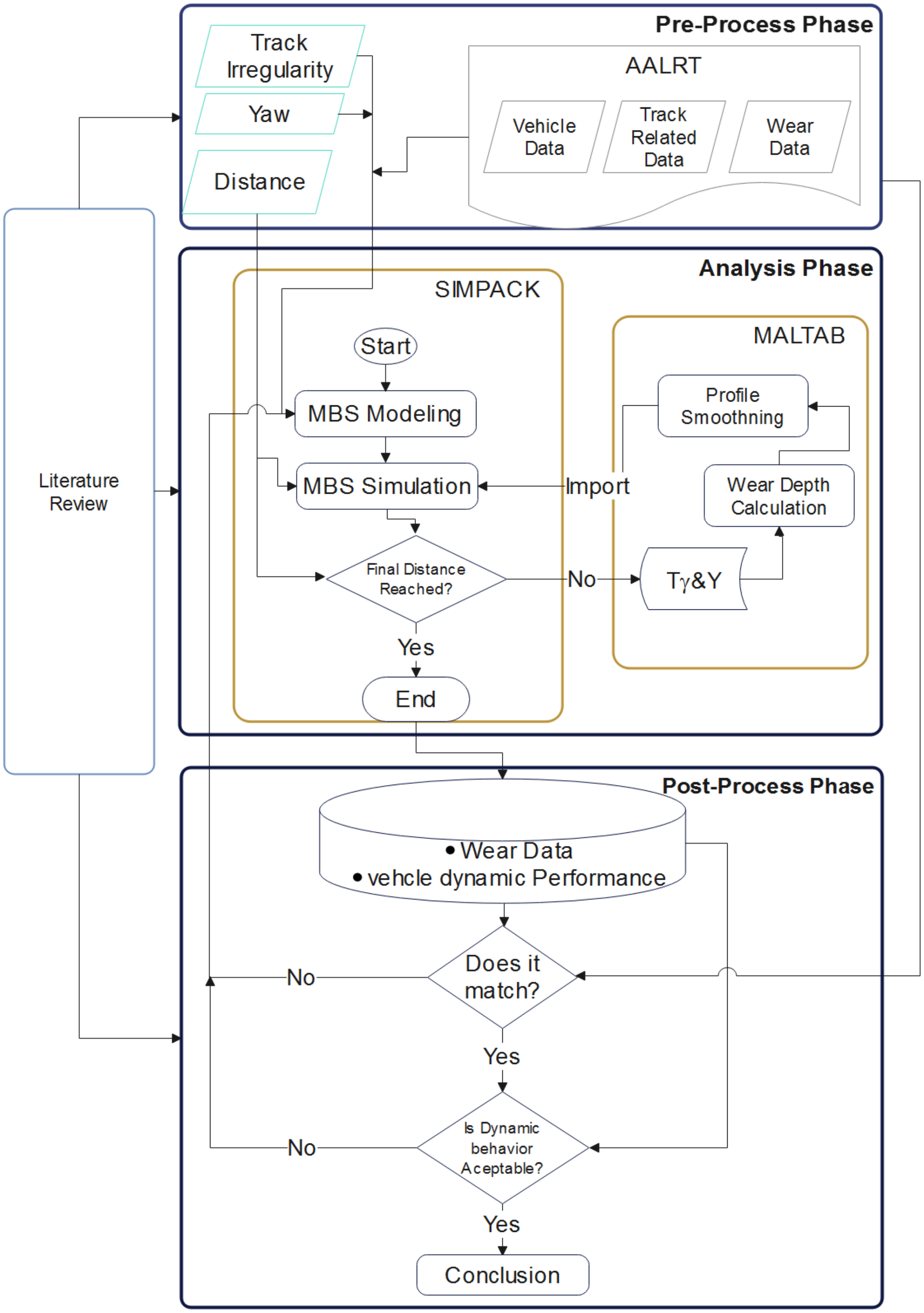

Figure 3.1-Schematic of Research Methodology

3.2. Data collection

In general, the railway is a service industry. This means especially in Ethiopia, its effectiveness and profitability is measured in terms of the service it provides for the public instead of the high revenue it makes interms of income. In this prospect, AALRT is also an organization serving the public in the transportation sector for the people of Addis Ababa. Even though it's doing a great job filling the transportation need, that doesn't mean it is a perfect system. Among the problems the organization faces the failure of rail cars to operate properly is one of the major. Specifically, the wear of wheels is one of them. Wear of wheels gives rise to different dynamic effects; the floor level of the carriages being lowered, exposing some components to impact from ground-level equipment and uneven wear leading to further aggravated wheel wear.

A newly installed wheel of AALRT has thread diameter and flange thickness of 660mm and 24mm, respectively which then starts to wear out from its profile and results from a worn profile, which could be even or uneven depending on the loading condition. To avoid the negative effect of the diameter variation, the Re-profiling operation is done on wheel lathe machine. Especially when steep curves exist on the rail lines, higher flange area wear is observed due to flange contact to negotiate curves. Re-profiling is then done to compensate for the wheel diameter reduction to gain an increment in flange thickness. Once repeated re-profiling is done, a final diameter threshold of 580mm and flange thickness of 14mm is reached and beyond these values, the wheels couldn't further be re-profiled and disposed accordingly.

The data collection process is from two typed of sources. These are primary and secondary sources of data. The primary source for data collection is the AALRT itself and its departments, including the rolling stock department, civil infrastructure department, and others. On the other hand, the secondary resources will be published literature and thesis works done by other researchers concerning the related topics. Some important parameters are retrieved from both of the data sources. To simulate the wear and dynamic behavior of the AALRT train on a pre-specified scenario, the following data is vital.

3.3. Vehicle and Track parameters

The vehicle and track-related parameters are important to construct the modeling of the multibody dynamic system in SIMPACK. In the vehicle related, most of the data has been retrieved from primary sources, i.e., AALRT rolling stock depot.

The rolling stocks of AALRT are 70% low-floor tram of the Chinese brand, at 750V DC, with a capacity of 317 passengers per train (standing capacity: 8 persons/m^2), and a maximum speed of 70km/h with a 3 car in one train set (two motored and one trailer cars).

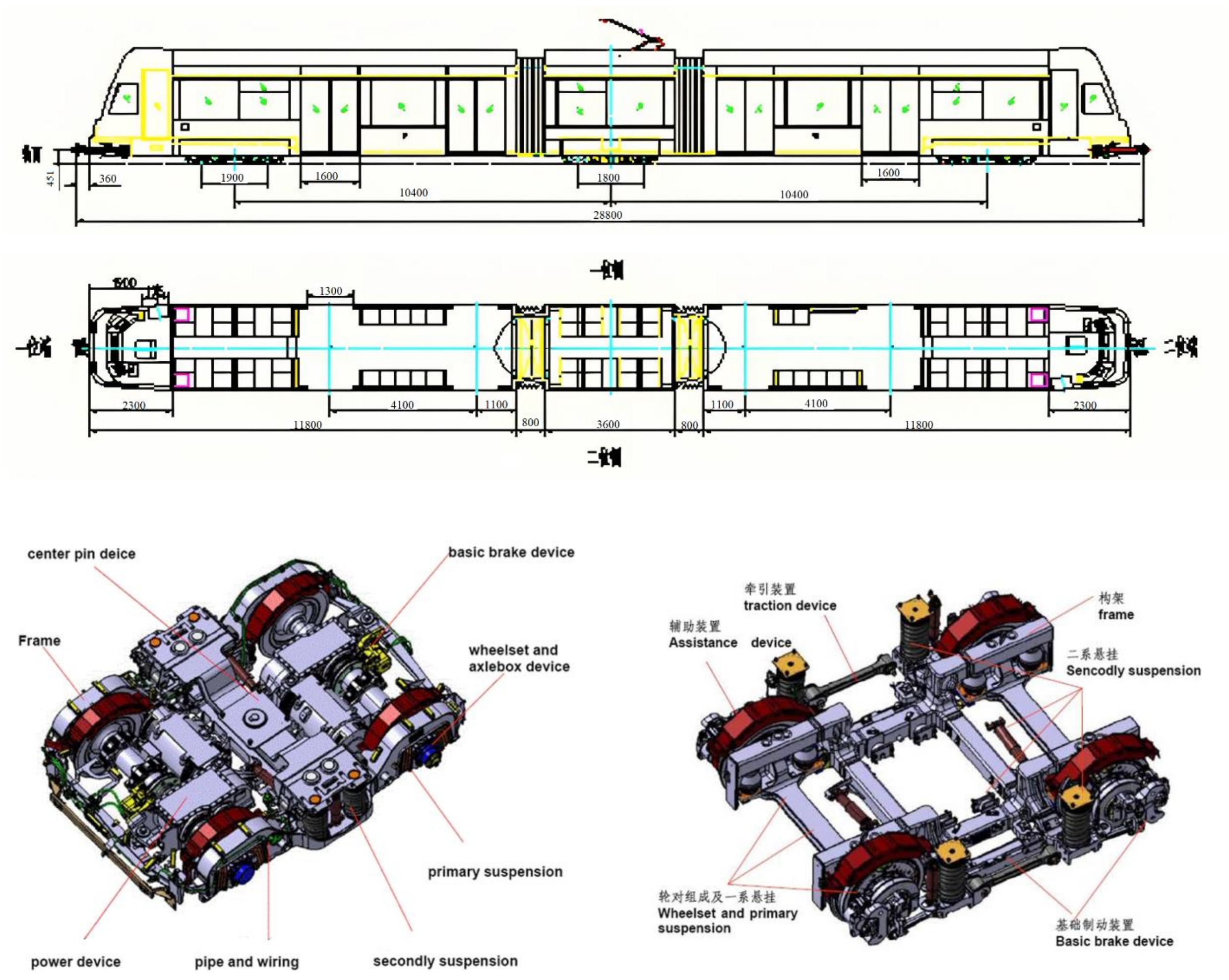

Figure 3.2-Structural and component Layout of AALRT Train (Courtesy of AALRT Train Maintenance Manual)

The critical curves found in the AALRT are mostly found in the Kality Rout, i.e., North to South, rather than the Ayat line. The most important track and vehicle parameters for the analysis are shown below.

Table 3.1- Vehicle and track model parameters (Courtesy of AALRT & Train repair Manual)

No	Vehicle Parameter	Unit	Value
1	Bogie base Distance	m	10.4
2	Wheel set base for motor bogie	m	1.9
3	Wheel set base for trailer bogie	m	1.8
4	Wheelset Mass	kg	880
5	Wheelset Moment of inertia in x	kgm^2	176
6	Wheelset Moment of inertia in y	kgm2	70
7	Wheelset Moment of inertia in z	kgm^2	176
8	Wheel Diameter (New)	m	660
9	Wheel Diameter (Worn)	m	580
10	Wheel Profile	-	S1002
11	Lateral Wheel Position	m	0.75
12	Bogie mass for motor bogie	kg	5120
13	Bogie mass for trailer bogie	kg	3120
14	Car Body Mass (Maximum Load)	kg	63000
15	Car Body Mass (Normal Load, Sitting and Standing)	kg	59200
16	Car Body Mass (Normal Load, only Sitting)	kg	48000
17	Car Body Mass (No Load)	kg	44000
18	Car body mass (MC1 and MC2)	kg	2/5 of total M
19	Car body mass TP	kg	1/5 of total M
20	Car body moment of inertia along x	kgm^2	4375
21	Car body moment of inertia along y	kgm^2	8750
22	Car body moment of inertia along z	kgm^2	8750
23	Car body mass (TP)	kg	12325
24	Car body moment of inertia along x	kgm^2	3081
25	Car body moment of inertia along y	kgm^2	6162
26	Car body moment of inertia along z	kgm^2	6162
27	Bogie Frame mass	kg	985
28	Bogie movement of inertia along x	kgm^2	1250
29	Bogie movement of inertia along y	kgm^2	1870
30	Bogie movement of inertia along z	kgm^2	2182
31	Train Total Length	m	28.8
32	MC car body length	m	12
33	TP car body length	m	3.6
34	Height car body excluding pantograph	m	3.61
35	Height of Car from ground	m	0.655
36	Width of car body	m	2.65
37	Primary spring stiffness along x	N/m2	7.00E+05
38	Primary spring stiffness along y	N/m2	7.00E+06
39	Primary spring stiffness along z	N/m2	8.00E+05
40	Primary damping along x	N.S/m	1.53E+05
41	Primary damping along y	N.S/m	1.53E+05
42	Primary damping along z	N.S/m	1.53E+05
43	Secondary spring stiffness value along x	N/m2	0.00E+00
44	Secondary spring stiffness value along y	N/m2	1.65E+07
45	Secondary spring stiffness value along z	N/m2	2.72E+08
46	Secondary damper along x	N.S/m	1.4E+03
47	Secondary damper along y	N.S/m	4.00E+06
48	Secondary damper along z	N.S/m	8.00E+06
No	**Track Parameter**	**Unit**	**Value**
1	Track Profile	-	UIC 60
2	Track Gauge	m	1.435
3	Track Length	m	1000
4	Track Super elevation	m	0.1
5	Minimum radius of horizontal curve	m	50,100,150 190
6	Operating Speed (Normal/Maximum)	km/hr	18/36/72
7	Friction Coefficient	-	0.4

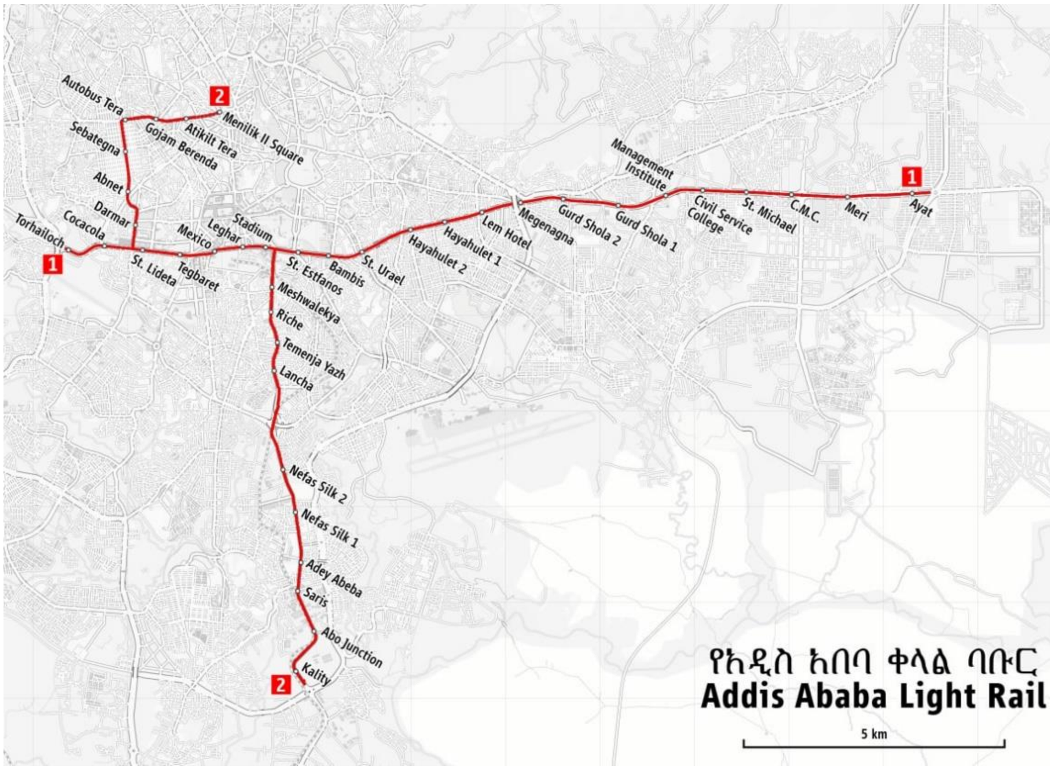

Figure 3.3-Addis Ababa LRT Route lines (transitmap)

Based on the track layout of AALRT shown in the above figiur, the following critical curves were extracted for simulation purpose.

Ayat Line (1): Torhayloch R-65m, Coca-Cola station area R-190m
Kality Line (2): Kaliti area R-150m, Saris Junction R-150m, Stadium R-50m, St. Lideta R-50, Darmar R-100m, Darmar R-100m, Autobistera R-50m, and Menilik-square underground R-65m.

3.4. Traffic Data Estimation

According to data collected, the daily rotation (2-way trip) achieved by AALRT trains could reach up to 94-122 at pick operation days in the North to South line. Taking the maximum value and having a total of 21 trains operating on the North to south line gives the following daily and annual traffic data for the rail transit. 122 rotations/day = 244 trip/day

Trip per train per day = (244 trip/day)/21 trains = 11.62 trip/train/day

Taking S = 16.9km and estimated 300 days of operation per year by considering different inspection, routine maintenance and repair related stoppages gives:

Distance traveled/train = 11.62trip * 16.9km/trip = 196.4 km/day = 58,920 ~ **60,000 km/year**

3.5. Wear Data

The wear data mainly consists of flange thickness and re-profiled thread diameters of trains for 2019 to 2022. Due to data availability issues, some records were missing for a few of the months for each train in the two depots of AALRT. But for kality depot, most of the data has been found to be complete, and nine trains have been chosen due to their relatively complete data set for the years indicated. Unlike the kality depot, for Ayat depot, not much of ready-made data has been found during data collection. Only may of 2022 data was available; the rest was not organized, and most of it is missing. As a result, the comparison has been made based on the available data despite not being enough for a concrete conclusion. A sample of the wear data has been given in Appendix 1 and 2 of this document for reference. For demonstration, sample of the May 2022 data comparison is shown below.

Kality Trains

Date	Train no	MC1				TP				MC2			
		WS1		WS2		WS3		WS4		WS5		WS6	
		L	R	L	R	L	R	L	R	L	R	L	R
May-22	201	21.08	21.38	22.44	22.96	19.65	19.49	19.60	19.93	23.00	23.00	22.85	22.75
	203	23.00	23.00	23.00	23.00	17.05	17.30	16.74	16.50	23.00	22.93	22.51	22.39
	207	22.3	22.25	22.85	23	19.55	20.1	18.55	19	22.8	23	21.85	22
	208	21.90	22.03	22.33	22.63	18.53	18.15	18.00	18.03	22.90	23.00	22.85	22.90
	211	21.5	22.4	23	23	18.45	17.6	15.75	18	21.1	21.65	19.6	19.8
	213	23.00	23.00	23.00	23.00	16.30	16.58	16.20	16.63	23.00	23.00	22.80	23.00
	215	22.9	23	23	23	18.35	17.9	18.5	18.85	23	23	21.7	21.45
	218	22.92	22.48	23.00	23.00	17.75	18.82	16.17	17.00	23.00	22.92	23.00	22.63
	219	21.25	22.3	22.75	23	17.85	18.85	18	19.1	23	23	22.1	23

Ayat Trains

Date	Train no	MC1				TP				MC2			
		WS1		WS2		WS3		WS4		WS5		WS6	
		L	R	L	R	L	R	L	R	L	R	L	R
May-22	102	23.3	23.25	23.35	23.45	17.05	17.85	18.6	18	24.1	23.15	23.65	22.8
	103	21.4	21.75	22.7	23	19.3	18.6	19.55	18.5	22.6	22.15	19.6	19.55
	105	22	23.3	23.15	24.1	17.75	18.35	16.55	17.75	24.1	23.9	22.1	22.65
	106	20.85	21.4	21.2	22.35	18.05	18.6	17.7	18.15	23	24	21.45	22.2
	108	23	23.15	23.3	24.45	18.45	17.45	19.15	18.35	22.8	22.85	22.15	22.1
	119	21	22.55	22.1	22.8	17.05	17	17.05	18	22	22.7	21.05	22.25
	121	22.9	23.85	22.95	22.9	17.55	18	17.3	18.4	23.15	23.85	23.3	24

Figure 3.3-Sample flange thickness data

This shows a sever flange wearing in the TP section of the trains where the most of the values for Kality trains are close to 16 and below which is due to the highly curved construction of the rail lines.

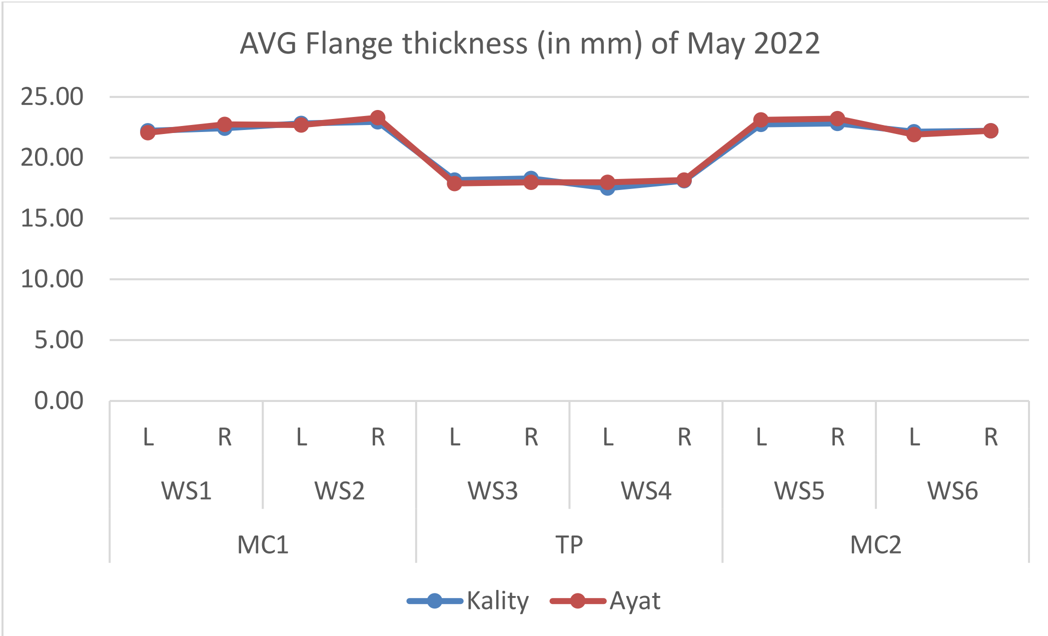

Figure 3.4-Average wheel flange thickness data in May of 2022

Based on the data collected, the following inferences has been made.

- High flange wear is observed on the TP (Trailer car) wheels rather than the motored wheelsets. Based on this fact, the possible reason based on the informal interviews and passenger data is that there are many standing passengers on the Trailor car than on the motored cars per square area which raises the load on the wheels of the TP. During curving also, the Trailor car is subjected to high wheel slippage due to the articulated construction of the rail vehicle twisting the TP from both sides, as observed in the simulation process.
- In about 60% of the whole train wheels, the Kality (north to south) trains have more worn flange profile than the Ayat (East to West) trains, based on average value. This is the case because of the curvy construction nature of the Kality (North to South) line of AALRT. As a result of the case, more flange contact of the wheels is expected in this line than in the other.

Re-profile Diameter

When flange thickness becomes lower than the threshold value, i.e., 14mm, re-profiling becomes a necessary activity, in order to regain the flange thickness by compromising part of the wheel thread diameter. Once the wheel reaches a geometric constraint of 580mm, it cannot be further re-profiled, rather disposed. Considering AALRT, since there's no wheel lathe machine in the Ayat depot, all the trains are transported to the Kality depot for re-profiling operation. The data recorded at the kality depot from 2019 to 2021 has been collected with each thread diameter of the wheel before and after re-profiling.

In summary, 38 of the 47 trains for which re-profiling action was taken during the specified period were from the Ayat line, and 9 of them were from the Kality line.. This was an unexpected phenomenon that indicates that even though the kality line was curvier than the two, there are factors related to overloading, which makes the Ayat train wheels wear out more frequently than anticipated, as shown in the figure 3.5 but since the only complete wear data available was for Kality depot trains, reasonable comparison couldn't be done between the two lines.

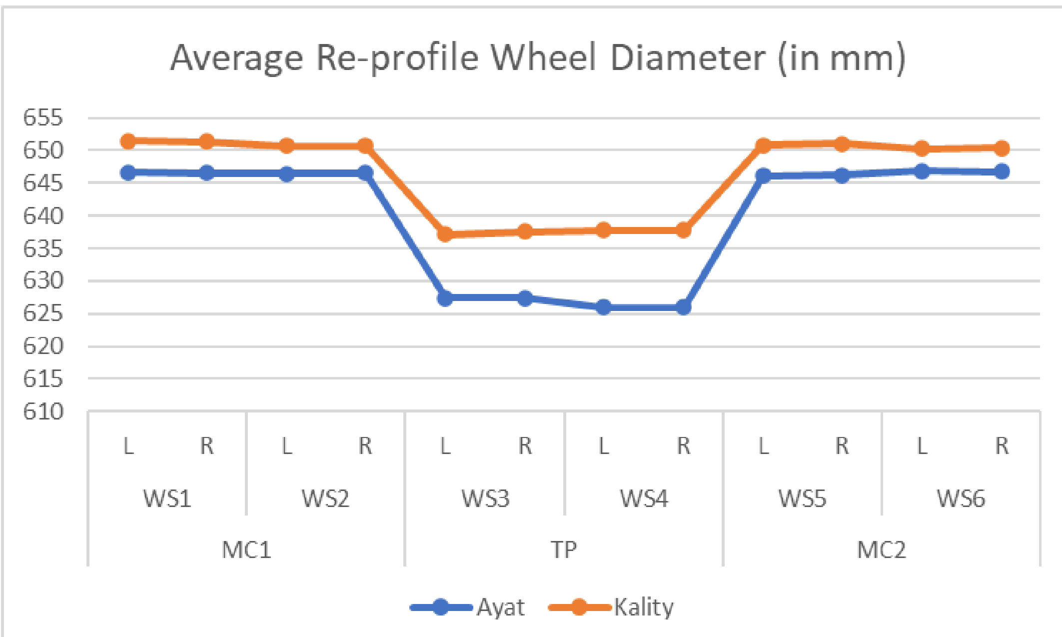

Figure 3.5-Average wheel re-profiling Diameter data

The below sown in figure 3.6 is the underground lathe machine found at the kality depot of AALRT. Trains are driven towards the lathe machine and primary measurement is performed befor the re-profiling task is done for the wheels. All of the pre and post re-profiling measurments are recorded and confirmed during each re-profiling operation.

Figure 3.6-Underfloor wheel lathe in AALRT (Courtesy of AALRT RS Depot)

The most repeatedly re-profiled wheels were from the TP (Trailer car) and these indicates that higher creepage and creep forces will be expected in these areas for the simulation results.

Summery

- High wear rate and depth is seen in the trailer bogies of AALRT Trains.
- Frequent wheel re-profiling operation performed on Ayat trains than Kality, but wear data is not readily available for Ayat trains.

Chapter 4 – Multibody Modeling and Analysis

4.1. Introduction

The first step in every software-based dynamic and wear analysis of a multibody system is to model the system in MBS software, in our case SIMPACK. There are two types of modeling processes involved in SIMPACK. These are:

- **Sub-Structure Approach**: which comprises wheel-set, bogie, and car bodies constructed in a separate model with different formulations using different variables and assembled to obtain a coupled mathematical system that can describe the whole system. The system is more simplified for very complex analysis but needs proper attention during variable assigning and assembly processes so that simple errors could lead to erroneous models.

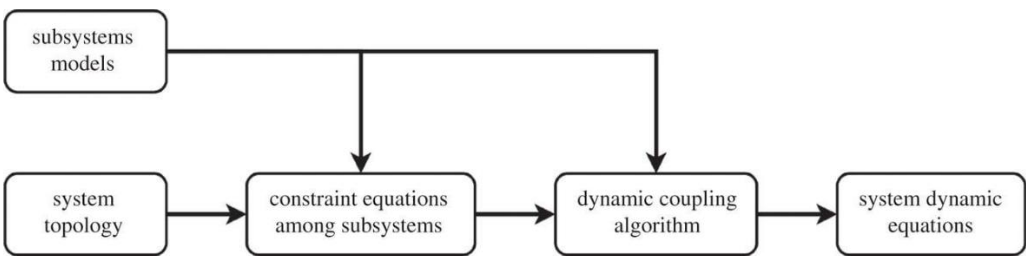

Figure 8-The sub-system approach dynamic modeling process [45]

- **All-in-one Approach**: here, all the components of the system be modeled inside the main model and it is the most straight forward methodology used by researchers. If system is not complex enough, modeling in this approach is the preferred way. As a result, for this research work, the all-in-one approach has been used for dynamic modeling.

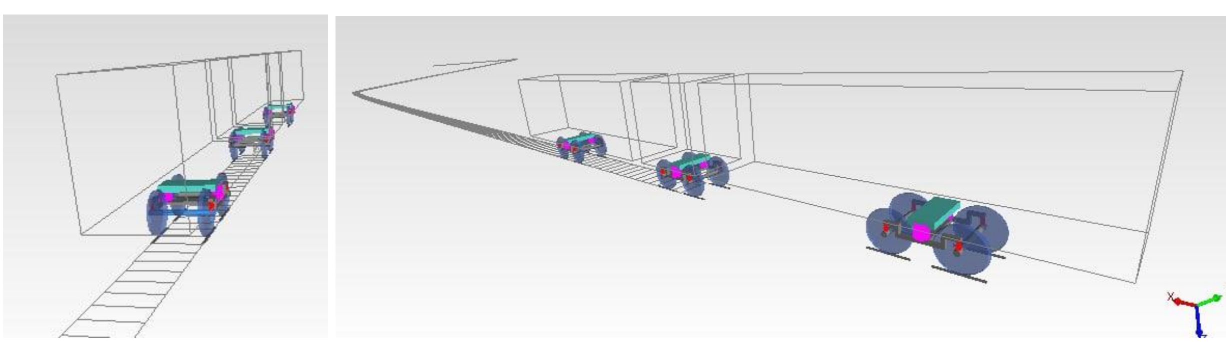

Figure 9-Isometric and perspective view of the model

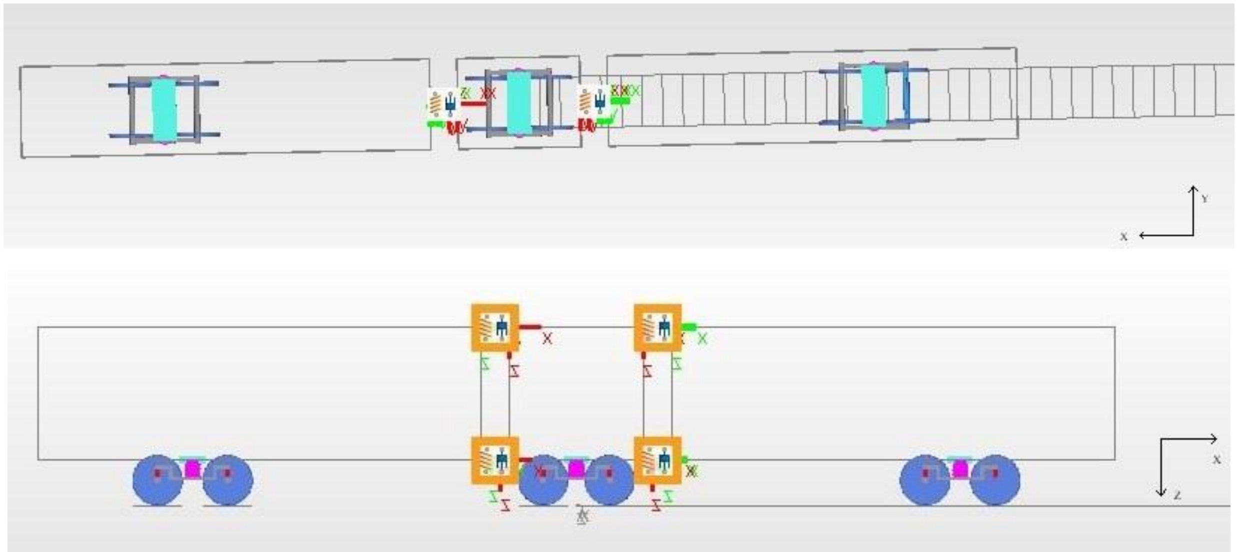

Figure 10-Top and Front View of Rail Vehicle Model

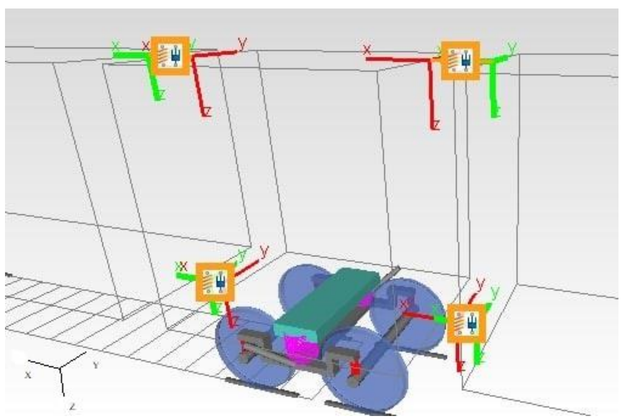

Figure 11-Coupling Force elements used between Carriages

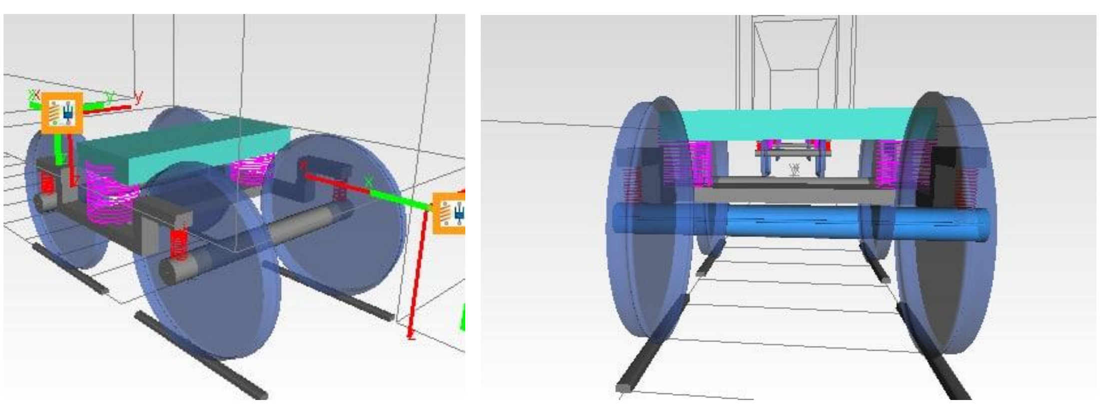

Figure 12-Layout of Rail vehicle and Bogies model on SIMPACK 2021

4.2. Degree of Freedom

Even though it has many definations in different fields of use, degree of freedom is defined as the number of independent variables that define the possible positions or motions of a mechanical system in space. [47] Based on this statement and taking small value of pitch and translation direction variation, each of the systems has 5 degrees of freedom with respect to the coordinate system except the coupling, which allows yaw and a little bit of roll during curving operation

Table 4.1- DoF of System

Component	Translation			Rotation			Qty	DOF
	X	Y	Z	X(Roll)	Y(Pitch)	Z(Yaw)		
Wheelset	✓	✓	✓	✓	X	✓	6	5*6=30
Bogie Frame	✓	✓	✓	✓	X	✓	3	5*3=15
Car Body	✓	✓	✓	✓	X	✓	3	5*3=15
Coupling	X	X	X	✓	X	✓	2	2*2=4

As a result of the above analysis, the DOF of the whole system is found to be:

$$DOF = 30+15+15+4 = 64$$

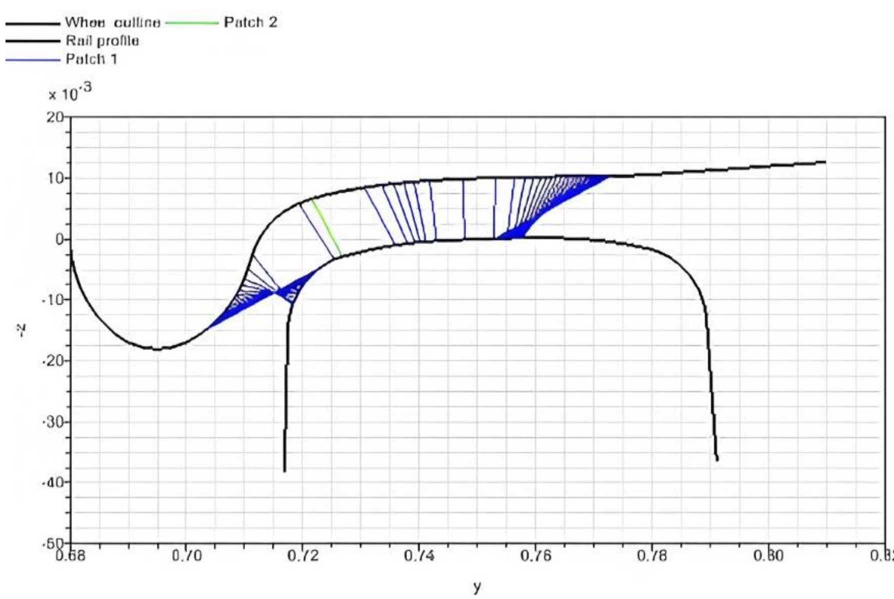

Figure 13-Sample contact model of wheel and rail MC-1 front wheel set right wheel

4.3. Track condition

The track was modeled in a way to contain the short critical curves of the North to South line of AALRT. The minimum value, i.e., 50, 100, 150, and 190 meters of curve radiuses with 100 m long approach curves of 1200m radius for transition purposes in between and a total length of 1km, has been used for analsysis. The curve length has been analyzed based on Hallade method found from the indian railway manual guideline as follows in order to limit the running simulation path at 1km for all radiuses.

$$R = \frac{125C^2}{V} \quad \text{Eq 4.1}$$

Where: R=Radius in meters, C = Chord length in meters, and V = Versine in millimeters

Track irregularities for the curved track have also been imported to the excitation part of the track layout and used during the analysis with a fade in and out the length of 10m. Maximum superelevation of 0.1 meters was also applied to one of the track sides on each curve based on SIMPACK recommendation on the curving direction (right or left) to aid the centrifugal effect of the loaded car bodies during the simulation to prevent early derailment of the vehicle's wheelsets.

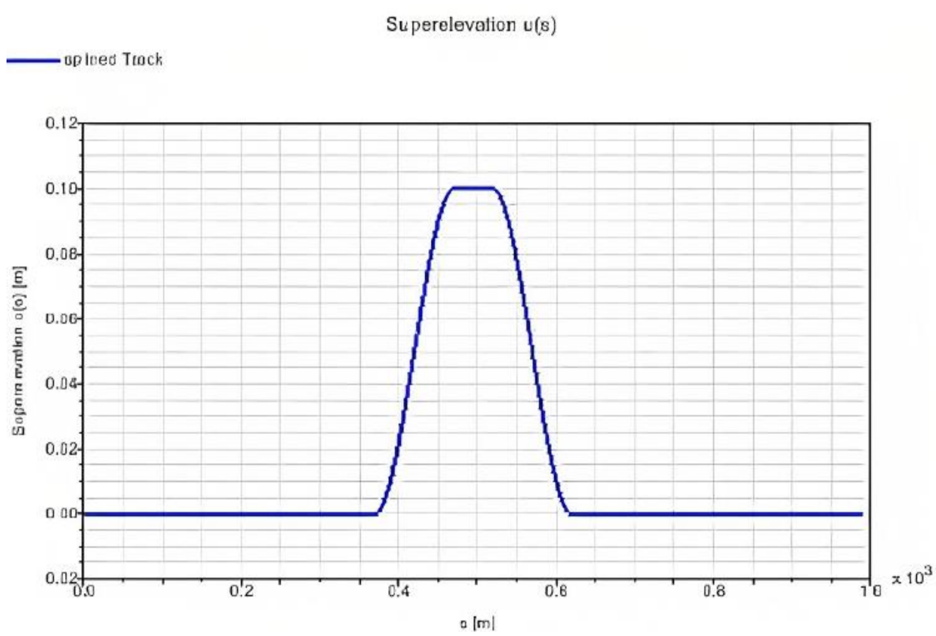

Figure 14- Super elevation of the track

In the analysis section, the model has been run several times in different scenarios of speed, irregularities, Yaw and other parameters variation and the results are summarized in the next chapter.

4.4. Simulation Parameters

In the simulation process, a short track of length 1km containing the critical curves of the north to south line, i.e. 50m (Min. Curve), 100m, 150m and 190m radiuses have been used with each approach and leave curves of 100m long with 1200m curve radius and super elevation of 0.1m high during the curving operation. The rail vehicle have been given a speed curve to run at a maximum cruising speed of 20m/s (72km/hr, Max op. Speed), 10m/s (36km/hr), and 5m/s (18km/hr). Also, a wear distance factor of 10,000 has been used for the overall track distance of approximately 1km in order to avoid the full modeling of the track length on the north-to-south line. Considering a yaw damper, 2.5×10^7 (found from local researches done on AALRT) and 4×10^7 Ns/m (Higher yaw value) pure damping elements were used separately for different cases and their effect on each parameter has been checked on the analysis. Each simulation process has been performed for a simulation clock of 75 seconds to complete the whole 1km path on a TOSHIBA C55A Windows 10 pro, 4GB Ram, 2.5 GHz processor laptop computer. Outputs of the simulation result have been discussed in detail in the following chapter.

Chapter 5 – Results and Discussion

5.1. Result

To check the truthfulness of the results and methodologies involved in the analysis, wear data provided from the AALRT depots has been used. The data included a re-profiling diameter record of all the trains admitted to the underground wheel lathe found at the Kality depot and flange thickness data recorded during each monthly inspection of the train vehicles from both depots. Even though no complete data has been found, especially for the flange thickness data of the Ayat depot trains, the available data has been converted to a suitable form to be compared to the analysis data shown below. This is done by getting the re-profiling diameter data before and after re-profile operation is performed and used as an approximate wear depth with the maximum and minimum confidence level ranges plotted based on 96% confidence level of probability distribution analysis. The values were then used to be compared to the 60,000 km analysis result explained in the validation section.

Considering the analysis, process mentioned in the methodology section of this document had been used until the estimated annual distance, 60,000 km is reached. For every 10,000 km analysis, i.e. 1km analysis with 10,000 distance factor, the lateral and longitudinal creepage values, contact patch area, wheel contact position, and worn wheel profile were extracted from the SIMPACK post-processor file and imported to the Matlab code indicated in Appendix 4, each values in .txt format. Once the resulting profile has been generated from, the value is plotted and is imported to the SIMPACK wheel profile .prw file format so that it can be smoothened. Next step of 10,000 km analysis is performed until it reaches the final termination distance. The wear depth values were then compared, as shown in the figure 5.1. It shall be noted that the analysis was performed for the +Y+Tr case, 190m radius of curvature, and 10m/s speed cases for all of the 12 wheels of a trainset, which is the general case. Based on this analysis, the results shown in the following figure 5.1 below were constructed and explained.

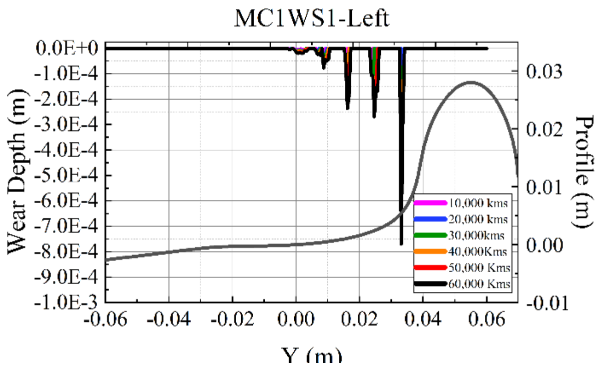
MC1WS1-Left
Wear Depth (m)
Profile (m)
Y (m)
10,000 kms
20,000 kms
30,000kms
40,000Kms
50,000 Kms
60,000 Kms

(a)

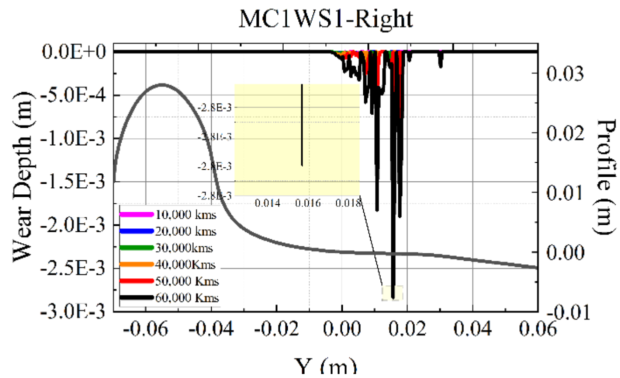
MC1WS1-Right
Wear Depth (m)
Profile (m)
Y (m)
10,000 kms
20,000 kms
30,000kms
40,000Kms
50,000 Kms
60,000 Kms

(b)

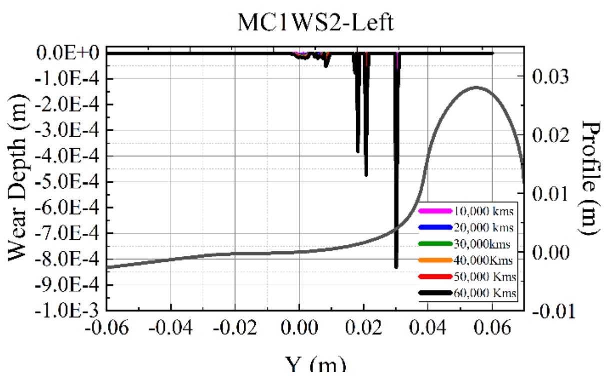
MC1WS2-Left
Wear Depth (m)
Profile (m)
Y (m)
10,000 kms
20,000 kms
30,000kms
40,000Kms
50,000 Kms
60,000 Kms

(c)

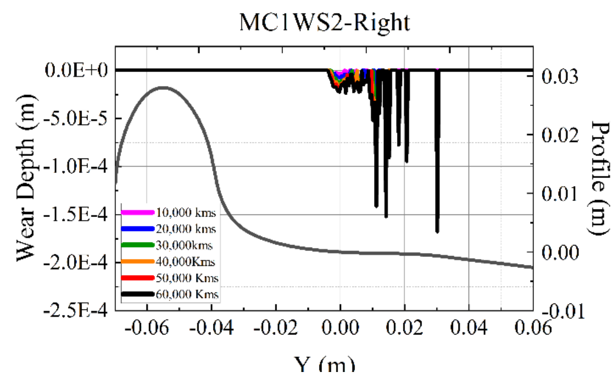
MC1WS2-Right
Wear Depth (m)
Profile (m)
Y (m)
10,000 kms
20,000 kms
30,000kms
40,000Kms
50,000 Kms
60,000 Kms

(d)

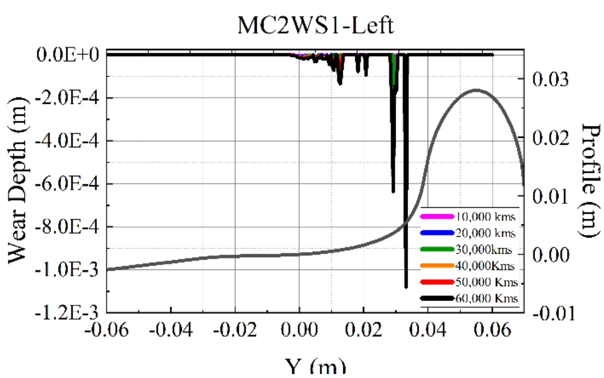
MC2WS1-Left
Wear Depth (m)
Profile (m)
Y (m)
10,000 kms
20,000 kms
30,000kms
40,000Kms
50,000 Kms
60,000 Kms

(e)

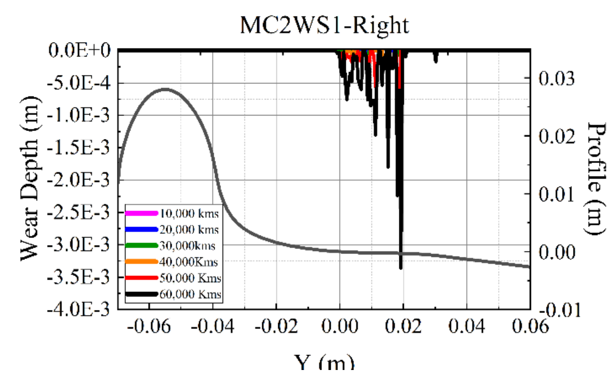
MC2WS1-Right
Wear Depth (m)
Profile (m)
Y (m)
10,000 kms
20,000 kms
30,000kms
40,000Kms
50,000 Kms
60,000 Kms

(f)

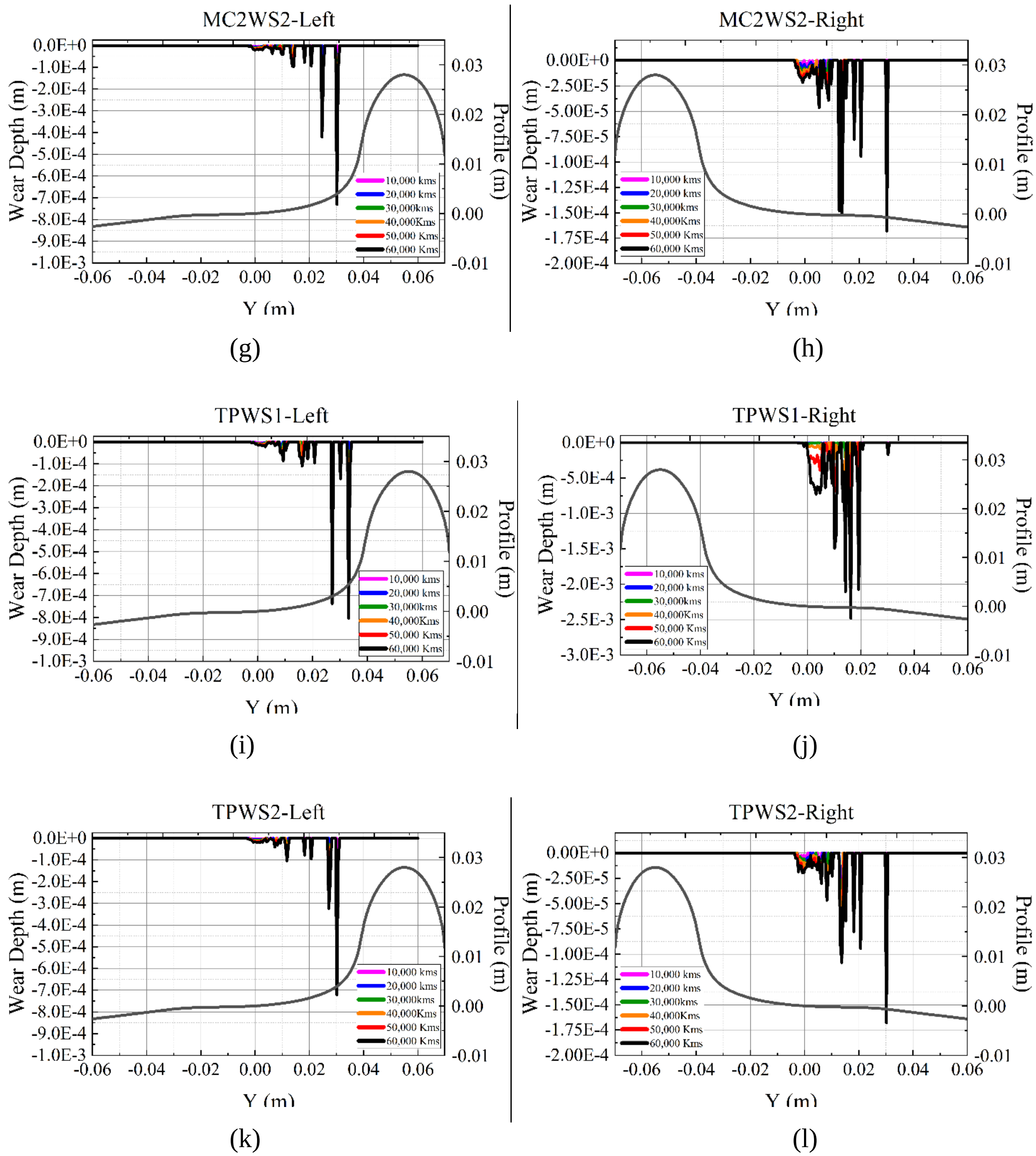

Figure 5.1-Wear depth updating from 10,000 to 60,000 kms based on analysis

5.2. Validation

Based on the above results, it can be observed that the maximum wear depth has been found to be 3.3mm for MC2 WS1 right wheel. The maximum wear depth for each analyzed wheel has been compared statistically to the measured wheel wear depth measurement data found from AALRT on confidence level of 96% probability distribution analysis. Based on this comparison, even though the upper confidence level for the TP is a bit elevated due to some unintended loading condition that weren't analyzed in the simulation but exist in the real scenario, the analysis closely estimated at some points of the lower and upper confidence levels of the wear depth of each wheel, as can be viewed in the figure 5.2 below. The results for the left and following right wheelsets of MC1 and MC2 were mostly found to be closer to the lower confidence levels while the leading right ones were closer to the upper confidence. This is because the leading wheels will face most of the sudden turning centrifugal force from the turning while the following wheelsets were simply be dragged forward by the front wheelsets and assisted by the already in the turn wheels through the body force being transferred to them. The slight variation of values some being closer to the upper confidence and lower are due to incompleteness of wear data which is used for validation.

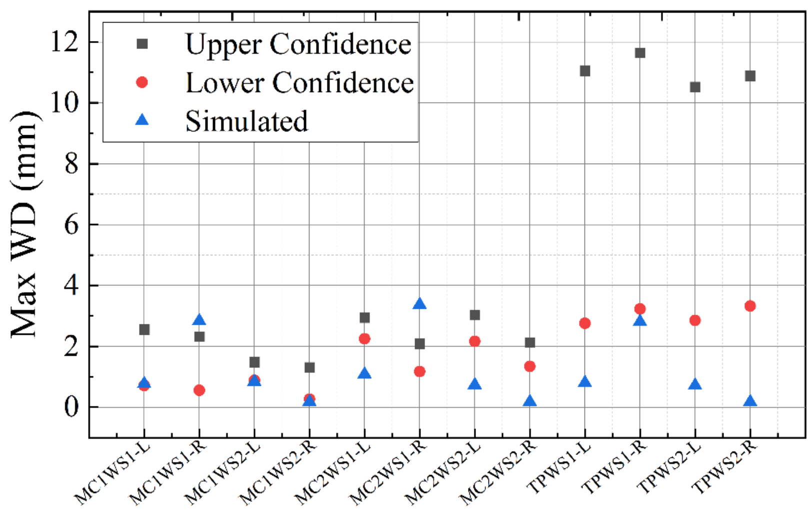

Figure 5.2-Maximum wear depth validation using wear data from AALRT

5.2. Case 1: Curve radius variation

5.2.1. Straight track

For a straight track of 1km and 10,000 wear distance factor, the result obtained for the unit kilometer is multiplied by this factor to get the desired wear depth at the specified distance since it is difficult to input the full distance of track on SIMPACK in order to minimize the computation time and memory usage. Based on this process, the wear depth was calculated in a MATLAB code that uses extracted values of Lateral and Longitudinal creepages, contact patch area and its axis a

& b and lateral wheel position using the Arcard wear analysis method. Even though analysis has been performed for all wheels, the leading MC2 WS-1 wheels were found to have the highest wear. As a result, the results for these wheels were under consideration. Note shall also be taken that 10m/s (36km/hr) running speed and 25MS/m yaw damper has been used for each simulation.

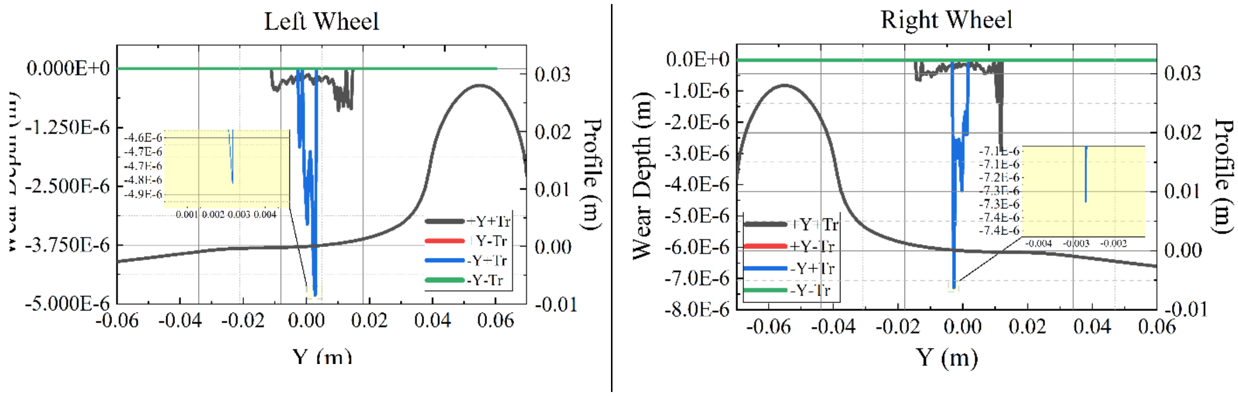

(a) (b)

Figure 5.3-Wear Depth of Straight line run simulated on MC1 WS1 Left (a) & Right (b) wheels

In the above figure 5.3, it can be observed on a straight-line simulation the maximum wear depth after 10,000kms reaches up to $4.8x10^{-3}$mm for the left wheel, figure 5.3 (a), and $7.3x10^{-3}$mm for the right wheel, figure (a) with track irregularity included and No-Yaw damper case (-Y+Tr) being the highest value. This shows adding yaw damper greatly influences the wear depth on a straight track. From the above figure 5.3, it can also be seen the wear depth is concentrated in the thread region and no significant flange wear was noticed on both wheels due to no curvature operation. Due to this wear, the derailment coefficient for the specific cases is shown the figure 5.4 below.

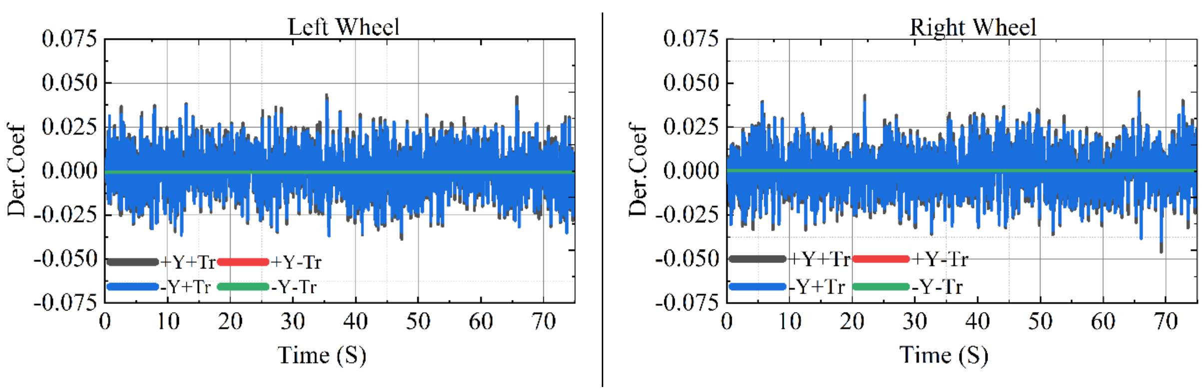

(a) (b)

Figure 5.4-Derailment coefficient result of MC1WS1 (a) Left and (b) Right wheels straight line

According to Nadal's derailment coefficient safety criteria, it can be seen the rail vehicle is safe from derailment as all values are way below the threshold limit of 0.8, 0.046 being the maximum at the yaw damper included, and no track irregularity case (+Y-Tr) on the right wheel. Minimum derailment coefficients are viewed when there is No yaw and track irregularities and both yaw and track irregularities exist. This is due to the fact that the vibration induced by the track irregularity is being damped by the yaw damper.

5.2.2. 50m curve run

Considering a 50m radius run (the actual minimum radius of curve at AALRT) simulation of the AALRT model for a track length of 1km and distance factor of 10,000, the maximum wear depth for the right wheel was found to be close to 0.952 mm on the case of yaw and track irregularity (+Y+Tr). For the left wheel, on the other hand, this value was found to be 6.18 mm which is a very high wear rate since the radius of curvature was too tight at the given curving speed of 36 km/hr. As a result, of this, the wheel is highly wearing on the left side, but the presence of the yaw damper has not improved much of the wear depth rather increased by 1.8 and 0.88% compared to without yaw (-Y+Tr) and no track irregularity (+Y-Tr) cases, respectively. It can also be noticed that the wear type on the right is purely thread type while on the left wheel a higher flange and thread wear were observed. As a result of this, care shall be taken to curvature speed at tight curves of AALRT since they aggravate wear rate in a great deal.

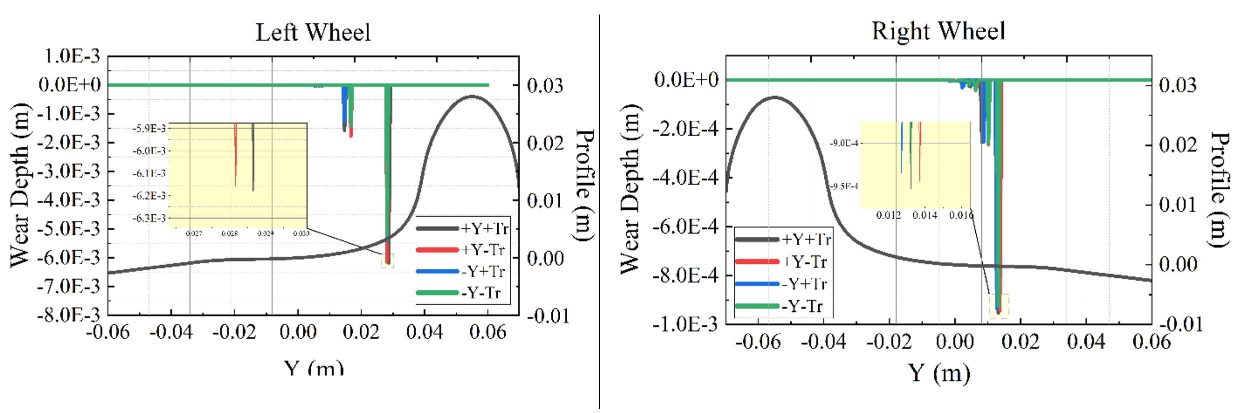

(a) (b)

Figure 5.5-Wear Depth result of MC1WS1 (a) Left and (b) Right wheels 50m Curve

In the same manner, as shown in the figure 5.6 below, the derailment coefficient for the left and right wheels between the curving periods of 46.5 to 49 seconds were 1.01 and 0.408 respectively, the left being 147.5 % higher than the right wheel. Since the limiting value is based on Nadal's stability condition of 0.8, the left wheel is expected to be unstable and possibly experience derailment to the rolling stock. As a result, care shall be taken while passing tight curves like this so that derailmentcan be avoided.

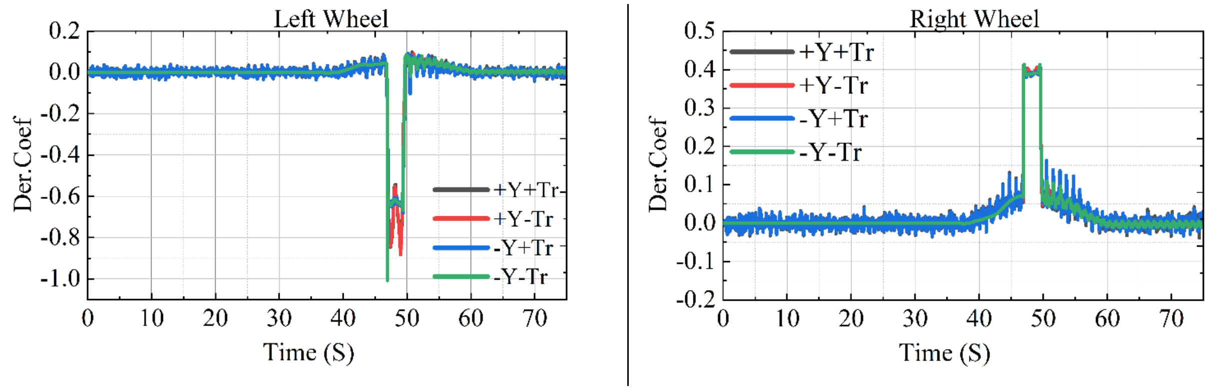

(a) (b)

Figure 5.6-Derailment Coefficient result of MC1WS1 (a) Left and (b) Right wheels 50m Curve

5.2.3. 100m curve run

In this simulation as well, a 100m curve was used. The maximum wear depth has reduced for the left wheel to 0.989 mm for the case of yaw and no rack irregularity (+Y-Tr), improving by 84% and 0.658 mm for the right wheel (-Y-Tr case) thereby decreasing by 30.9%, which is due to the radius of curvature being increased by 50m. As a result, the spiked wear depth in the 50m radius of curvature has been reduced significantly, especially for the left wheel. Yet here also, the presence of the yaw damper made a 2.1% increment to the wear depth compared to no yaw case, as shown in the figure 5.7 below.

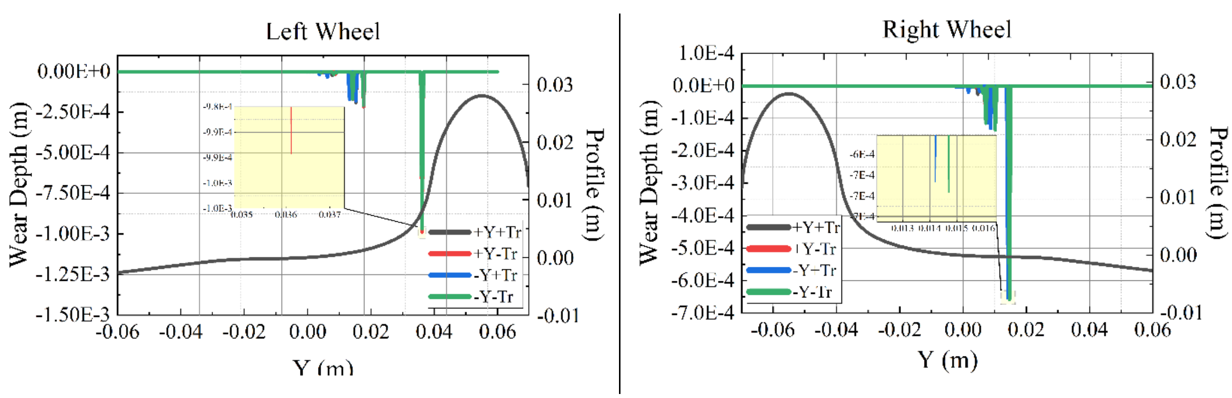

(a) (b)

Figure 5.7-Wear Depth result of MC1WS1 (a) Left and (b) Right wheels 100m Curve

This in turn also resulted in a reduced maximum derailment coefficient of 0.78 and 0.41 for the left and right wheels, respectively. This is a 22.77% reduction to the left wheel, while the right one increased by 0.5%. This shows that the wear region on the right wheel is still the thread region, and no significant increment has been seen on the derailment coefficient, as shown below.

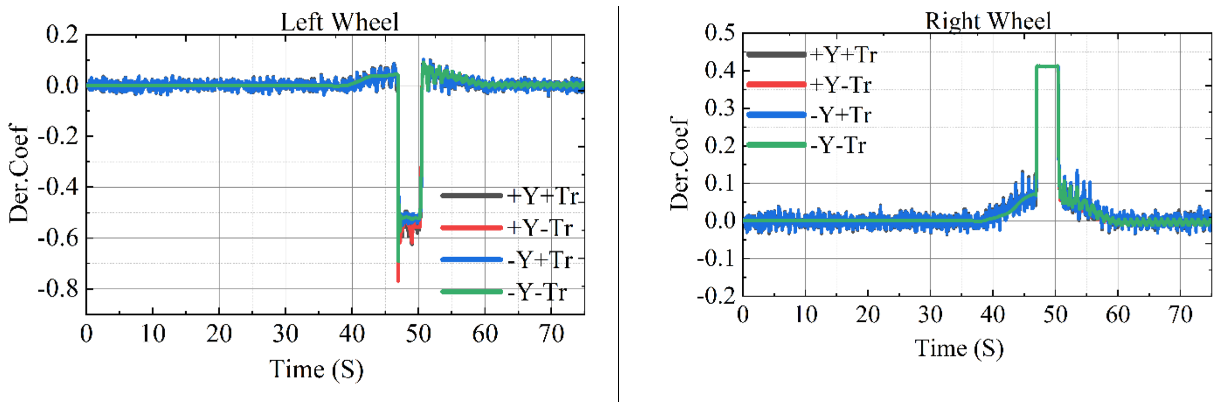

(c) (d)

Figure 5.8-Derailment Coefficient result of MC1WS1 (a) Left and (b) Right wheels 100m Curve

5.2.4. 150m curve run

The wear depth for the 150m curve radius run is found to be 0.26mm and 0.306mm for the right and left wheels, respectively, as shown below for a case of no yaw and no track irregularity (-Y-Tr) case for the left wheel while no yaw and track irregularity (-Y+Tr) case for the right wheel. This is 69.1% lower than the wear depth registered for the left wheel, while the right wheel's reduced by 60.5%. This is also a great improvement registered due to increased radius of curvature to 150m with the other factors kept constant. Unlike the previous cases, the presence of yaw resulted in a 6.7% improvement in wear depth to the right wheel.

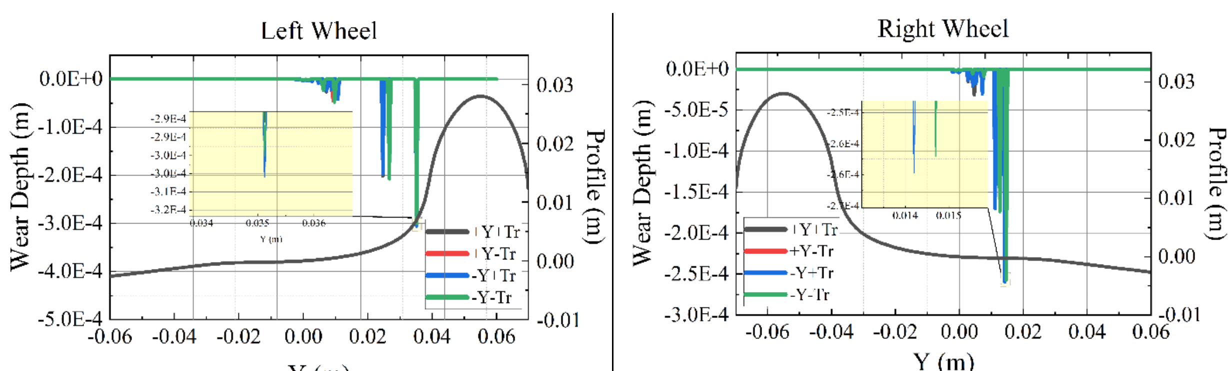

(a) (b)

Figure 5.9-Wear Depth result of MC1WS1 (a) Left and (b) Right wheels 150m Curve

On the other hand, the derailment coefficient improved for this case to 0.4 and 0.65 for the right and left wheels, respectively. This is a reduction of 16.7% and 2.44% for the left and right wheels. In this series of cases, it can be seen that the derailment coefficient is reducing steadily with a significant amount, while for the right wheel, only slight improvement is observed since the wear region hasn't yet changed.

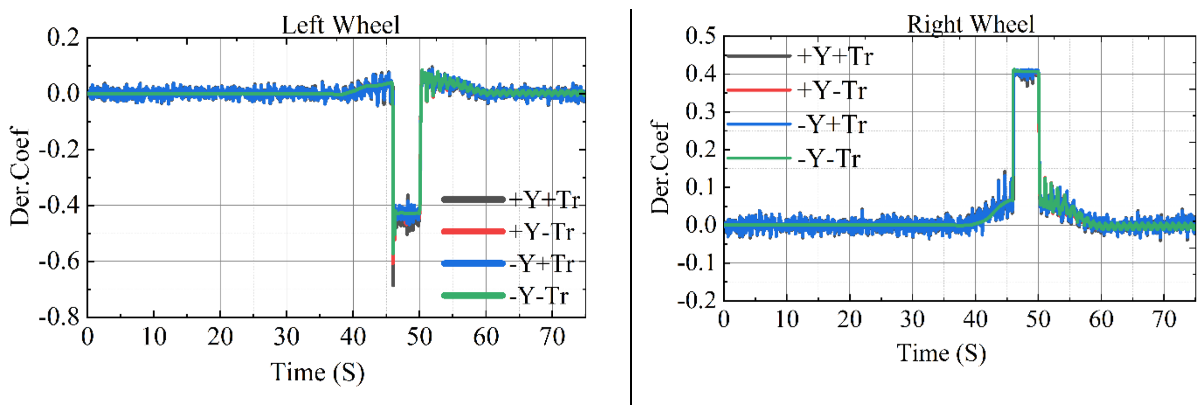

(a) (b)

Figure 5.10-Derailment Coefficient result of MC1WS1 (a) Left and (b) Right wheels 150m Curve

5.2.5. 190m curve run

Finally, for this specific scenario of curve radius variation, the wear depth improved to 0.151 and 0.1mm for the left and right wheels, respectively as shown in the figure 5.11 below. From the previous cases, this radius of curvature resulted in a 50.7% and 61.5% reduction to the wear depth, which is significantly lower and it can also be observed that the left wheel flange wear has become very much reduced. This is due to the reduction of lateral and longitudinal creep forces at the flange location when the radius of curvature increases from 50m to 190m. This is very important information that shall be considered to reduce the wear depth during the design of railway infrastructure.

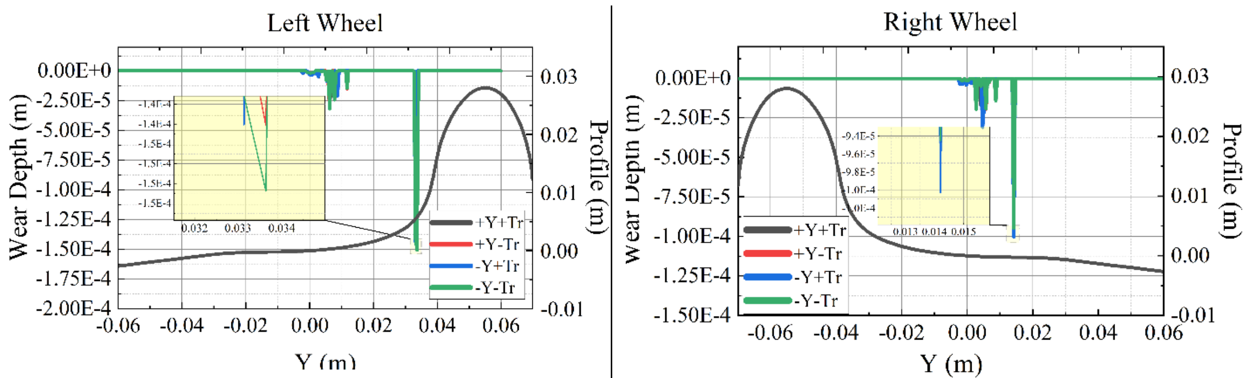

(a) (b)

Figure 5.11-Wear Depth result of MC1WS1 (a) Left and (b) Right wheels 190m Curve

On the other hand, derailment coefficient of left wheel can be seen for zero yaw with track irregularity (-Y+Tr) case increased to 0.78 (20%) and right wheel is still close to 0.41, yet still below the Nadal's stability and safety criteria and we can consider derailment is well minimized for this scenario.

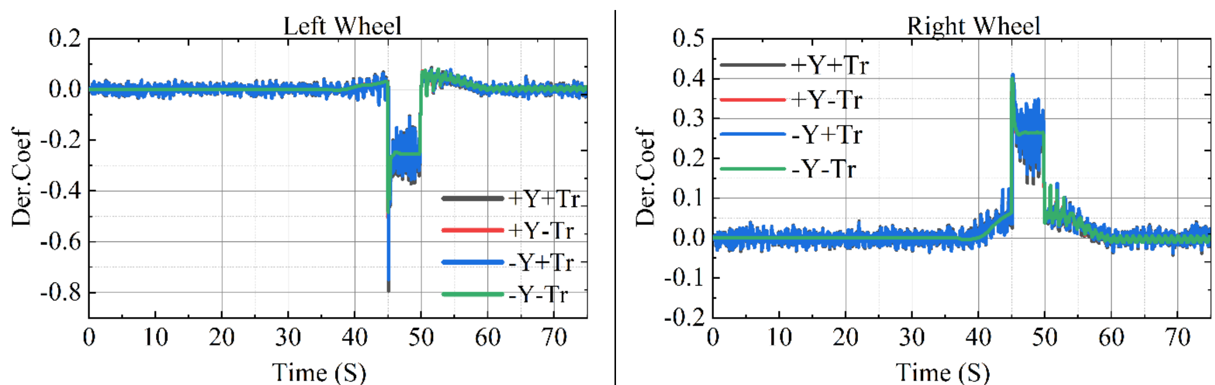

(a) (b)

Figure 5.12-Derailment coefficient result of MC1WS1 (a) Left and (b) Right wheels 190m Curve

5.2.6. Comparison of Maximum wear depth

Based on the data analyzed above, a clear picture of elevated wear depth has been viewed at the smaller radius of curvature (50m), being the highest for the left wheel since the case considers a right-hand curve during analysis. This is because of the conical construction of the railway wheel, and in order to perform the steering operation, the wheel slides to the left, causing significant flange wear damage to the left wheel of the train set. This can all be easily manifested by the maximum wear depth comparison figure 5.13 below.

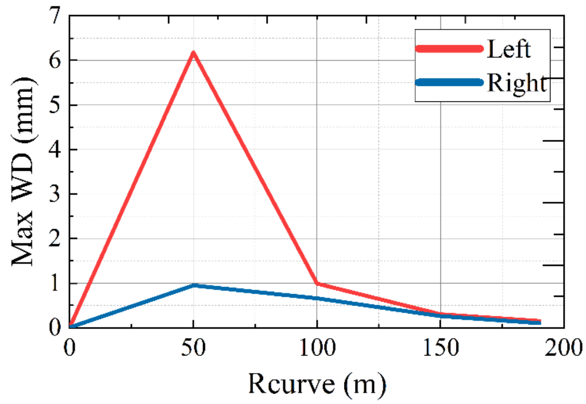

Figure 5.13-Maximum Wear depth variation for different Radiuses

5.2.7. Ride index variation

Considering the ride index, the value has been computed for each of curve variations and found to be close values between each radius variation case. Even though there are small variations due to presence of tack irregularities on all of the car bodies, the yaw damper has minimal effect on the vertical ride index. This is expected since the yaw damper is acting significantly in the lateral and longitudinal direction instead of vertical. But that doesn't mean it has no effect at all, rather not much significant as it can be seen in the figure 5.14 below.

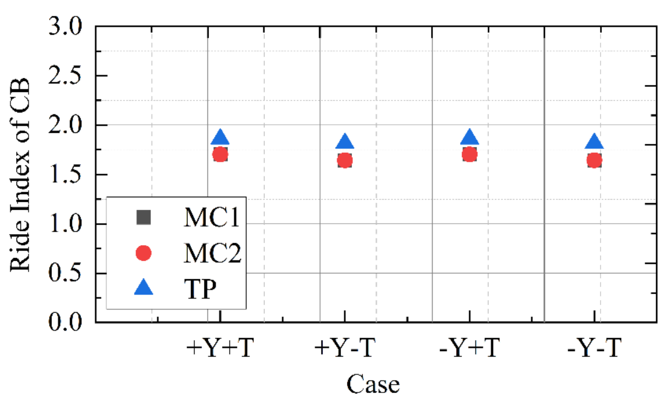

Figure 5.14-Ride index Variation for different cases of Yaw and track irregularity

The RI values were close to 1.7 at the MC1 and MC2, and 1.85 at the TP is a moderately comfortable riding experience since not much further from the boundary of recommended comfort level at 1.6 or below. It can also be seen that maximum discomfort is felt at the TP since it is the shortest car body and most articulated one. This is because turning force from the rail at curves is transmitted to the wheels through both couplings at the front and back, causing maximum slip at the wheels. This trend is also repeated in the following simulation scenarios.

5.3. Case 2: Speed Variation

In this speed variation analysis, the simulations have all been performed for 190m radius curve, 25Ms/m yaw damper, and 1km of distance with 10,000 distance factor with the variation of the train speed set at 5m/s, 10m/s, and 20m/s. This is intended to analyze the effect of speed variation on the wear depth of wheels based on varying combinations of yaw and track irregularity. Maxmimum operational speed of AALRT,i.e. 70km/hr or 19.44m/s, was used as a reference to select the speed ranges to see the trend due to high and low speed variation. Even though there are other speed values in between, selecting these values is representative for the low and higher operational cases of the trains.

5.3.1. Speed of 5m/s (18 km/hr)

For this simulation case, 5m/s has been used for the initial velocity of the vehicle, and the rest of the parameters have been made the same for the other speed variation simulations. Based on this analysis, the maximum wear depth is 0.1481mm and 0.102mm for the left and right wheels for both -Y+Tr cases, respectively. It can be seen that the existence of yaw has improved the wear depth by 5.9% and 3.8% for the left and right wheels, respectively, compared to the other cases.

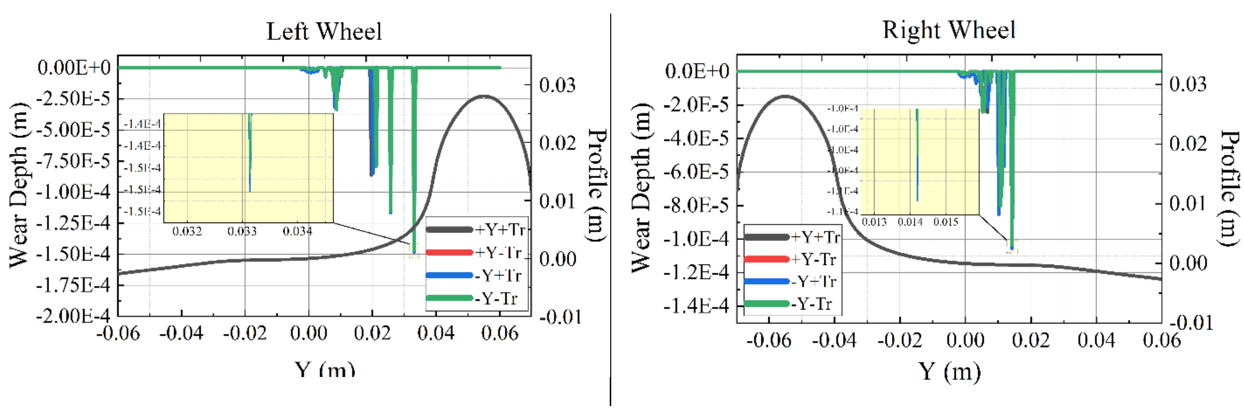

(a) (b)

Figure 5.15-Wear depth Variation for MC1WS1 (a) Left and (b) Right wheel at 5m/s speed

The maximum derailment coefficients for the right and left wheels are 0.43 and 0.4 for the left and right wheels which is way below the Nadal's safe threshold (0.8) and it is visible that the local derailment coefficients for the Yaw damper available cases are damped while the rest had local fluctuation leading to a higher local derailment coefficient at specific points as it can be demonstrated in the figure 5.16 below (indicated in blue and green).

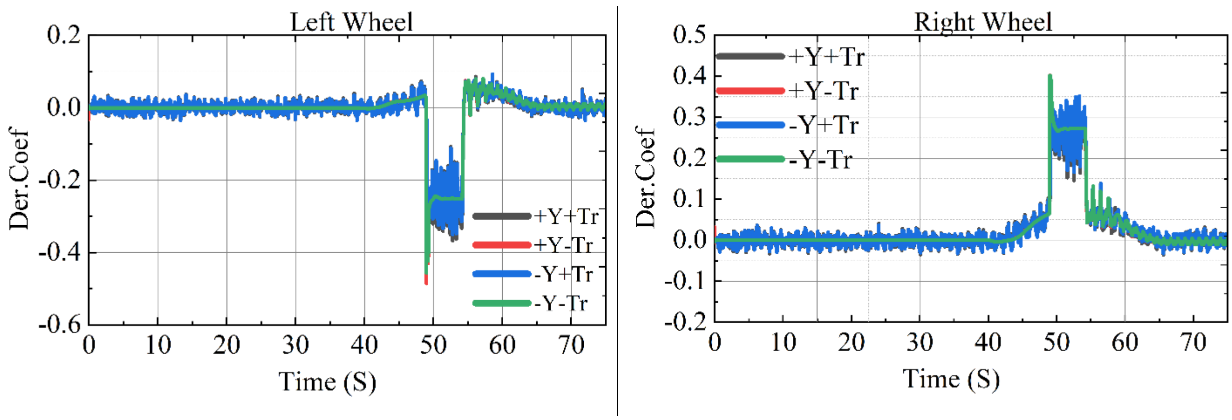

(a) (b)

Figure 5.16-Derailment Coefficient Variation for MC1WS1 (a) Left and (b) Right wheel at 5m/s speed

The ride indexes for the cases of zero yaw are the least state, fig 5.17 below. Introducing the yaw damper has elevated the ride index of the TP and MC2 vehicles, while it had a smaller increment to the MC1 compared to the others. This compared to the previous result indicates that the introduction of yaw damper increases the ride index while reducing the wheels' wear depth by damping forces leading to vibration in yaw direction. Since the values are between 2.25 and 1.5, a slight comfort loss is viewed, but acceptable comfort condition is preserved during the operation.

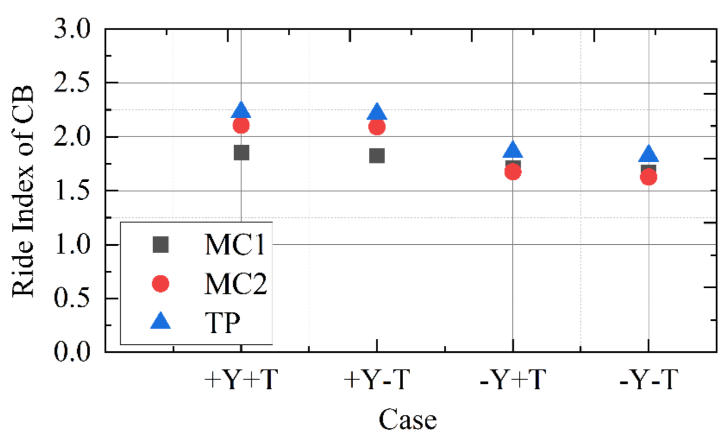

Figure 5.17-Ride Index Variation for MC1WS1 Yaw and track irregularity cases at 5m/s speed

5.3.2. Speed of 10m/s (36 km/hr)

Increasing the speed of the trainset to a higher value of 10m/s has changed the wear to 0.1507mm and 0.144mm for the case of -Y-Tr and -Y+Tr of the left wheel and 0.1003mm also for the -Y+Tr case of the right wheel. Considering same -Y+Tr case, wear depth reduced slightly for both of the wheels.

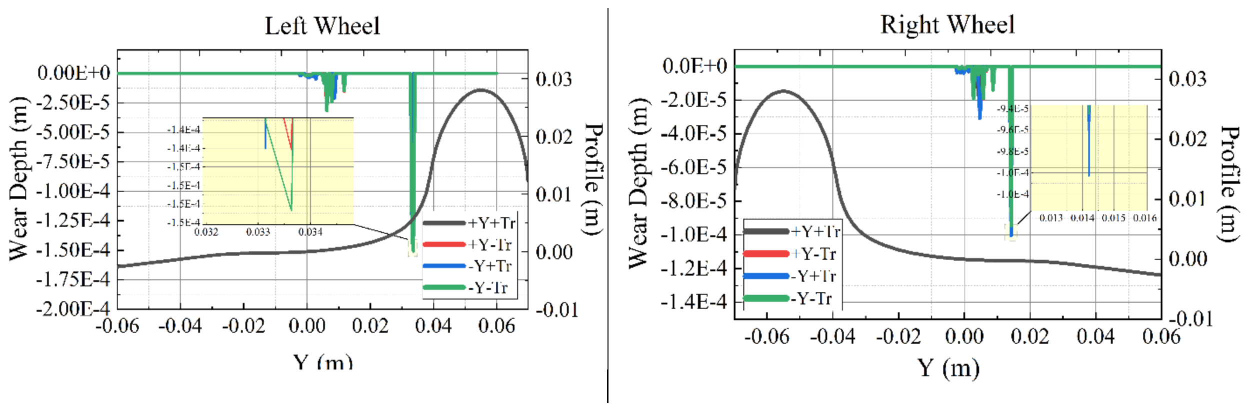

(a) (b)

Figure 5.18-Wear depth Variation for MC1WS1 (a) Left and (b) Right wheel at 10m/s speed

The derailment coefficient also increased to 0.793 and 0.41 for the left and right wheels. This is an 84.4% increment for the left wheel, and this exists due to the increased curving speed and is clearly shown that this existed on the +Y+Tr case.

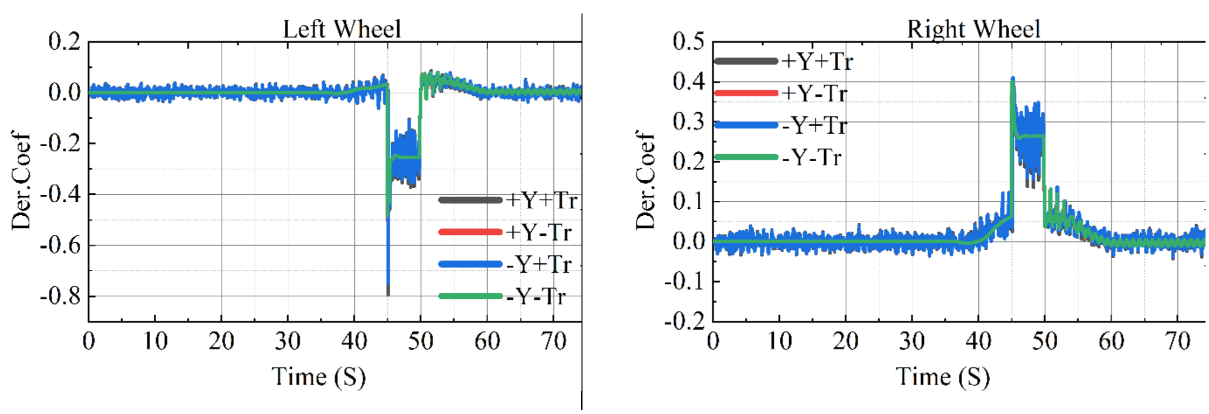

(a) (b)

Figure 5.19-Derailment Coefficient Variation for MC1WS1 (a) Left and (b) Right wheel at 10m/s speed

The ride index has not much varied for the cases with and without yaw damper but showed a slight 2.5% increment due to the existence of track irregularities. But since the values are close to the 1.6 threshold, not much comfort loss is expected during the operation of the trainset. But compared to the previous case, the ride index has improved especially for the yaw-included cases.

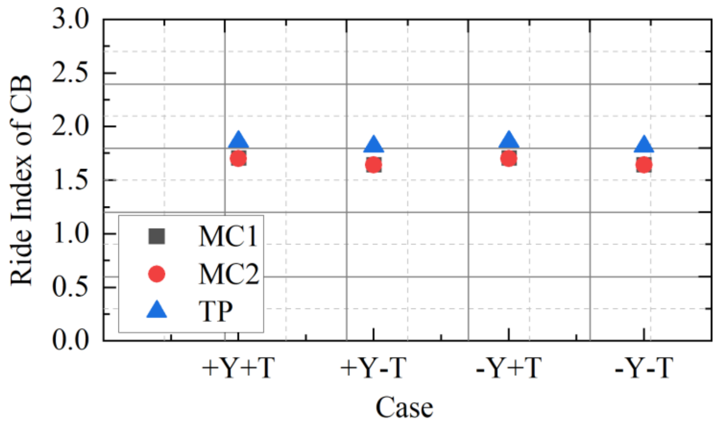

Figure 5.20-Ride index variation for different yaw and track irregularity cases at 10m/s speed

5.3.3. Speed of 20m/s (72 km/hr)

The maximum wear depth for this case has dramatically reduced to 0.1353mm and 0.0912mm for the left and right wheels showing a 6.04% and 9.07% reduction, respectively, compared to the 10m/s case. This shows that when speed increases, the wear depth decreases significantly due to the limited time to create adhesion for wear between the rail and wheel materials. This reduces the probability there might exist defects on the wheel and rail materials that disrupt this effect.

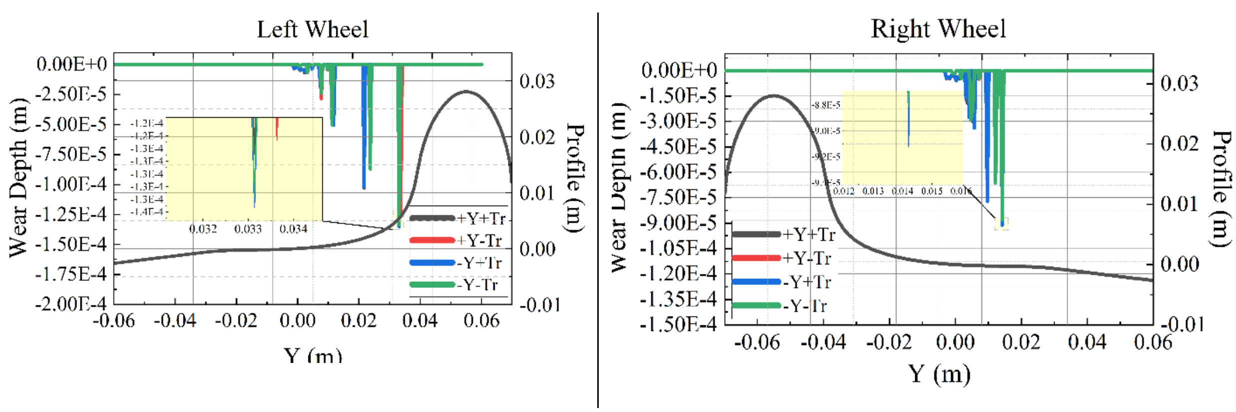

(a) (b)

Figure 5.21-Wear depth Variation for MC1WS1 (a) Left and (b) Right wheel at 20m/s speed

On the contrary, the derailment coefficient of the left wheel increased beyond the safe limit to 0.872 by the right wheel staying at a similar region as before. This show that the left wheel's maximum derailment coefficient is steadily increasing as the wheel's speed increases while the right wheel's not changing much. Yet since the value is not much distant from Nadal's limit, certain derailment might not be expected during the actual operation since the trainset reduces its speed when approaching tight curves.

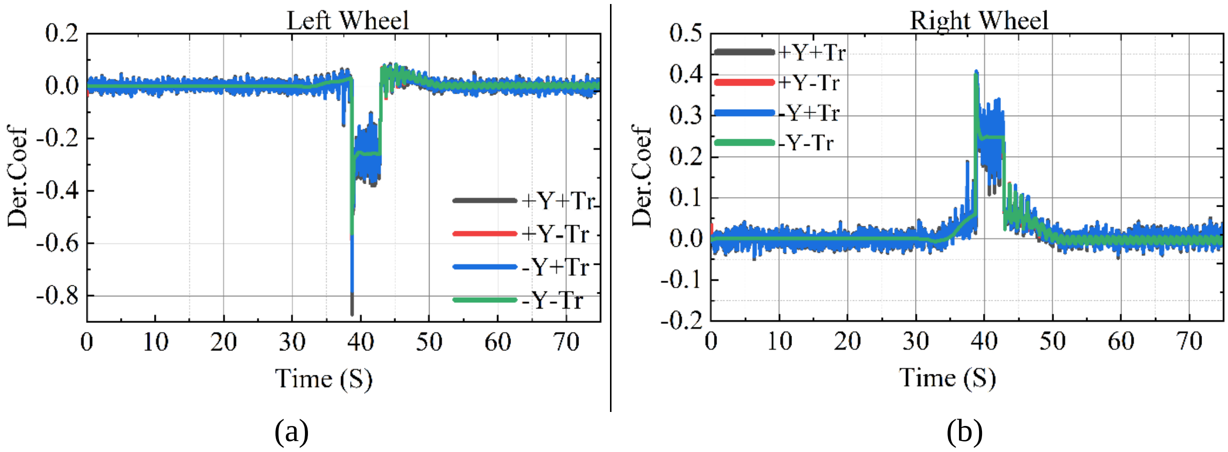

Figure 5.22-Derailment coefficient Variation for MC1WS1 (a) Left and (b) Right wheel at 20m/s speed

The ride index of the TP and MC1 also increases greatly when the speed increases to the stated value for this case, when the yaw damper is introduced while it stays in the safe zone close to 1.6 while no yaw damper is applied in the region. As a result, significant discomfort might be felt when the train passes through the line with 20m/s based on the findings indicated in the figure 5.23 below, since RI >2.5.

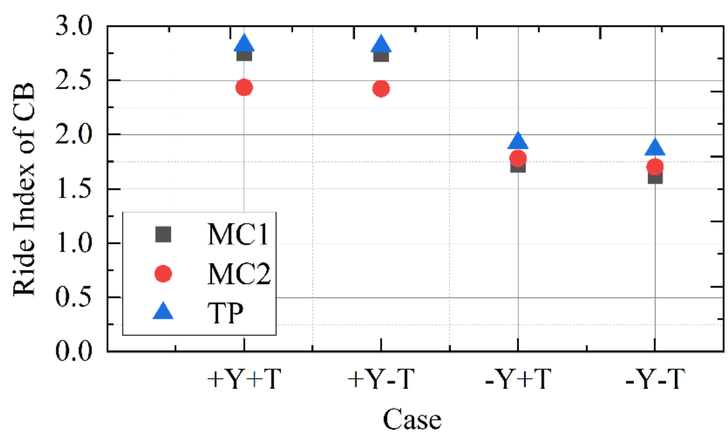

Figure 5.23-Ride index variation for different Yaw and track irregularity cases at 20m/s speed

5.3.4. Comparison of Maximum Wear depth

As explained earlier and shown in the figure 5.24 below, the maximum wear depth for the speed variation for the case of –Y+Tr started decreasing for both wheels when the speed of the vehicle increased. This is because adhesive force is minimum when speed is increased which has a direct influence to the wear depth. Note shall also be taken that we are using a wide curve for simulation and this shows that there is a specific speed limit that the maximum wear depth is seen for a specific radius of curvature for case of of the left wheel (more loaded for right hand curve) as this wouldn't have been the case if the radius of curvature is increased or decreased from what it is now. On the other hand, the derailment coefficient for the left wheel and the ride index for the car bodies showed a significant increase when the speed of the rail vehicle increased due to increment of lateral forces arrsing from centrifugal force effect at curvatures directly related to speed. Also the wear depth is different for right and left wheel since the curve is right hand curve and higher flange wear is expected on the left wheel than the right wheel. This si a similar trend on the other cases as well. In addition, the value can be seen to be higher at low speeds because of the chance to have more of adhesive wear to occure since plenty of time is available for the high load to be concentrated in the small contact patch and easier material removal during movment.

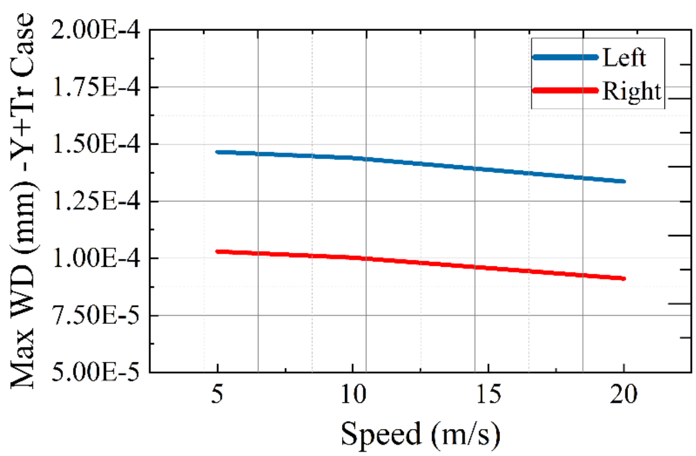

Figure 5.24-Maximum wear depth due to different speed variation cases

5.4. Case 3: Yaw damper variation

The comparison in this section is based on 10m/s speed, 190m radius of curvature line of 1km distance considering 10,000 distance factor by varying the yaw damper value between No yaw damper, 25MNs/m and 40MNs/m. This will identify the effect of increasing or decreasing the yaw damper value demonstrated on the rail vehicle's wear depth, derailment coefficient and ride index.

As referred to earlier to the 10m/s speed simulation, the wear depth and derailment coefficient of the right and left wheels and the ride index for the car bodies of 25MNs/m and no yaw case have already been computed and results described. As a result, the next task will be expressing the results of 40MNs/m result and making the comparison.

5.4.1. Yaw damper of 40MNs/m

The yaw damper being increased to a value of 40MNs/m has resulted in a decrement of wear depth of 0.13mm and a dramatic elevation of 0.85mm for the left and right wheels, respectively, as it can be seen in the figure 5.25 below. This is a 13.3% reduction for the left wheel and a significant increment for the right wheel for the yaw and no track irregularity case.

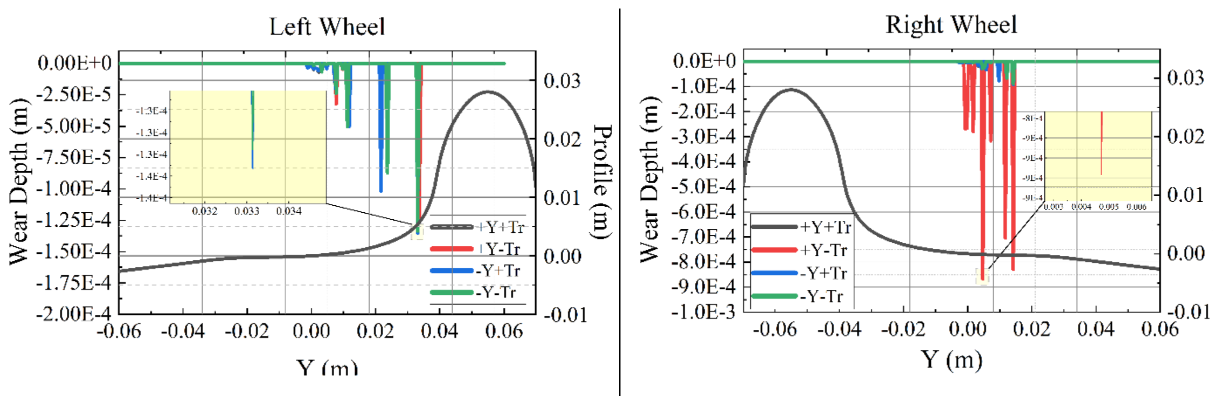

(a) (b)

Figure 5.25-Wear depth Variation for MC1WS1 (a) Left and (b) Right wheel at 40MNs/m Yaw

On the other hand, the derailment coefficient stayed leveled up as that of the 25 MNs/m case while increasing by only 2.5% for the 40 MNs/m case. Yet here also, the derailment coefficients are in the safe region as they are close to the threshold value of 0.8 as specified by the Nadal stability criteria.

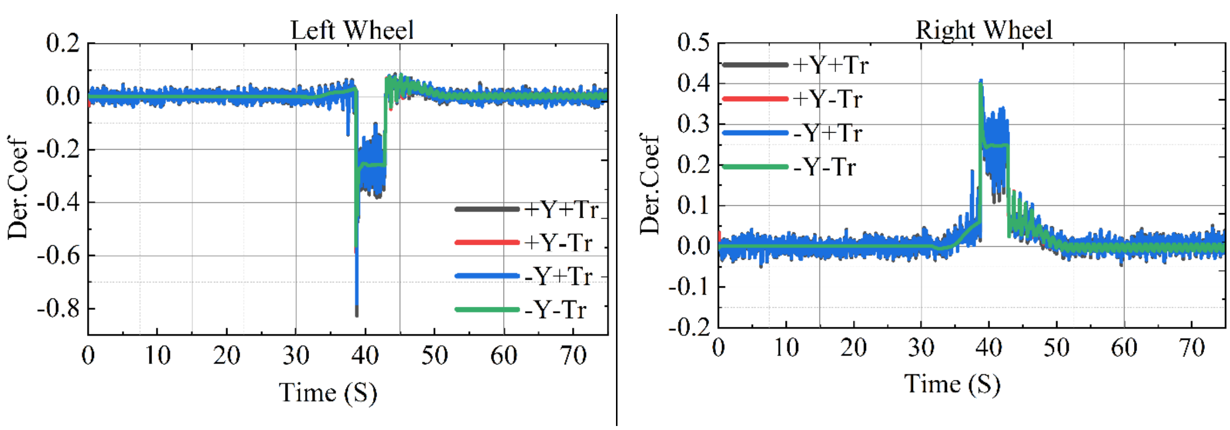

(a) (b)

Figure 5.26-Derailment coefficient Variation for MC1WS1 (a) Left (b) Right wheel at 40MNs/m Yaw

The ride index on the reverse is elevated for the yaw-included cases reaching up to 2.8, while without yaw cases were kept close to 0.75 area where not much discomfort is felt. This a clear indicator that the increase in yaw damper capacity increased the wear depth of the right wheel, kept the derailment coefficient, and elevated the rail vehicle's ride index, as seen in the figure 5.27.

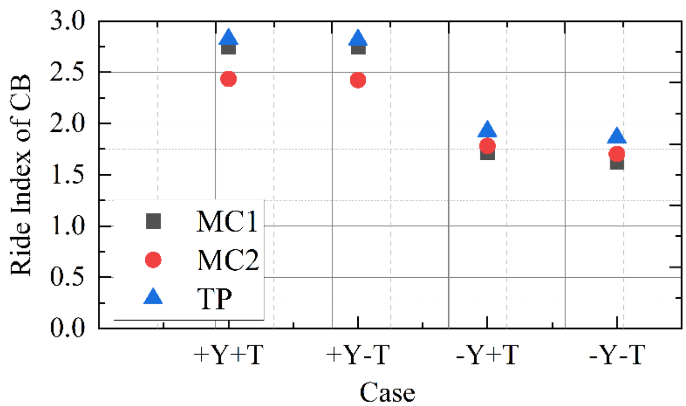

Figure 5.27-Ride index variation for Different Yaw damper values

5.4.2. Comparison of Maximum Wear depth

Based on the above analysis and below figure 5.28, it can be observed that the increment in the yaw damping value resulted in reduced wear depth for the left wheel of the rail vehicle by making the trainset more adaptable to the yaw effect and brought improvement yet resulting in more discomfort based on the ride index deterioration, shown in the figure 5.27, to the passengers as chances of vibration or shock being transmitted to the car bodies and the passengers is higher when the damper becomes higher (more rigid). Yet, the wheelsets will have better yaw negotiating capability shown as a decrement of the wear depth.

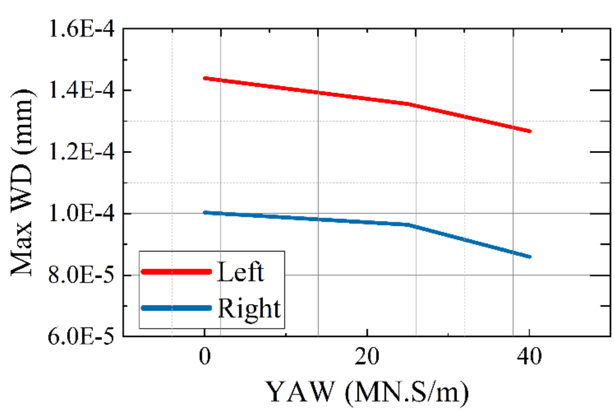

Figure 5.28-Maximum wear depths due to Yaw damper value variation

Chapter 6 – Conclusion, Recommendations, and Future work

As explained in previous chapters, the intention of the research was to investigate the effect of the yaw damper and track irregularity manifested in terms of wear depth and vehicle dynamic behavior, i.e., Derailment coefficient and Ride index by considering factors like curve radius, travel speed, and Yaw damper value variation. Based on the analysis performed, it has been found that the radius of curvature increment resulted in reduced wear depth due to reduction in creepe and creep forces accompanied by reduced derailment coefficient and improved ride index which are directly related to lateral force reduction. The yaw damper inclusion also didn’t much bring change the ride index at low speeds since vertical ride index case has been considered for the analysis but its higher value resulted in higher derailment coefficient and ride index with reduced wear depth. The track irregularity included results also introduced some noise to the derailment coefficient plot, bringing a slight increment to the ride index.

The speed increment on the other hand brought a reduced wear depth due to the reduced time for adhesion wear to occur, yet resulting in more flange wear to the left wheel since the test line was a right hand curve and specific speed limit is expected for each radius of curvature to result in maximum wear depth, for this specific research case 10m/s for 190m radius. It also brought an increment to the derailment coefficient and deteriorating ride index due to lateral forces increased especially at curves.

Introducing a yaw damper and increasing its value at low speed reduced wear depth, slightly increasing the derailment coefficient thereby significantly increasing the ride index due to the rigidity of wheelsets in the lateral direction. On the other hand, only a slight increment on ride index and derailment coefficient has been seen when track irregularity has been included in the analysis since most of it will be damped by the primary and secondary suspension of the rail vehicle. Yet it introduced significant disturbance when combined with factors like yaw.

Finally, validation step revealed that the devised methedology resulted close match for the actual wear data collected, and AALRT can use this system to analyze and predict the wear profile generation of train wheels so that they can improve their maintenance process by focusing on mitigating factors that result in the highest wear and vehicle dynamic issues, including discomfort and increased derailment coefficients so that the best service can be availed for their passengers.

Future Work: - Further research can be performed to analyze the specific case of TP wheel wearing for articulated type of trainsets like AALRT and validate the use of different new and improved wear analysis methodologies like USFD for this application and other non-hertzian contact modeling techniques to get a more refined result for the process. Other parameters like loading, environmental and operational condition that cause higher wear depth, discomfort, and dangerous derailment conditions could also be analyzed and incorporated in up coming reseachs where their effects can be reasoned out in detail, and priority of maintenance activities can be focused on minimizing these factors to improve the service life of railway wheels for AALRT as well as other railway operators.

References

[1] "Trains: A history | Institute for Transportation." https://intrans.iastate.edu/news/trains-a-history/ (accessed Jul. 04, 2022).

[2] "History of Railroad - Development of Rail Transport." http://www.trainhistory.net/railway-history/railroad-history/ (accessed Jul. 04, 2022).

[3] "A brief history of the railways." https://www.raildiscoveries.com/the-discovery-blog/2018/september/a-brief-history-of-the-railways/ (accessed Jul. 04, 2022).

[4] "Railways in Ethiopia." https://www.sinfin.net/railways/world/ethiopia.html (accessed Jul. 04, 2022).

[5] "Cities100: Addis Ababa - Sub-Saharan Africa's First Light-Rail Train - C40 Cities." https://www.c40.org/case-studies/cities100-addis-ababa-sub-saharan-africa-s-first-light-rail-train/ (accessed Jul. 04, 2022).

[6] "Light Rail Transit in Addis Ababa|Centre For Public Impact (CPI)." https://www. Centre forpublicimpact.org/case-study/light-rail-transit-in-addis-ababa (accessed Jul.04 ,2022).

[7] "green-line-east-west.jpg (1200×900)." https://dynamic-media-cdn.tripadvisor.com/media/photo-o/14/19/14/50/green-line-east-west.jpg?w=1200&h=-1&s=1(accessed Jul.04,2022).

[8] "Three major challenges for the railway market in 2021 | Segula Technologies." https://www.segulatechnologies.com/en/news/three-major-challenges-for-the-railway-market-in-2021/ (accessed Jul. 04, 2022).

[9] "Well-to-wheel (wake/wing) GHG intensity of motorised passenger transport modes – Charts – Data & Statistics - IEA." https://www.iea.org/data-and-statistics/charts/well-to-wheel-wake-wing-ghg-intensity-of-motorised-passenger-transport-modes (accessed Jul. 04, 2022).

[10] N. K. Myshkin and I. G. Goryacheva, "Tribology: Trends in the half-century development," *Journal of Friction and Wear*, vol. 37, no. 6, pp. 513–516, Nov. 2016, doi: 10.3103/S106836661606009X.

[11] F. Braghin, S. Bruni, and R. Lewis, "Railway wheel wear," in *Wheel-Rail Interface Handbook*, Elsevier Ltd, 2009, pp. 172–210. doi: 10.1533/9781845696788.1.172.

[12] F. Braghin, S. Bruni, and R. Lewis, "Railway wheel wear," in *Wheel-Rail Interface Handbook*, Elsevier Ltd, 2009, pp. 172–210. doi: 10.1533/9781845696788.1.172.

[13] J. Tondo and J. Sekasi, “Capacity assessment of railway stations: a case of Addis Ababa light rail’s Menilik Square Station,” 2021. [Online]. Available: https://ssrn.com/abstract=3868579

[14] G. quan Tao, X. Du, H. ji Zhang, Z. feng Wen, X. song Jin, and D. bin Cui, “Development and validation of a model for predicting wheel wear in high-speed trains,” *Journal of Zhejiang University: Science A*, vol. 18, no. 8, pp. 603–616, Aug. 2017, doi: 10.1631/jzus.A1600693.

[15] R. Enblom and M. Berg, “Simulation of railway wheel profile development due to wear influence of disc braking and contact environment,” in *Wear*, Mar. 2005, vol. 258, no. 7–8, pp. 1055–1063. doi: 10.1016/j.wear.2004.03.055.

[16] A. Tsujimoto *et al.*, “Wear of resin composites: Current insights into underlying mechanisms, evaluation methods and influential factors,” *Japanese Dental Science Review*, vol. 54, no. 2. Elsevier Ltd, pp. 76–87, May 01, 2018. doi: 10.1016/j.jdsr.2017.11.002.

[17] H. Pourasiabi, M. Babazadeh, and H. Pourasiabi, “Wear characteristics of ADIs; A Comprehensive Review on Mechanisms and Effective Parameters,” *Article in Journal of Basic and Applied Research International*, vol. 3, no. 2, pp. 646–656, 2013, [Online]. Available: www.textroad.com

[18] R. Lewis and U. Olofsson, *Wheel-rail interface handbook*. CRC Press, 2009.

[19] H. Soleimani and M. Moavenian, “Tribological Aspects of Wheel–Rail Contact: A Review of Wear Mechanisms and Effective Factors on Rolling Contact Fatigue,” *Urban Rail Transit*, vol. 3, no. 4, pp. 227–237, Dec. 2017, doi: 10.1007/s40864-017-0072-2.

[20] S. Pradhan, A. K. Samantaray, and R. Bhattacharyya, “Prediction of railway wheel wear and its influence on the vehicle dynamics in a specific operating sector of Indian railways network,” *Wear*, vol. 406–407, pp. 92–104, Jul. 2018, doi: 10.1016/j.wear.2018.03.020.

[21] A. Wickens, “Fundamentals of Rail Vehicle Dynamics: Guidance and Stability,” 2005.

[22] J. Piotrowski and W. Kik, “A simplified model of wheel/rail contact mechanics for non-Hertzian problems and its application in rail vehicle dynamic simulations,” *Vehicle System Dynamics*, vol. 46, no. 1–2, pp. 27–48, Jan. 2008, doi: 10.1080/00423110701586444.

[23] E. Vollebregt, “Detailed wheel/rail geometry processing with the conformal contact approach,” *Multibody System Dynamics*, vol. 52, no. 2, pp. 135–167, Jun. 2021, doi: 10.1007/s11044-020-09762-w.

[24] S. (Simon) Iwnicki, *Handbook of railway vehicle dynamics*. CRC/Taylor & Francis, 2006.

[25] "Archard Wear Equation - About Tribology." https://www.tribonet.org/wiki/archard-wear-equation/ (accessed Jul. 12, 2022).

[26] S. Chen, C. Casanueva, S. Hossein-Nia, S. Stichel, *Modified Wear Modelling for Fast Wear Calculation.* In: Orlova, A., Cole, D. (eds) Advances in Dynamics of Vehicles on Roads and Tracks II. IAVSD 2021. Lecture Notes in Mechanical Engineering. Springer, Cham, 2022, https://doi.org/10.1007/978-3-031-07305-2_56

[27] Y. Q. Sun, N. K. Mandal, and Q. Wu, "Rail wear modelling Rail joints View project International benchmarking of longitudinal train dynamics simulators View project." [Online]. Available: https://www.researchgate.net/publication/330913874

[28] F. Braghin, R. Lewis, R. S. Dwyer-Joyce, and S. Bruni, "A mathematical model to predict railway wheel profile evolution due to wear," *Wear*, vol. 261, no. 11–12, pp. 1253–1264, Dec. 2006, doi: 10.1016/j.wear.2006.03.025.

[29] T. Karis, *Correlation between Track Irregularities and Vehicle Dynamic Response Based on Measurements and Simulations*. KTH Royal Institute of Technology, 2018.

[30] B. An; D. Ma, P. Wang,J. Zhou, R. Chen, J. Xu, D. Cui, "Assessing the fast non-Hertzian methods based on the simulation of wheel–rail rolling contact and wear distribution," *Proceedings of the Institution of Mechanical Engineers, Part F: Journal of Rail and Rapid Transit*, vol. 234, no. 5, pp. 524–537, May 2020, doi: 10.1177/0954409719848592.

[31] Y. Ye, Y. Sun, D. Shi, B. Peng, and M. Hecht, "A wheel wear prediction model of non-Hertzian wheel-rail contact considering wheelset yaw: Comparison between simulated and field test results," *Wear*, vol. 474–475, Jun. 2021, doi: 10.1016/j.wear.2021.203715.

[32] J. Auciello, M. Ignesti, M. Malvezzi, E. Meli, and A. Rindi, "Development and validation of a wear model for the analysis of the wheel profile evolution in railway vehicles," *Vehicle System Dynamics*, vol. 50, no. 11, pp. 1707–1734, Nov. 2012, doi: 10.1080/00423114.2012.695021.

[33] J. Pombo *et al.*, "Development of a wear prediction tool for steel railway wheels using three alternative wear functions," *Wear*, vol. 271, no. 1–2, pp. 238–245, May 2011, doi: 10.1016/j.wear.2010.10.072.

[34] R. Luo, H. Shi, W. Teng, and C. Song, "Prediction of wheel profile wear and vehicle dynamics evolution considering stochastic parameters for high-speed train," *Wear*, vol. 392–393, pp. 126–138, 2017, doi: 10.1016/j.wear.2017.09.019.

[35] G. Tao, Z. Wen, Q. Guan, X. Zhao, Y. Luo, and X. Jin, "Locomotive wheel wear simulation in complex environment of wheel-rail interface," *Wear*, vol. 430–431, pp. 214–221, Jul. 2019, doi: 10.1016/j.wear.2019.05.012.

[36] M. A. Abdullah, M. A. A. Solahudin, S. A. Shamsudin, A. E. Mohan, and H. A. Habeeb, "Railway Wheel Wear Analysis," 2020.

[37] M. Asplund, M. Palo, S. Famurewa, and M. Rantatalo, "A study of railway wheel profile parameters used as indicators of an increased risk of wheel defects," *Proceedings of the Institution of Mechanical Engineers, Part F: Journal of Rail and Rapid Transit*, vol. 230, no. 2, pp. 323–334, Feb. 2016, doi: 10.1177/0954409714541953.

[38] B. Zhu, J. Zeng, D. Zhang, and Y. Wu, "A non-Hertzian wheel-rail contact model considering wheelset yaw and its application in wheel wear prediction," *Wear*, vol. 432–433, Aug. 2019, doi: 10.1016/j.wear.2019.202958.

[39] S. Sui, K. Wang, L. Ling, and Z. Chen, "Effect of wheel diameter difference on tread wear of freight wagons," *Engineering Failure Analysis*, vol. 127, Sep. 2021, doi: 10.1016/j.engfailanal.2021.105501.

[40] U. Spangenberg, R. D. Fröhling, and P. S. Els, "The effect of rolling contact fatigue mitigation measures on wheel wear and rail fatigue," *Wear*, vol. 398–399, pp. 56–68, Mar. 2018, doi: 10.1016/j.wear.2017.11.012.

[41] N. Zhang, J. Zhang, L. Lu, M. Zhang, D. Zeng, and Q. Song, "Wear and friction behavior of austempered ductile iron as railway wheel material," *Materials and Design*, vol. 89, pp. 815–822, Jan. 2016, doi: 10.1016/j.matdes.2015.10.037.

[42] A. B. Rezende *et al.*, "Wear behavior of bainitic and pearlitic microstructures from microalloyed railway wheel steel," *Wear*, vol. 456–457, Sep. 2020, doi: 10.1016/j.wear.2020.203377.

[43] Y. Lyu, Y. Zhu, and U. Olofsson, "Wear between wheel and rail: A pin-on-disc study of environmental conditions and iron oxides," *Wear*, vol. 328–329, pp. 277–285, Apr. 2015, doi: 10.1016/j.wear.2015.02.057.

[44] "Types of Trains - BayRail Alliance." https://www.bayrailalliance.org/types_trains/ (accessed Jul. 14, 2022).

[45] R. M. M. Orsino and T. A. Hess-Coelho, "A contribution on the modular modelling of multibody systems," *Proceedings of the Royal Society A: Mathematical, Physical and Engineering Sciences*, vol. 471, no. 2183, Nov. 2015, doi: 10.1098/rspa.2015.0080.

[46] S. Bair, "The contribution of roller compliance to elastohydrodynamic traction Development, Fabrication and Delivery of an Ultra-High-Pressure Viscometer View project," 2016. [Online]. Available: https://www.researchgate.net/publication/288743452

[47] "What is degrees of freedom (mechanics)?" https://www.techtarget.com/whatis/definition/degrees-of-freedom (accessed Apr. 21, 2023)

[48] F. Dula, *Investigating the wheel wear of Addis Ababa Light Rail Transit (AALRT)*. Addis Ababa University, Addis Ababa Institute of Technology, 2017.

[49] G. Eyob, *Analyzing Wear Condition of Wheel on Crossing a Case of Addis Ababa Light Rail Transit Line*. Addis Ababa University, Addis Ababa Institute of Technology, 2018.

[50] S. Kizanye, *Investigation of Wheel Wear Behaviors Subjected Under Dry and Wet Loading Conditions: A Case study of Addis Ababa Light Rail Transit*. Addis Ababa University, Addis Ababa Institute of Technology, 2020.

Appendices

Appendix – 1:

Table A1-Sample re-profiling History of AALRT Trains

Criteria	
New Diameter (mm)	660
Worn Dia. limit (mm)	580

	Date	Train No	Status of Mesur.	MC1				TP				MC2			
				WS1		WS2		WS3		WS4		WS5		WS6	
				L	R	L	R	L	R	L	R	L	R	L	R
2021			Before	639.29	640.94	641.27	641.99	621.1	620.92	618.98	619.12	639.26	639.66	638.76	636.79
	Dec-21	121	After	638.58	637.72	640.36	640.09	604.46	604.47	602.51	602.42	638.32	638.34	637.1	636.84
			Before	636.28	636.76	637.23	636.98	632.26	631.88	631.7	631.28	641.48	640.44	642.25	642.4
	Jul-21	108	After	635.29	634.76	634.47	634.86	614.5	614.67	614.81	614.75	639.64	639.99	641.55	641.32
			Before	643.02	643.03	640.83	641.44	594.28	594.63	594.57	594.84	642.97	642.42	642.43	642.3
	Jul-21	110	After	641.36	641.45	639.47	639.6					641.4	641.67	641.27	641.24
			Before	643.12	643.54	643.64	643.67	637.2	637.43	637.85	638.27	643.64	645.28	643.58	643.55
	Jul-21	101	After	642.25	642.2	641.65	641.78	620.62	620.71	621.36	621.47	641.9	641.52	641.78	642.02
			Before	638.77	638.1	638.06	638.8	649.28	649.34	648.88	649	637.36	638.06	636.52	637.07
	Jul-21	102	After	636.53	637.13	637.33	636.75	646.25	646.27	646.38	646.56	635.88	635.95	634.85	634.77
			Before	642.53	642.94	641.45	641.74	618.24	618.25	620.63	620.87	644.27	643.84	643.19	642.64
	Jul-21	104	After	639.03	639.16	639.53	640.18	598.59	598.79	598.55	598.5	641.03	641.4	640.58	641.29
			Before	646.82	648.18	648.12	647.64	599.89	599.76	597.27	598.33	647.17	648.03	648.52	646.65
	Apr-21	114	After	643.44	643.21	644.48	644.4					643.57	643.68	643.39	643.15
			Before	651.34	651.83	652.34	652.54	651.63	651.27	650.76	649.68	652.85	652.08	652.79	652.26
	Apr-21	205	After	649.72	649.38	650.82	651.18					650.01	650.93	649.94	650.75
			Before	648.02	648.44	647.2	648.64	639.46	639.58	655.82	656.89	649.22	648.66	647.48	647.51
	Mar-21	105	After	643.73	643.66	642.09	642.57	637.01	637.23	638.72	638.89	644.82	644.36	643.64	644.01
			Before	648.91	647.31	645.61	646.89	632.48	632.24	631.51	631.35	647.31	649.3	648.61	647.06
	Mar-21	111	After	642.6	642.5	641.64	641.42	628.46	628.48	627.81	627.95	642.32	642.36	643.55	643.33
			Before	648.85	647.99	648.81	647.58	655.12	654.84	655.16	655.29	653.4	653.32	653.22	652.94
	Mar-21	201	After												
			Before	653.95	653.93	653.68	653.41	653.7	655.05	655.09	654.99	654.83	655.07	655.26	655.04
	Feb-21	214	After	653.26	653.24	652.59	653.12	652.43	652.35	654.26	654.28	652.05	652.97	652.38	652.83
			Before	653.22	652.26	651.85	651.72	631.9	631.9	631.55	632.53	628.65	628.88	624.91	624.8
	Feb-21	209	After	650.63	651.08	650.91	650.99	630.7	631.06	630.03	629.26	626.46	627.22	622.82	623.3

Appendix – 2:

Table A2-Sample flange Thickness Measurement

Criteria	
New Flange thickness (mm)	24
Worn Flange limit (mm)	15

Train 201													
Date		MC1				TP				MC2			
		WS1		WS2		WS3		WS4		WS5		WS6	
		L	R	L	R	L	R	L	R	L	R	L	R
2019	Jan-19												
	Feb-19												
	Mar-19												
	Apr-19	21.95	21.75	22.25	22.65	20.9	20.7	20.45	21.05	22.1	22.7	21.8	22.25
	May-19	22	22	22.5	22.8	20.85	20.8	20.45	21.1	23	23	23	23
	Jun-19	21.9	21.9	22.5	22.8	20.7	20.85	20.5	20.75	22.95	23	23	23
	Jul-19	21.7	21.75	22.5	22.7	20.5	21.05	20.45	20.4	22.7	22.95	22.95	23
	Aug-19	21.7	21.85	22.45	22.8	20.45	21.7	20.4	20.95	22.85	22.8	22.8	22.85
	Sep-19	21.5	22.5	23	23	21.25	21.15	21.1	21.4	23	23	23	23
	Oct-19	22	22	23	23	20.6	20.4	20.6	20.95	23	22.95	22.9	23
	Nov-19	22.05	22	23	23	20.7	20	20.55	20.95	22.9	22.95	22.85	23
	Dec-19	22	22	23	23	20.45	20.2	20.25	20.7	23	23	23	23
2020	Jan-20	21.85	21.8	21.7	21.75	20.3	19.95	19.9	19.95	21.85	21.85	21.9	21.85
	Feb-20	22.2	22.1	23	23	20.55	20.4	20.45	20.75	23	23	23	23
	Mar-20	22.15	21.85	23	23	20.6	20.4	20.35	20.6	23.05	23.2	23	23
	Apr-20	22.05	22.35	23	23	20.7	20.45	20.45	20.85	23	23	23	23
	May-20	23	23	23	23	20.6	20.1	20.35	20.6	22.7	22.45	22.1	22.5
	Jun-20	22.6	22.4	23	23	20.65	20	20.2	20.65	23	23	23	23
	Jul-20	23	23	23	23	20	20	20.1	20.2	22.3	22.3	22.1	22.9
	Aug-20	22	22	23	23	20	20	20.5	20	23	23	23	23
	Sep-20												
	Oct-20	22	22	23	23	20	20	20.3	20.7	23	23	23	23
	Nov-20	23	23	23	23	19.7	20.15	20.15	20.7	23	23	23	23
	Dec-20	22.1	22.1	23	23	20.45	20.35	20.15	20.65	23	23	23	23
2021	Jan-21	22.15	21.2	23	23	20.05	20.1	20.15	20.55	23	23	23	23
	Feb-21	22.45	22.5	23	23	20.3	20.35	20.15	20.15	23	23	23	23
	Mar-21	22.65	21.15	23	22.65	20.25	19.95	19.9	20.4	23	23	23	23
	Apr-21	21.95	21.05	23	22.95	20.45	20.35	20.35	20.4	23	23	23	23
	May-21	22.15	21.25	23	22.75	20.2	20.4	20.55	20.4	23	23	23	23
	Jun-21	22.05	21.45	20.15	20.4	19.8	20.35	19.9	20.4	23	23	23	23
	Jul-21	22.25	21.75	22.6	23	20.05	19.65	19.6	20.25	23	23	23	23
	Aug-21	20.5	21.3	22.25	22.85	20.05	19.65	19.7	20.15	23	23	23	23
	Sep-21	20.65	20.9	22.15	22.75	19.65	19.55	19.75	20.25	23	23	22.95	23
	Oct-21	20.75	21.25	22.35	23	19.7	19.6	19.4	20.25	20.75	22.2	19.6	21.3
	Nov-21	21	21	22	22.8	19.55	19.4	19.7	20.35	23	23	23	23
	Dec-21	22.7	22.75	22.55	22.9	20	19.45	19.6	20	23	23	23	23

Appendix – 3:

Kalker's Hertzian creep coefficients table [46]

Materials	G/GPa	σ	$C_{11}\left(\frac{a}{b}=1\right)$	$C_{22}\left(\frac{a}{b}=0.62\right)$	$C_{23}\left(\frac{a}{b}=0.62\right)$
Steel	78	0.30	4.34	3.20	1.08
Titanium	45	0.36	--	3.24	1.12
SiC	179	0.16	--	--	--
SiN	127	0.27	--	--	--
SiC/SiN	149	0.225	4.05	--	--

	C_{11}			C_{22}			C_{23}		
a/b	$\sigma=0$	0.25	0.5	$\sigma=0$	0.25	0.5	$\sigma=0$	0.25	0.5
0.1	2.51	3.31	4.85	2.51	2.52	2.53	0.334	0.473	0.731
0.2	2.59	3.37	4.81	2.59	2.63	2.66	0.483	0.603	0.809
0.3	2.68	3.44	4.80	2.68	2.75	2.81	0.607	0.715	0.889
0.4	2.78	3.53	4.82	2.78	2.88	2.98	0.720	0.823	0.977
0.5	2.88	3.62	4.83	2.88	3.01	3.14	0.827	0.929	1.07
0.6	2.98	3.72	4.91	2.98	3.14	3.31	0.930	1.03	1.18
0.7	3.09	3.81	4.97	3.09	3.28	3.48	1.03	1.14	1.29
0.8	3.19	3.91	5.05	3.19	3.41	3.65	1.13	1.25	1.40
0.9	3.29	4.01	5.12	3.29	3.54	3.82	1.23	1.36	1.51
1.0	3.40	4.12	5.20	3.40	3.67	3.98	1.33	1.47	1.63
1.11	3.51	4.22	5.30	3.51	3.81	4.16	1.44	1.59	1.77
1.25	3.65	4.36	5.42	3.65	3.99	4.39	1.58	1.75	1.94
1.43	3.82	4.54	5.58	3.82	4.21	4.67	1.76	1.95	2.18
1.67	4.06	4.78	5.80	4.06	4.50	5.04	2.01	2.23	2.50
2.00	4.37	5.10	6.11	4.37	4.90	5.56	2.35	2.62	2.96
2.50	4.84	5.57	6.57	4.84	5.48	6.31	2.88	3.24	3.70
3.33	5.57	6.34	7.34	5.57	6.40	7.51	3.79	4.32	5.01
5.0	6.96	7.78	8.82	6.96	8.14	9.79	5.72	6.63	7.89
10	10.7	11.7	12.9	10.7	12.8	16.0	12.2	14.6	18.0

Appendix – 4:

Matlab Code for Arcard Wear Analysis

```
dat1 = importdata('Contact postion.txt');
dat2 = importdata('Vertical Force.txt');
dat3 = importdata('Contact patch Area.txt');
dat4 = importdata('LongCreep.txt');
dat5 = importdata('LatCreep.txt');
dat6 = importdata('Velocity.txt');
dat7 = importdata('Wheel profile.txt');
dat8 = importdata('ab ratio.txt'
PC = zeros(size(dat2));
for i = 1:numel(PC);
    if dat3(i) == 0
        PC(i) = 0;
    else
        PC(i) = dat2(i)/dat3(i);
    end
end
PC; % unit is N/m2=Pa
a = zeros(size(dat2));

for i = 1:numel(a);
    if dat8(i) == 0
        a(i) = 0;
    else
        a(i) =
sqrt(abs(dat3(i)*dat8(i)/pi));
    end
end

ds = zeros(size(PC));
for i = 1:numel(PC);
        ds(i) =
sqrt((dat4(i)^2)+(dat5(i)^2))*2*a(i);
end

K = 0.01*10^-4;
H = 3*10^9;
V = zeros(size(PC));
for i = 1:numel(PC);
    if PC(i) == 0
        V(i) = 0;
    else
        V(i) = (K*dat2(i)*ds(i)/H);
    end
end
V;
WD = zeros(size(PC));
for i = 1:numel(V);
    WD(i) = K*PC(i)*ds(i)/H;
end
WD = WD*10000; % Unit is m for 10,000
Distance factor
w = [dat1, WD];
sortrows(w,1);

n1=1;
n2=((length(w)/30));
A = zeros(); c = zeros();
for i = n1:n2
    A(i) = sum(w(n1:n2,2));
    c(i) = mean(w(n1:n2,1));
    n1=n2+1;
    n2=n2+((length(w)/30));
    if n1 > length(w)
        break
    end
end
A(A==0) = [];
ea=A'; ec=c';
b = ea(end:-1:1); d = ec(end:-1:1);
x = dat7(:,1);
z = zeros();
for i = 1:numel(d)
    [val,idx] = min(abs(x-d(i)));
    z(i) = x(idx);
end
Z = z';
format shortg;
disp('      WD       WD Act.Loc    Closest
WD loc. Wheel Profile')
D = [b,d,Z];
disp(D)
disp('All value are in m')
disp('---')
disp('---')
y = dat7(:,2);
[matches,Ix,IZ]=intersect(x,Z);
dif=y(Ix)-b(IZ);
Depth = [Z(IZ),dif,b(IZ)];
disp('Prof.Y-Location----wheel Z-------WD
')
disp(Depth)
Xx = dat7(:,1);
Xy = dat7(:,2);
Dx = Z(IZ);
Dy = dif;
EX = zeros();
for i = 1:numel(Xx)
    for j = 1:numel(Dx)
        if Dx(j)== Xx(i)
            EX(i) = Dy(j);
            break
        else EX(i) = Xy(i);
        end
    end
end
EZ = EX';
EV = EZ - dat7(:,2);
EW = dat7(:,3) - dat7(:,2);
format shortg
Figure(1)
plot(Xx,EZ,'blue')
hold on
plot(Xx,dat7(:,3),'red')
hold on
plot(Xx,dat7(:,2),'green')
legend({'Matlab worn Profile','SIMPACK worn
Profile','Unworn
profile'},'Location','north','Orientation','
horizontal')
Figure(2)
plot(Xx,EV,'red')
hold on
plot(Xx,EW,'blue')
legend({'WD-Matlab','WD-
SIMPACK'},'Location','Southeast','Orientatio
n','horizontal')
T = table(Xx, EZ, EV, 'VariableNames', { 'Y'
'Zworn'  'WD'} );
writetable(T, 'Matlab Worn
Profile_MC_WS_L.xlsx')
```